CHALMERS

Derivation of Forces on a Sail using Pressure and Shape Measurements at Full-Scale

Master of Science Thesis

DALE MORRIS

Department of Shipping and Marine Technology
Division of Sustainable Ship Propulsion
CHALMERS UNIVERSITY OF TECHNOLOGY
Göteborg, Sweden, 2011
Report No. X-11/267

REPORT NO. X-11/267

Derivation of Forces on a Sail using Pressure and Shape Measurements at Full-Scale

DALE MORRIS

Department of Shipping and Marine Technology
CHALMERS UNIVERSITY OF TECHNOLOGY
Gothenburg, Sweden 2011

Derivation of Forces on a Sail using Pressure and Shape Measurements at Full-Scale

DALE MORRIS

Report No. X-11/267
Department of Shipping and Marine Technology
SE-412 96 Gothenburg
Sweden
Telephone +46 (0)31-772 1000

Cover: Orange neon stripes, detected by the sail recognition software VSPARS, and pressure sensors on full-scale sails

Printed by Chalmers Reproservice
Gothenburg, Sweden 2011

Derivation of Forces on a Sail using Pressure and Shape Measurements at Full-Scale
DALE MORRIS
Department of Shipping and Marine Technology
Chalmers University of Technology

Abstract

Aerodynamic forces are usually computed numerically or measured in a wind tunnel. These forces may be used to predict the performance of a yacht at full-scale. The aim of this project was to develop a new method to measure the forces and moments directly at full-scale. The theory was that by simultaneously measuring the shape of the sails and the pressures around them the force normal to the surface could be derived by summation of the product of the pressure, unit normal vector and the relevant area of the discretised sail shape.

A code was written for the interpolations of the discrete shape and pressure measurements to the full sail shapes and pressures over them. The shape was then discretised and the pressure at the centre of each cell was assumed constant over it. The results were validated through testing at model-scale. The calculated forces and moments were compared directly to the results obtained from a force balance on which the model yacht was mounted. The results were also used in a VPP to assess the accuracy when predicting heel angle and boat speed.

The first test was conducted on a set of semi-rigid sails with surface mounted pressure taps. A study of the pressure distributions found using a VLM was used to optimise the pressure tap locations. The results were encouraging; however it appeared that the interference on the flow caused by the taps resulted in large under-predictions of the forces and moments. This lead to a second round of model testing using sails with internal pressure taps leaving the sail surfaces smooth. The results showed good agreement, although there was still a significant under-prediction of the drive force.

Full-scale testing was carried out using a purpose built pressure measuring system. Although full-scale testing is extremely difficult due to the unsteady environment, good results were obtained where clear trends in the boat speed and heel angle were also seen in the calculated drive force and heeling moment.

Keywords: pressure measurement, force measurement, full-scale, model-scale, shape recognition, sails

Acknowledgements

First and foremost I would like to thank the Rolf Sörmans Fund and the Jewish Maritime League for sponsoring my trip to New Zealand.

I would like to thank Lars Larsson for providing me with the opportunity to go and for accepting the role of examiner and to Peter Richards in the role of supervisor for guiding my work and providing a deep insight into the theory of sailing.

This work would not have been possible without the help of David Le Pelley. His input into this project was immense, not only his time spent on developing the pressure system but also the help provided in his advice for writing the code, instruction on how to use the wind tunnel and thoughts on the analysis of the results. Of course I also have much gratitude for him providing the use of his beautiful Stewart 34.

Julien Pilate was gracious enough to let me use his VLM code in this work. He was always helpful and any questions or problems I had regarding the use of or the theory behind it were always taken care promptly.

A big cheers to the boys at the YRU for helping with the full-scale testing. Alex Blakely was always ready to lend a hand down in the workshop or to discuss any issue I was having, often with him providing the epiphany I needed. He was also always up for a weekend of testing when the schedule was too full during the week. Boris Horel and Rafaelle Ficco were also always ready to jump in and help out where they could, and not to mention Boris' contribution he made for this work with his measurements of the heel angle, boat speed and AWS.

My loving parents, Ian and Dalene Morris, are my biggest inspiration in everything I do and I cannot thank them enough.

Lastly I would like to thank Cathrine Waldebjer for always being close by even when she was on the other side of the world.

(From L to R) Peter Richards, Raffaele Ficco, Alex Blakely, Dale Morris, Boris Horel & David Le Pelley

Table of Contents

Abstract iii
Acknowledgements iv
Table of Contents v
List of Figures viii
List of Tables x
Nomenclature xi
Symbols xi
Abbreviations xii
1 Introduction 1
1.1 Background to the Current Work 1
1.2 Objective 2
1.3 Methodology 2
1.4 Scope & Limitations 3
2 Previous Work 4
2.1 Pressure Measurements on Sails 4
2.2 Full-Scale Force Measurements on Yachts 6
2.3 Sail Shape Measurements 8
2.4 Summary of Previous Work 8
3 Theory 9
3.1 Sail Theory in Brief 9
3.1.1 Sail Geometry and Terminology 9
3.1.2 Pressure Difference and Lift 12
3.1.3 Flow Phenomena Affecting the Pressure Field 13
3.1.4 Forces and Moments Generated by the Sails and Rig 15
3.2 Difficulties in Measuring Pressure 19
3.2.1 Issues due to Measuring Equipment 19
3.2.2 Fluctuations in Readings due to Pressure Environment 19
3.2.3 Difficulties to Zero the System at Full-Scale 20
3.3 Theory behind VSPARS 20
3.4 Full-Scale vs. Model-Scale or Numerical Testing 21
3.4.1 Details of the Twisted Flow Wind Tunnel (TFWT) 22
3.5 Curve Fitting Techniques 22
3.5.1 Interpolation 22

3.5.2 Least Squares 23
4 Pressure Integration over Sail Shapes 25
4.1 Inputs for the Integration 25
4.1.1 Shape Input 25
4.1.2 Pressure Input 26
4.1.3 User Input 26
4.2 Sail Shape Generation 27
4.3 Pressure Integration over the Sail 30
4.4 Force & Moment Calculation 32
4.5 Verification & Validation 32
4.5.1 Sail Area Calculation 32
4.5.2 Sail Dimensions 33
4.5.3 Integration of Uniform Pressure Field 33
5 Model Test 1: Semi-Rigid Sails 34
5.1 Test Setup: Semi-Rigid Sails 34
5.1.1 Details of Semi-Rigid Sails and Pressure System 34
5.1.2 Test Procedure for the Semi-Rigid Sails 37
5.2 Results: Semi-Rigid Sails 37
5.2.1 Semi-Rigid: Recorded Pressures 37
5.2.2 Semi-Rigid: Forces & Moments 42
5.2.1 Semi-Rigid: VPP Results 43
5.3 Summary of Results for the Semi-Rigid Test 46
5.3.1 Possible Sources of Error for the Semi-Rigid Test 46
6 Model Test 2: Coreflute Sails 47
6.1 Test Setup: Coreflute Sails 47
6.1.1 Description of the Coreflute Sails 47
6.1.2 Test Procedure: Coreflute Sails 49
6.2 Results for the Coreflute Sails 49
6.2.1 Coreflute: Recorded Pressures 49
6.2.2 Coreflute: Sail Area and Depth 53
6.2.3 Coreflute: Forces & Moments 54
6.2.4 Coreflute: VPP Results 55
6.3 Summary of the Results for the Coreflute Test 58
7 Full-Scale Testing 59

7.1 Test Equipment 59
7.1.1 Details of the Pressure Measuring System 59
7.1.2 Calibration of the Pressure Transducers 61
7.1.3 Setup of the VSPARS Stripes 61
7.1.4 Setup of the Pressure Taps 61
7.1.5 The Sails Used 63
7.1.6 Additional Equipment 63
7.2 Test Procedure and Observations 63
7.3 Results for the Full-Scale Test 64
7.3.1 Full-Scale: Recorded Pressures 64
7.3.2 Full-Scale: Comparison of Various Measurements 68
7.4 Summary of the Results for the Full-Scale Test 72
8 General Discussion 73
9 Conclusions 74
10 Recommendations for Future Work 75
11 Bibliography 76
APPENDIX 1 – Base Code 78
APPENDIX 2 – Formulas used in Code 81
Cross-Product Theorem 81
Arc Length 82
Least Squares Curve Fitting 83
APPENDIX 3 – Pressure Tap Testing 84
Taps for the Semi-Rigid Sails 84
Various Full-Scale Tap Geometries 84
Full-Scale Taps with Sail Patches 85
APPENDIX 5 – Pressure Tap Locations 87
APPENDIX 5 – Results 88
Results for the Semi-Rigid Test 88
Results for the Coreflute Test 91

List of Figures

Figure 3-1: Terminology of a sail 9
Figure 3-2: Sail Shape Parameters 10
Figure 3-3: Windward and leeward on port tack 10
Figure 3-4: Sail dimensions 11
Figure 3-5: Pressure distribution over a thin foil (19) 12
Figure 3-6: Flat plate with circulation (9) 12
Figure 3-7: The boundary layer under various pressure gradients: 14
Figure 3-8: Pressure distributions over a main and headsail (7) 14
Figure 3-9: Stagnation streamlines on the main- and headsail 15
Figure 3-10: Force components on a sail 16
Figure 3-11: Change in force components due to sail trim 16
Figure 3-12: Forces and moments created by the sails 17
Figure 3-13: The heeling force balance 17
Figure 3-14: Comparison of different interpolation schemes used for a typical chordwise pressure distribution 23
Figure 3-15: The "best" fit curve through a scatter of data points (inset: vertical offsets) 23
Figure 3-16: Two examples of a 3rd degree least squares curve fitted to a typical pressure distribution compared to a linear interpolation 24
Figure 4-1: Stripes with user defined number of points 27
Figure 4-2: The basic sail shape extrapolated to the head and foot 28
Figure 4-3: Sails generated at a high resolution 29
Figure 4-4: Picture showing the cut and skewed cells on the headsail 30
Figure 4-5: Area of a parallelogram 32
Figure 5-1: Overhead view of the Semi-Rigid test setup in the wind tunnel 34
Figure 5-2: Graph showing the recreated pressure distribution along a chord 35
Figure 5-3: Coin tap (dimensions in mm) 35
Figure 5-4: Block tap (dimensions in mm) 35
Figure 5-5: Picture of taps on the top stripe at the leading edge of the mainsail 36
Figure 5-6: Picture of mainsail, PVC tubing and stand from astern 36
Figure 5-7: Figures of pressure distribution around the Semi-Rigid sails 37
Figure 5-8: Differential pressure reading on Semi-Rigid headsail for the sweep of the headsail 38
Figure 5-9: Differential pressure reading on Semi-Rigid mainsail for the sweep of the headsail 38
Figure 5-10: Pressure contour plot of Semi-Rigid mainsail for JS0 40
Figure 5-11: Pressure contour plot of the Semi-Rigid headsail for JS0 40
Figure 5-12: Pressure contour plot of the mainsail using a VLM 41
Figure 5-13: Pressure contour plot of the headsail using a VLM 41
Figure 5-14: Results for each trim position in the combined sweep of the Semi-Rigid Sails 44
Figure 5-15: VPP predicted boat speed (Vs) for Semi-Rigid 45
Figure 5-16: VPP predicted heel angle for Semi-Rigid 45
Figure 5-17: Heel moment (Mx) vs VPP predicted heel angle for Semi-Rigid 45
Figure 5-18: Photo of ridges found on the leeward, flush mounted taps 46
Figure 6-1: Overhead view of the Coreflute test setup in the wind tunnel 47
Figure 6-2: Cross-section of the Coreflute sails and location of pressure tap rows (15) 48

Figure 6-3: Figures of pressure distribution around Semi-Rigid and Coreflute sails 50
Figure 6-4: Differential pressure reading on Coreflute headsail for the sweep of the headsail 51
Figure 6-5: Differential pressure reading on Coreflute mainsail for the sweep of the headsail 51
Figure 6-6: Pressure contour plot of Coreflute mainsail 52
Figure 6-7: Pressure contour plot of Coreflute headsail 52
Figure 6-8: Comparison of VPARS to measured values for camber and draft 54
Figure 6-9: Results for each trim position in the combined sweep of the sails 56
Figure 6-10: VPP predicted boat speed (Vs) for Coreflute 57
Figure 6-11: VPP predicted heel angle for Coreflute 57
Figure 6-12: Heel moment (Mx) vs VPP predicted heel angle for Coreflute 57
Figure 7-1: Two piece housing for the pressure transducer (25) 60
Figure 7-2: Schematic of the wired pressure system (25) 60
Figure 7-3: Pictures of the pressure taps being mounted to the sail 62
Figure 7-4: Rough representation of the course sailed 64
Figure 7-5: Pressure distribution on the main top stripe for main sweep for both tacks 66
Figure 7-6: Pressure distribution on the main mid stripe for main sweep for both tacks 66
Figure 7-7: Pressure contour plot of full-scale mainsail 67
Figure 7-8: Pressure contour plot of full-scale headsail 67
Figure 7-9: Comparison of SOG and Vs to Fx for both jib sweeps 68
Figure 7-10: Comparison of Vs to F_x for all stbd sweeps 69
Figure 7-11: Comparison of heel angle to heeling moment for all stbd sweeps 70
Figure 7-12: Comparison of heeling angle to boat speed for all stbd sweeps 70
Figure 7-13: Comparison of heeling moment, heel angle, AWA, drive force, boat speed and AWS for all stbd sweeps 71
Figure 11-1: Calculation of arc length 82
Figure 11-2: Graph of pressure readings for model-scale taps for one sweep of the headsail 84
Figure 11-3: Various tap geometries (from L-R: Volcano, Steep, Gradual, Rounded) 85
Figure 11-4: Graph of pressure readings for various full-scale tap geometries 85
Figure 11-5: Top and side views of the testing of full-scale pressure taps 85
Figure 11-6: Graph of pressure readings for full-scale taps with sail patches 86

List of Tables

Table 4-1: Data sheet for code 25
Table 4-2: Example of a pressure matrix with varying number of taps 31
Table 5-1: Force & moment results for Model Test 1: Semi-Rigid 42
Table 6-1: Rows used and corresponding percentages 48
Table 6-2: Percentage difference between VSPARS and measured values 53
Table 6-3: Force & moment results for Model Test 2: Coreflute 55
Table 7-1: Relative contribution of main and headsail on F_x and M_x 69
Table 11-1: Table of average difference of different model-scale tap geometries 84
Table 11-2: Table of average difference and standard deviations for various full-scale tap geometries 85
Table 11-3: Table of average difference and standard deviations for full-scale taps with sail patches 86

Nomenclature

Symbols

α	Angle of Attack
A_{head}	Area of the headsail
A_{main}	Area of the mainsail
A_{ref}	Reference Area
B	Heeling Angle
b	Righting Arm
C	A constant value
C_F	Force Coefficient
C_M	Moment Coefficient
C_P, C_{Pmax}, $\triangle C_P$	Pressure Coefficient, Maximum C_P, Differential C_P
$\triangle$	Buoyancy of the boat
E	Maximum dimension of the foot of a mainsail
F_A	Aerodynamic Force
F_H	Hydrodynamic Force
F_{side}, F_S	Side Force
F_T	Resultant Force
F_{vert}	Vertical Force
$F_{x,}$ F_R	Drive Force
F_y	Force perpendicular to the mast
F_z	Force parallel to the mast
θ, θ_{zero}	Analogue signal in bits, Value in bits for the zero reading
h	Heeling Arm
H	Luff Height, Length of Head
I	Maximum hoist height of the headsail
J	Distance from fore face of the mast to the forestay
LP	Luff Perpendicular
m	Gradient of the slope
P	Maximum hoist height of the mainsail
p, p_∞	Static Pressure, Static Pressure of the free stream
q, q_∞	Dynamic Pressure, Dynamic Pressure of the free stream
ρ	Density
U, U_∞	Flow Velocity, Free Stream Velocity
V	Flow Velocity
V_a	Apparent Wind Velocity
V_b	Boat Velocity
Vs	Boat Speed
V_t	True Wind Velocity
W	Weight of the boat
x/c	x coordinate divided by chord length
x_{ij}	x coordinate for the i^{th} data point in the chordwise direction and the j^{th} in the spanwise direction

Abbreviations

A/D	Analogue to Digital
AoA	Angle of Attack
AWA	Apparent Wind Angle
AWS	Apparent Wind Speed
CB	Centre of Buoyancy
CE	Centre of Effort
CFD	Computational Fluid Dynamics
CG	Centre of Gravity
CLR	Centre of Lateral Resistance
CNC	Computer Numerical Control
CS	Combined Sweep
GPS	Global Positioning System
HM	Heeling Moment
IDC	Insulation Displacement Connector
IMU	Inertial Measurement Unit
JS	Jib Sweep
MDF	Medium Density Fibreboard
MS	Main Sweep
PCB	Printed Circuit Board
PVC	Polyvinyl Chloride
RANSE	Reynolds Averaged Navier Stokes Equations
SOG	Speed Over Ground
STBD	Starboard
TFWT	Twisted Flow Wind Tunnel
TWA	True Wind Angle
TWS	True Wind Speed
UoA	University of Auckland
USB	Universal Serial Bus
VLM	Vortex Lattice Method
VPP	Velocity Prediction Program
VSPARS	Visualisation of Sail Position And Rig Shape
YRU	Yacht Research Unit

1 Introduction

This project is believed to be the first attempt to calculate the generated forces and moments from full-scale or model-scale sails by measuring the pressures across them and integrating these over the measured sail shape.

1.1 Background to the Current Work

Predicting the potential speed of a yacht is an important tool for the designer and for the sailor. Whether being used to design the best sails for the yacht or to trim the sails to their optimum the more accurate these predictions are the better the yacht will perform.

It is possible to use empirical formulas to predict the performance of a certain sized sail but generally, if a higher accuracy is required, testing is done either numerically or at model-scale. These methods have their limitations; computational power limits the accuracy of numerical testing while scaling of all parameters is basically impossible in a wind tunnel.

Knowing this there is still few other options. Ideally all potential sails would be tested at full-scale but this is economically not viable as the cost of doing wind tunnel tests on a full range of sails is roughly the same as making one full-scale sail and numerical testing is even cheaper. However if an easy and accurate method existed to test full-scale sails it could provide priceless feedback for future designs. Specifically flying shapes, pressures and ultimately the forces and moments generated by the sails would be the most valuable.

There have been a few sail dynamometers built over the years which have been successful (1) (2) (3). These are yachts constructed with an internal force balance in order to measure the forces from its sails. The results are however specific to the dynamometer and cannot be used to predict the forces for others. Another method to look at the fluid-structure interaction between the sails and rig is to measure the loads directly on the rigging using strain gauges (4). According to the material available these have been the only previous attempts to measure the forces at full-scale.

Until recently full-scale pressure tests had been few and far between, the earliest was done in 1923 by Warner and Ober (5) followed by the next recorded attempt in 2006 by Puddu et al. (6). Subsequently there has been a revival of this thread of research thanks to more appropriate equipment being developed. Viola (7) was successful in obtaining a good resolution of the pressure distribution over a jib and mainsail while working at the Univeristy of Auckland Yacht Research Unit (YRU).

Le Pelley and Modral have developed a commercial package, VSPARS, which is capable of recording the chord shapes at specific heights along the sail. This package is currently being used by top-flight racing teams in the Volvo Ocean Race, America's Cup and the TP52 circuit plus many more. Teams that use it are easily identified by the bright orange or green day-glow stripes across their sails (8).

The hypothesis for this work then is that by coupling a pressure measurement system and a sail shape recognition package it would be possible to calculate the magnitude and direction of the resultant force generated by the sails by integrating the pressure over their surface.

1.2 Objective

The primary objective of this project was to simultaneously measure the shape of a set of sails and the pressure distribution around it at full-scale. Then, by multiplying said pressures by the area and unit normal vector of a corresponding surface, calculate the generated drive force and roll moment

A number of secondary objectives were identified in order to achieve the primary goal:

- Recreate the full sail shape and pressure distribution from discrete measurements.
- Validate the calculations through wind tunnel testing.
- Optimise the number of pressure taps necessary to obtain a reasonably accurate pressure distribution.
- Test various geometries of pressure taps for model- and full-scale for the least interference on the air flow.
- Assemble and test a new pressure measurement system designed for full-scale.

1.3 Methodology

Shape measurements were recorded using a commercial sail recognition package, VSPARS, developed within the YRU. Pressures were obtained in the wind tunnel through a system developed and used successfully in previous projects. For full-scale a new system was developed by David Le Pelley.

Discrete measurements for both shape and pressure are interpolated in order to describe the full sail shape and pressure distribution of the sails. Some assumptions were necessary to achieve this.

A program was needed to handle the inputs and perform the interpolations to a high density. This was written in Matlab. It was developed using inputs obtained through model testing in a wind tunnel before being implemented at full-scale.

A force balance in the Twisted Flow Wind Tunnel (TWFT) at the YRU was used to validate the calculated forces. The calculated forces and results from the balance were also used in a Velocity Prediction Program (VPP) to assess the influence on boat speed and heel.

Initially results from a Vortex Lattice Method (VLM) numerical simulation, developed by Julien Pilate at the YRU, were used to optimise the number of pressure taps and their locations. Once sufficient data had been recorded an analysis of it helped to assess the effectiveness of the layout.

A brief study was conducted in the wind tunnel to assess a couple of tap geometries and their effect on the pressure readings on a model-scale sail. Further testing was conducted on proposed full-scale taps. These were limited by the size of the pressure transducer that they were required to house.

Assembly, installation and calibration of the full-scale pressure system were carried out by the author.

Full-scale testing was conducted on a Stewart 34, courtesy of David Le Pelley, out on the Hauraki Gulf in Auckland, New Zealand.

1.4 Scope & Limitations

The project was primarily focused on the recreation of the sail's geometry from the data output from the sail shape capturing and the extrapolation of discrete pressure readings into a full distribution over the sail.

The scope was limited to upwind sails, i.e. a mainsail and jib or genoa. The work required to incorporate downwind sails was thought to be excessive for the time allotted to this project. These sails were trimmed using only the primary controls, i.e. the sheets, to simplify the problem.

Although some analysis of the pressure distributions was done to determine if the recorded data was valid or not, this work does not focus on the details as to what was occurring in the pressure plots for each test run.

Leeway angle was ignored completely. The results can easily be transformed if the leeway angle is known. However it is very complicated to measure this angle accurately for a time averaged period and therefore was not accounted for.

The full-scale testing was conducted two weeks prior to the author commencing work at Southern Spars NZ and therefore time was too limited for a repeat test. The delay was caused by the late delivery of parts for the pressure system.

2 Previous Work

This was a multifaceted project that can be divided into three main parts when examining the previous work leading up to it. Namely these are pressure measurement, shape measurement and full-scale force measurement. The previous work conducted in each area is reported here in chronological order. Some previous work combined elements from two or more categories making it difficult to categorise and so the relevant content is discussed in each section.

2.1 Pressure Measurements on Sails

In 1923, according to Marchaj (5), full-scale pressure measurements were carried out by Warner & Ober on the yacht *Papoose.* They used a number of manometers connected to small holes in the sails using rubber tubing on only one side of the sails. Three lines or sections were measured on the mainsail and one on the jib. There was a slightly higher density of measurement points at the leading edge than on the remainder of a line. Simultaneous measuring was achieved by photographing the bank of manometers and windward and leeward pressures were measured by changing tack. The readings were then of the pressure difference between the static pressure on the sail and the static atmospheric pressure at the deck. This eliminated the effect of wind speed variations between different tests.

In 1971 Gentry (9) investigated sail interactions in 2D by using an Analogue Field Plotter. This was essentially a device that uses electrical current to simulate the streamlines around a 2D foil in lines of constant voltage across a conducting sheet. The analogy neglects viscosity in the same way as potential flow theory. Velocities and pressures were then calculated from the readings using Bernoulli's equation and some significant observations were made with respect to the influence of the headsail on the main and vice versa.

Wilkinson (10) conducted experiments in 1989 that looked at the pressure distribution on a 2D variable camber aerofoil. The model also included a circular mast. The pressure tappings were integral and did not disturb the flow. An investigation was done on the effect of Reynolds number, camber ratio, incidence angle, mast diameter/chord ratio and mast angle.

In the past 5 years pressure measurements have seen a resurgence. The realisation of compact equipment that does not significantly affect the flow field or sail shape has allowed researchers to look at the underlying phenomena that creates the forces and moments in more detail. This has served to better understand the problem as well as to provide full-scale validation for numerical techniques.

In 2006 Pudda et al (6) investigated the static pressures at full-scale on the mainsail of a tornado class catamaran. 25 wired taps were regularly spaced per side and staggered relative to the other side to measure either the suction or pressure on the sail. The measurements were then combined to obtain the differential pressure. They reported a full pressure distribution derived from these measurements and compared them to numerical results but there was no mention of how the pressures were interpolated across the sail. Where or how the reference pressure was measured was not mentioned either. The taps were not placed very close to the leading edge where phenomena such as separation and recirculation are known to occur and create high gradients in the pressure.

In the same year Flay and Millar (11) published their work describing the considerations needed when attempting to measure pressures on sails. Their full-scale attempt, which used 120 pressure taps placed at 1/4, 1/2, and 3/4 luff lengths to measure static pressures connected to a reference pressure through PVC tubing, was unsuccessful. They concluded that squashed tubing had resulted in incorrect backing pressure to the transducers.

In 2008 a team working for BMW Oracle (12) developed their own wireless pressure measuring system. In order to validate the system they tested it on a 25m sloop and recorded boat speed, TWS and TWA and compared these with the changes in pressure. The results correlated well and they suggested that the pressure readings could be highly useful as it pre-empted change in boat speed. Pressures were also compared to computer models with good agreement. The sail shapes for the CFD analysis were recorded through photographs and recreated using North Sails' sail design software, Membrain©. The number of pressure taps used was very limited, as few as five per side at five different heights. They recommend using as many as 56 evenly spaced taps per side on the main and 33 for the headsail in order to obtain a complete pressure map across the sail.

Richards and Lasher (13) conducted a $1/25^{th}$ model-scale experiment on downwind sails using Semi-Rigid, fibre glassed sails with PVC tubing embedded inside. The main advantage of these sails was that there was no interference with the flow by the pressure tappings, as opposed to having surface mounted taps on a flexible sail. They were also able then to tap the sails at a high resolution of 47 per side on the spinnaker and 30 per side for the main distributed over 7 chords or horizontal sections on each sail. The results of the pressure measurements were integrated over the known sail shape taken from the geometry file used for the mould to calculate the drive and side force generated by the sails. These were compared with the force balance measurements in the wind tunnel with good agreement. The pressure distributions were also compared to numerical computations using Fluent, again with good agreement.

In 2009 Viola and Flay (14) tested a range of asymmetric spinnakers at $1/15^{th}$ scale. The sails tested were an A1, A2 and A3 and the results correlated well to the intended uses of the sails, i.e. they each generated the maximum drive force at the AWA's that they were designed to be flown at. They used the same pressure measurement system as Richards and Lasher (13) albeit with different pressure taps. It was determined that the system had a resolution of 0.1 Pa when used at this scale. The sails this time were flexible cloth sails and the pressure taps were mounted on the sail surface. To minimise interference from the taps only one side was tested at a time with the taps mounted on the other side and connected to the test side through a small hole in the sail cloth. Firstly 5 chord sections were tested with 11 taps per chord for a range of AWA's and heel angles. Then one chord section was tested using 34 taps to investigate the effect of sail trim. The pressure measurements showed good agreement with sail aerodynamic theory and it was obvious to see where the leading and trailing edge separation occurred.

Encouraged by their results on the pressure measurements, in 2010 Viola and Flay (7) used the same system at full-scale on a Sparkman and Stephens 24ft yacht, this time at a resolution of 1.2 Pa. The experiment was conducted on a mainsail and genoa heading upwind with taps arranged at 3 different heights along each sail. The number of taps varied along the span with 6 at the top, 9 in the middle and 16 at the bottom. As before the taps were connected to transducers through PVC tubing which had to be taped onto the sail to avoid disturbing the flow. The pressure taps themselves were

truncated cones with a base of 20mm and a height of 5mm. All this apparatus was deemed to be within the sail boundary layer and thus would not alter the flow. The taps were only placed on one side of the sail with the transducers connected to a reference pressure. This meant that the boat needed to change tack in order to measure both the leeward and windward pressures. In order to obtain useful corresponding pressures there were a few pressure taps placed on the other side of the sail as well as a few taps placed on either side of the mast which then needed to match the pressure recorded on the previous tack before recording the new tack. The effects on the sails from sheet trim, leech and backstay tension, the gap between the sails and various AWA were investigated.

Around the same time Fluck et al. (15) were working on more model-scale pressure testing. They believed that it was not sufficient to validate numerical codes with force alone. If the code could match the experimental pressure data then it could prove that the code is accurate to a much higher degree. This prompted them to build Semi-Rigid pressure tapped sails with a Coreflute® core and fibreglass and epoxy skin. The fabrication of these sails is described in section 6.1.1. The advantage of them being semi-rigid is that the shape was known for the numerical simulations. The pressure tubing could then also be inside the sail and not disturb the airflow. The results compared very well to the VLM code that was used. These sails and the VLM code have been used extensively for the research in the current work.

2.2 Full-Scale Force Measurements on Yachts

Since the 1930's there have been efforts to predict the performance of yachts in order to design better ones or to make racing more competitive through handicapping systems. Although initially done by hand calculations, they are now handled by velocity prediction programs (VPPs). A VPP essentially balances the hydro- and aerodynamic forces acting on a yacht using empirical formulas in order to find the speed and attitude of the yacht when in equilibrium. All they require are the force coefficients of the hull and the sails. The hydrodynamic forces from the hull and appendages are estimated through mathematical models derived from series of tow tank tests conducted systematically on varying hull shapes at different attitudes and speed. The aerodynamic forces from the sails have in the past been found in various ways.

Model-scale sails can be tested in a wind tunnel, such as the Twisted Flow Wind Tunnel (TFWT) at the Yacht Research Unit (YRU) in Auckland, by mounting the model on a force dynamometer. The TFWT has overcome many of the issues associated with model testing, namely the wind shear from the atmospheric boundary layer and varying apparent wind angle (AWA) over a change in height. Hansen (16) discusses this in detail. However testing conducted at model-scale rarely matches the Reynolds number which is associated with the transition from laminar to turbulent flow. This would require excessive wind speeds and the delicate sail fabric necessary at model-scale would not be able to withstand this.

Another method is to measure the maximum speed of a full-scale yacht and then replicate the boat's attitude and speed in a tow tank. It is then possible to calculate the corresponding sail forces. This method includes scale effects and the added resistance from waves may not be accounted for accurately.

Numerical simulations, although rapidly becoming more powerful and robust, have not been able to account for the large amounts of separation on downwind sails.

The drawbacks from these methods have encouraged some to attempt to measure the sail force at full-scale. The first instance of this was van Hemmen (17), in 1986, who derived empirical formulas from tests done using 50 strain gages mounted on the rigging on a yacht. He was then able to measure the loads on these components and thus calculate the forces created by the sails. The major problem with this method was that it was not very accurate due to the changes in the load were in some cases less than 1% of the total load.

Herman (1) , in 1988, designed and built a 35ft test boat that connected all the rigging to a frame that was free floating inside the hull. This frame was then connected to the hull through six load cells which could then measure the six principal forces and moments. This essentially turned the full-scale yacht into a six component dynamometer much like the one mentioned previously in the wind tunnel. Milgram et al. (18), in 1995, used this boat, named the MIT Sailing Dynamometer, to develop a sail force model for a VPP. For this the induced drag needed to be calculated so that it could be separated from the form and parasitic components, therefore the sails' shape was recorded. How this was done is covered in the next section on sail shape measurement. Using this model resulted in better agreement between the VPP and actual performance. The major drawbacks of this method is that the results are only relevant to that boat which is time consuming and expensive to design and build.

In 1996 at the University of Berlin another sailing dynamometer was designed and built in order to investigate the differences between model-testing, numerical simulations and full-scale. The boat was called DYNA and it also incorporated a separate force balance that measured the hydrodynamic forces on the appendages (3).

Also based on this sailing dynamometer Masuyama & Fukasawa (2) built their own, named Fujin, in 1997. They used it to validate numerical calculations of the forces using a vortex lattice method. In this case the sail shapes again needed to be recorded so that the geometry could be used for the CFD analysis. How the shape was captured is discussed in the following section 2.3. The results between the numerical and experimental testing were fairly good but more insight into the effect on sail performance from trim and AWA was found. The experimental method and its drawbacks are the same as for Milgram (18).

More recently in 2011 Augier et al. (4) conducted a full-scale validation experiment for their numerical FSI model. The outputs from their code were compared with test results of the loads in the rig and the sail shape, which is also discussed in section 2.3. Turnbuckles and shackles were equipped with stress gauges to measure the loads in the shrouds and the running rigging respectively. 16 load sensors were used all together. The experiment was run as a steady state and then in an unsteady run. The steady state results from their code compared well but more work was needed for the unsteady.

2.3 Sail Shape Measurements

The sail shape measuring technique used by Milgram et al. (18) was based on videography from a chase-boat instead of onboard photography. At the time, in 1995, they deemed this to be more effective than other onboard methods. Their method required the chase-boat to circle the yacht in order to capture the sails from all necessary angles, eight all together. The stripes marking the sails were fairly intricate in that one stripe was made up from three lines, two horizontal and one diagonal, chord length calibration stripes and markings called a 'calibration arc'. The shape could then be recreated using software developed by them. The sail shapes were then used in a CFD analysis.

The method used by Masuyama & Fukusawa in 1997 (2) was what is known as a 2D approach. There were six CCD (charge-coupled device) cameras mounted on the yacht to record the sails' shape. Three on the port side and three on the starboard side to record either tack. Their mounting positions were at the top of the mast to record the bottom of the mainsail, on the boom to record the head of the mainsail and at the termination of the forestay on the mast to record the headsail. The images were analysed using SSA-2D software which is able to capture lines drawn across the sail at varying heights. The necessary input data was the line length and vertical position of it on the sail.

Augier et al. (4) used a similar approach as Masuyama & Fukusawa to record their sail shapes. They used ASA and ISIS image processing software to manually extract marked stripes along the sail. Calibration grids placed on deck were used to find the cameras' angle and position during post-processing. The results of this were used for comparison with a numerical model, which showed good agreement.

2.4 Summary of Previous Work

In summation, measuring pressures on sails is a maturing field but recent successes can be learnt from. The pressure tap numbers and locations vary significantly from one work to the next and no ideal layout has been found as yet.

The force measurement technique proposed in this work has not been seen before. Previous work in this field in the past has little relevance to other designs. The major advantage the concept has is that theoretically it can easily be used from one boat to the next as it is cheap and easy to setup.

Many different techniques in measuring the sail shape are known. Generally they are labour intensive or require various pieces of expensive hardware. The package used in this work appears to be vastly more user-friendly and less time consuming to post-process.

3 Theory

The following section details some basic theory that is necessary to understand the content of the work conducted for this paper.

3.1 Sail Theory in Brief

This section explains the basic concept of how a yacht functions starting with some sailing terminology to help understand these concepts.

3.1.1 Sail Geometry and Terminology

Sail makers have their own language when it comes to describing a sail. The front of a yacht is called the *bow* while the *stern* is the rear. From Figure 3-1 one can then see that the *luff* is the leading edge of the sail and the leech is the trailing. The *foot* is the bottom edge which can be attached to the *boom* or left loose. Sails generally come to a point at the *head*, the attachment point to the mast at the top of the sail, but it is more and more common to find mainsails with a square top as seen in the figure. The *tack* and *clew* are then the attachment points of the foot at the luff and leech respectively. *Battens* are stiffeners in the sail, normally made of composite plastic or wood. They can be full-length, as shown in the figure, or short, where they extend from the leech forward but not all the way to the luff. This keeps the shape of the sail, especially the leech, stiff and improves the sail's performance.

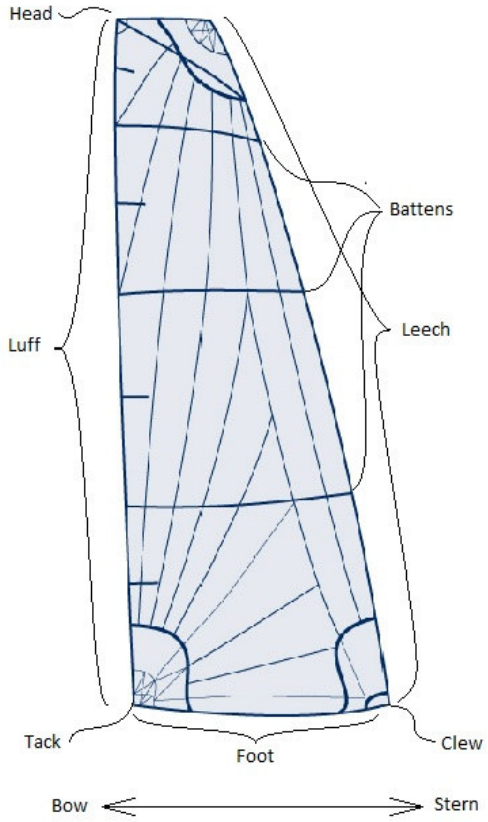

Figure 3-1: Terminology of a sail

Although the shape of a sail can vary along its height, or span, and has almost no thickness, a horizontal section can still be classified using the terminology of a wing. The following terms are graphically explained in Figure 3-2.

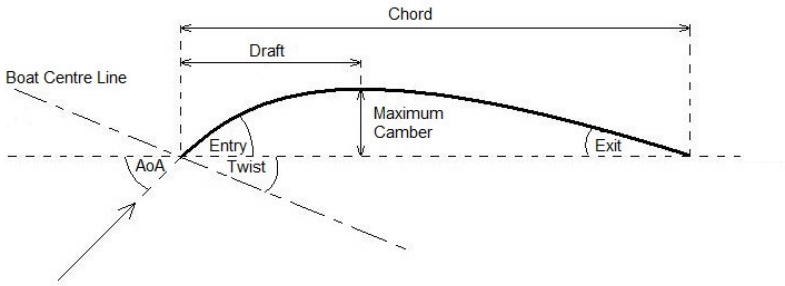

Figure 3-2: Sail Shape Parameters

The *Chord* is defined as the straight line between the leading and trailing edge. *Camber* is then the perpendicular distance from the chord line to the foil. *Draft* is the position of the maximum camber along the chord line

Entry and *exit* angles of the foil are, respectively, the angles of the leading and trailing edge to the chord line. *Angle of attack* (AoA) is the angle between the oncoming flow and the chord line and the twist angle is the angle between the chord line and the boat's centre line. The *twist* angle ideally varies along the span in order to keep the AoA constant for all sections. More about that can be read in detail in Marchaj (5) or Fossati (19).

In this paper only basic sail controls were used. The *sheet* is the primary line for trimming the sails. For the headsail it is attached to the clew and for the mainsail it is attached towards the aft end of the boom. The term used to indicate if the sheet is being tightened is *trim* and released is *ease*. By trimming a sail the AoA is increased while easing it will decrease the AoA.

Depending on the tack of the boat, the side from which the wind is blowing from depicted in Figure 3-3, will determine which side of the sail is the *windward* and which is the *leeward* side of the sail. The windward side will generally have positive pressures while the leeward will have negative.

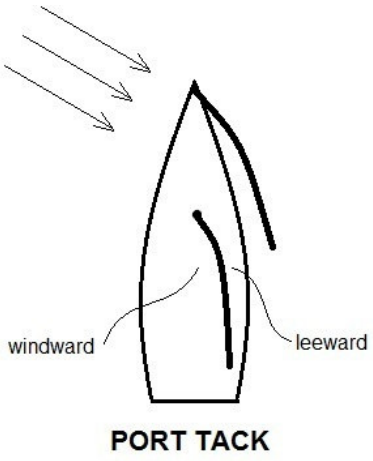

Figure 3-3: Windward and leeward on port tack

The maximum sail dimensions of a boat are limited by the mast height, boom length and the distance to the bow. These are defined as the lengths I, J, P and E where:

- I : height from headsail halyard hoist to shroud chainplate or sheerline.
- J : distance from the forestay termination on deck to forward surface of the mast.
- P : height of maximum halyard hoist of mainsail to top surface of boom.
- E : distance from aft surface of mast to the allowable aftmost position of the clew.

Other dimensions useful for calculating the nominal surface area of the sails hoisted on a yacht are:

- LP : Luff Perpendicular – length perpendicular from luff to clew of foresail
- H : Head Length – length of the top side of a square top mainsail

These can be seen graphically in Figure 3-4.

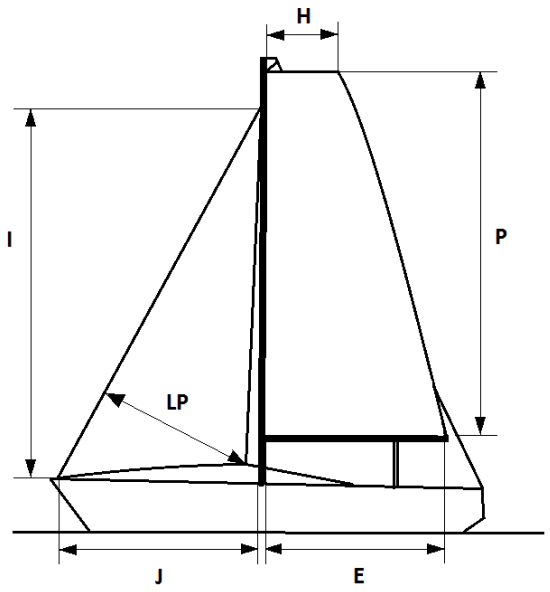

Figure 3-4: Sail dimensions

To calculate the areas the following equations are used (20).

For the headsail:

(3.1)

For a triangular mainsail:

(3.2)

For a square-top mainsail:

(3.3)

3.1.2 Pressure Difference and Lift

Sails function much like wings do, albeit with some significant differences. They both generate a force due to a pressure difference acting over their area as seen in Figure 3-6. The major differences are that a sail has almost no thickness but often has a large camber and generally operates at higher angles of attack. The flow around them is also usually disturbed by the mast or stays leading to large areas of separation (5) (9) (20).

From Bernoulli's equation we know that pressure is inversely related to velocity and so it can be seen through the contraction of the streamlines over the leeward side that the flow will accelerate creating a drop in pressure or a *suction*. Note that the pressure distribution in Figure 3-5 is displayed in the accepted convention of negative pressures above the x-axis (20).

The simplified explanation of how lift is created due to the particles travelling further over the leeward side does not hold much substance for thin aerofoils such as sails. Gentry (9) gives a more detailed explanation by looking at the numerical solution of a flat plate. Early attempts to model the flow around the plate resulted in the solution shown in Figure 3-6, labelled as the *Non-Lifting Solution,* even though it satisfied all the governing equations. It was seen through experiments that the flow at the trailing edge followed the angle of the plate along an imaginary extension of it before turning back towards the free-stream direction, known as the Kutta condition. This is due to a circulation that is created around the plate increasing the velocity on top and decreasing it on the bottom (9).

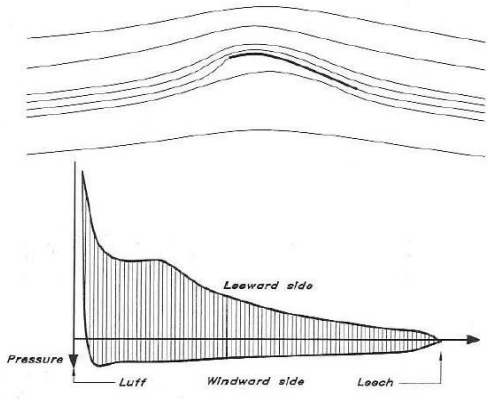

Figure 3-5: Pressure distribution over a thin foil (19)

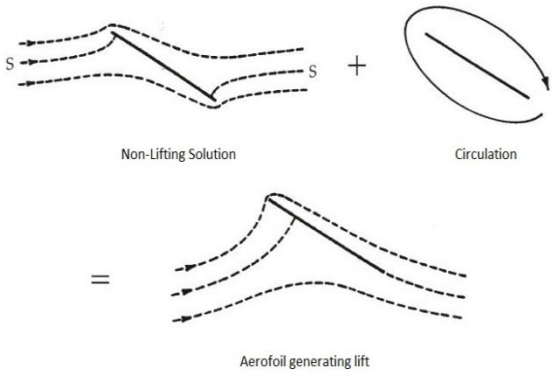

Figure 3-6: Flat plate with circulation (9)

Thus a low, suction pressure develops on the leeward side of the sail while a high pressure develops on the windward side. At any one point along the sail the difference of these pressures multiplied by a relevant area equals a force acting normal to the surface. If this calculation is done over an infinite number of areas making up the full sail area the resultant force magnitude and direction of the sail can be found. This is the fundamental theory behind this work (13).

The energy balance along a streamline can approximately be calculated using Bernoulli's equation:

$$p + q = C \tag{3.4}$$

Where p is the static and q is the dynamic pressure, which can be expressed in terms of the air density (ρ) and the fluid velocity (V):

$$q = \frac{\rho V^2}{2} \tag{3.5}$$

The change in dynamic pressure therefore drives the change in static. With an increase in speed there will be a decrease in static pressure and vice versa. It is the differential static pressure that loads the sail and this is what is measured.

A pressure coefficient is given in eq 3.6 as the ratio of the static pressure at a point less the ambient static pressure to the ambient dynamic pressure. This helps to compare pressure measurements between model and full-scale tests (19).

$$C_P = \frac{p - p_\infty}{q_\infty} \tag{3.6}$$

Note the streamlines in both Figure 3-5 and Figure 3-6 that terminate on the foil. This is known as the stagnation streamline and it is assumed that it comes to rest at the surface thus converting all of its kinetic energy into pressure. From equation 3.5 and 3.6 it can also be found that here the maximum pressure is achieved as the velocity (V) becomes zero. Thus $C_{Pmax} = 1$ where $p = C = p_\infty + q_\infty$ (21).

The difference in pressure between the two sides of a sail is referred to as $\triangle C_P$, for the windward pressure minus the leeward. The minimum leeward C_P from past experiments was found to be around -3, therefore the approximate maximum $\triangle C_P = \pm 4$ (7).

3.1.3 Flow Phenomena Affecting the Pressure Field

The previous section discussed how a pressure difference is created. This section discusses how this pressure distribution behaves and why.

There is a boundary layer around any external surface with a fluid flowing over it due to viscosity, where the flow velocity is less than the free-stream velocity far from the surface. The velocity is zero at the surface but as one moves perpendicularly away the velocity *recovers*. Figure 3-7A shows a classic example of this. The boundary layer is extremely thin and can almost be neglected when calculating the pressure distribution, that is until separation occurs (19).

When flow moves from a high pressure to a low pressure it is known as a favourable pressure gradient where separation of the flow is impossible. However when the flow moves from a low pressure to a high pressure, known as an adverse pressure gradient, the recovery of the velocity profile begins to slow down as can be seen by the inflection point in Figure 3-7B. If the gradient becomes too high then the flow will eventually separate and the flow will reverse, as seen in Figure 3-7C (22).

As mentioned earlier, the flow around a sail is disturbed by a number of elements such as the mast or the forestay which creates excessive adverse pressure gradients. Figure 3-8 shows a typical

pressure distribution over a head- and mainsail operating together. Below that the phenomena that affect this distribution have been illustrated. It is clear that the leeward side low pressure contributes the most to the pressure differences that creates lift. It is also more sensitive to separation.

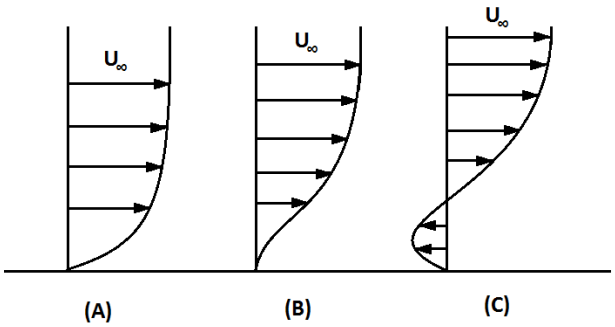

Figure 3-7: The boundary layer under various pressure gradients:

(A**) favourable (B) adverse (C) excessive adverse**

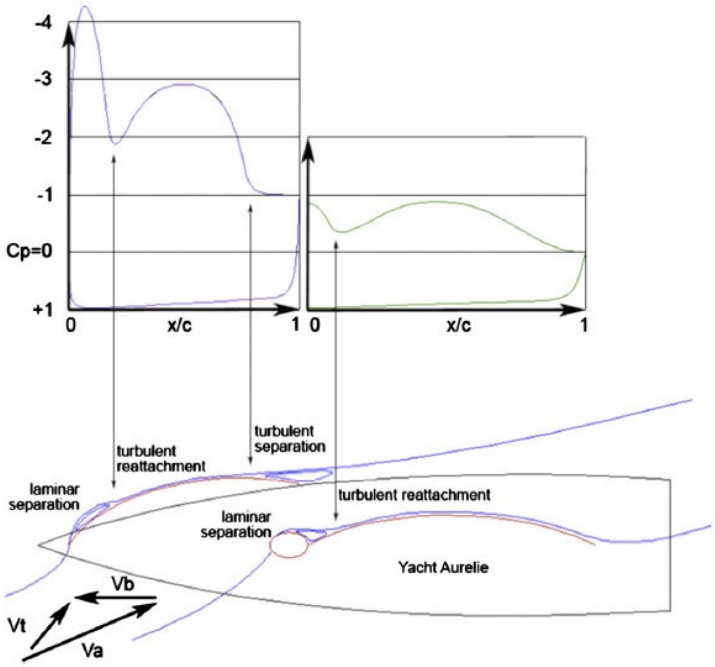

Figure 3-8: Pressure distributions over a main and headsail (7)

The stagnation streamlines shown in Figure 3-9 are enough to explain the interaction between the main- and headsail. As the distance, or *gap*, between the two sails is reduced the streamlines are deviated to windward, especially on the headsail, and also the flow rate over the leeward side of the mainsail is reduced. This phenomenon is known as *upwash*. The interaction between the sails has negative and positive attributes but overall the product is improved performance, and not just due to the increase in sail area (19).

- Effects on the mainsail
  - The oncoming flow deviates less towards the leeside and the stagnation point moves closer to the leading edge (*downwash*). This reduces the pressure gradients and therefore reduces the risk of separation.

- Effects on the headsail
  - The AoA and the amount of flow on the leeward side are increased and therefore the sail can produce more power.
  - The flow velocity is also increased on the leeward side which improves the efficiency and reduces the risk of stall.

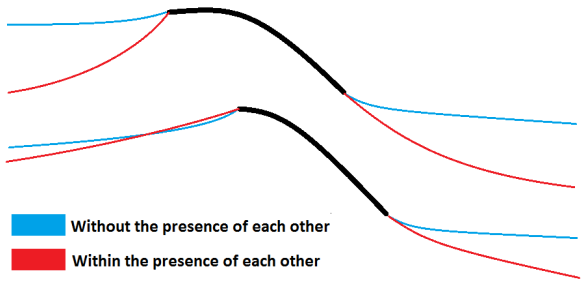

Figure 3-9: Stagnation streamlines on the main- and headsail

The flow off the trailing edge of the headsail may also impinge on the leeward side of the main. This can create a high pressure where the headsail overlaps the main. It is very noticeable where the mainsail takes on an *S* shape. This is known as back-winding.

As a sail has a finite length and a pressure difference between the two sides there is a flow at the head and foot between these two sides, from the high to low pressure. This circulation creates tip vortices and reduces the efficiency of the sail through loss of energy. This reduction is called induced drag (19). As a result of this cross-flow it can be assumed that the pressure difference across the sails approach zero towards the head or foot. Exactly how quickly and over what distance this occurs is not known at present. It was therefore difficult to incorporate into this work.

3.1.4 Forces and Moments Generated by the Sails and Rig

The resultant force from a foil for a given application generally has a component that does positive or useful work and another that acts in an undesired direction. How this force is resolved into these components depends on the application. Lift and drag are the components resolved into the perpendicular and parallel directions relative to the oncoming flow, or *apparent wind*, whereas drive and side force are relative to the direction of motion (5). In the case of a yacht the latter is more relevant, which can be seen graphically in Figure 3-10.

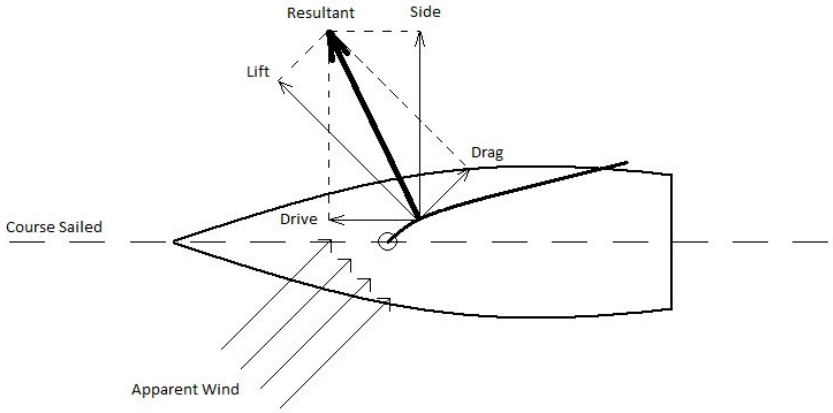

Figure 3-10: Force components on a sail

Depending on the hydrodynamics of the boat used the performance tends to deteriorate rapidly beyond a certain heel angle. Depowering the sails so as to reduce the heel angle may result in a faster boat speed, even if the drive force is also reduced. Depowering can be achieved by twisting, flattening or reefing the sails (16).

It is possible that for two identical boats, one with their sail trimmed to the maximum lift while the other has theirs slightly eased, that the latter will have a larger drive force and smaller side force resulting in a smaller heeling moment. This is the case when the latter's resultant force points more into the direction of motion due to the easing of the sail (5). This observation was confirmed by Viola and Flay (7).

These points highlight the relevance of being able to measure the drive force and heeling moment directly on a set of sails while sailing.

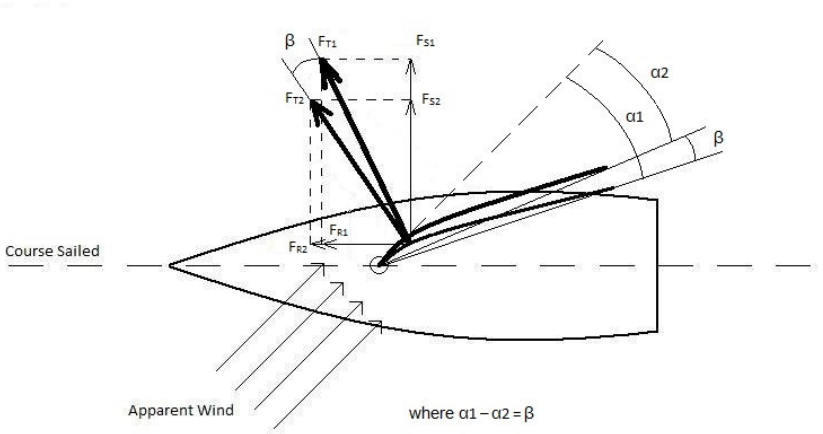

Figure 3-11: Change in force components due to sail trim

Below in Figure 3-12 the forces and moments produced by the sails of a yacht and the sign conventions used for them in this paper are shown. Take note that these forces are named differently to the boat motions due to waves. For example the translation in the X direction would then be called surge. The moments however have been labelled the same but these are relatively

steady moments that along with the hydrostatic and –dynamic behaviour of the yacht would determine the steady heel, trim and leeway angles.

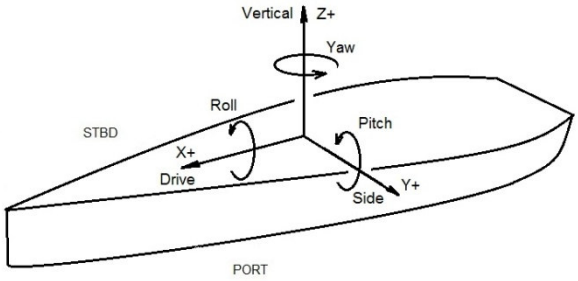

Figure 3-12: Forces and moments created by the sails

The origin of the coordinate system is at the aft base of the mast. The moments are positive in the directions according to the *right-hand rule* where if one points their thumb in the direction of the positive axis then the fingers on that hand point in the positive moment direction.

The aerodynamic force (F_A) creates the moment that heels the boat over. There is also a contribution from the hydrodynamic forces (F_H) and these moments are balanced by the gravitational and buoyant forces. F_A and F_H are distributed loads but their resultants can be assumed to act through singular points which are approximated by the geometrical centres of the sails and the underwater body, known as the *Centre of Effort* (CE) and *Centre of Lateral Resistance* (CLR) respectively. This approximation is used for simplicity as these points will migrate depending on the sails' trim or the boat's attitude (19). To better understand the force balance that occurs in heel refer to Figure 3-13. This is highly simplified 2D case which does not include the force components in the x direction. The positive direction of the moment is indicated around the *centre of gravity* (CG). The buoyancy force acts through the *centre of buoyancy* (CB).

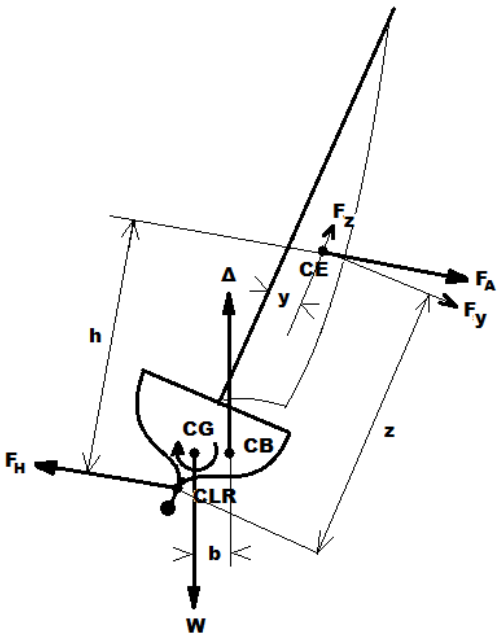

Figure 3-13: The heeling force balance

The heeling moment (HM) calculated around the CLR is:

$$HM = F_A.h \tag{3.7}$$

This is balanced by the righting moment (RM) taken around the CG:

$$RM = \Delta.b \tag{3.8}$$

F_A can be resolved into the components acting parallel (F_z) and perpendicular (F_y) to the mast. The HM can then be calculated using the horizontal and vertical distances to the CLR as moment arms.

$$HM = -F_z.y - F_y.z \tag{3.9}$$

Note the sign convention for F_y is negative to starboard and therefore the contribution to the moment is positive in this direction.

If the forces and location of many discrete points are known for i points at j heights then HM can be approximated by:

$$HM = \sum_i \sum_j (-F_{z\,ij}.y_{ij} - F_{y\,ij}.x_{ij}) \tag{3.10}$$

The structures that make it possible for a boat to carry its sails, such as the mast, stays and even the boat itself, do not generate drive themselves however they do generate a force. This drag force, known as *windage*, generally slows the boat down and heels it over more. When measuring the forces in a wind tunnel using a force balance or simulating the boat speed in a VPP these forces need to be accounted for. A common method for testing windage in a wind tunnel is to remove the sails and measure the forces of the structure independently. This gives a reasonable prediction, however it should be noted that the air flow is drastically changed when the sails are removed. Richards et al. (23) conducted a study of how much the windage measurements were affected by this and found that the force in the x direction was reduced by as much as 2/3 and the force in the y direction increased by as much as 1.7 times.

Forces and moments are expressed in non-dimensional coefficients in order to compare results between different tests conducted at different wind speeds or with different sails thus making scaling of the results simple.

Force coefficient:

$$C_F = \frac{F}{qA_{ref}} \tag{3.11}$$

Moment coefficient:

$$C_M = \frac{M}{qA_{ref}{}^{1.5}} \tag{3.12}$$

where F is the force, M is the moment, q is the dynamic pressure upstream and A_{ref} is a reference area. The reference area can be the actual surface area of the sails, which is useful if skin friction or viscous stress is being assessed, or it can be the planform area of the sails. This is can be calculated using the sail area formulas from section 3.1.1.

This is the area used in this paper. For C_M a reference dimension is needed, such as the mast length; however this does not take into account the extra area of a square top rig compared to a triangular mainsail. Thus $A_{ref}^{0.5}$ is used as the reference moment arm (16).

3.2 Difficulties in Measuring Pressure

There are numerous difficulties in measuring pressures, especially at full-scale. The following sections detail a few of these issues.

3.2.1 Issues due to Measuring Equipment

The YRU has developed through various projects a sound understanding when it comes to measuring the pressure on sails. In this section some of the issues that had to be solved are discussed.

A transducer can either have one side connected to the point of interest and the other connected to a reference pressure or it can read a differential pressure by connecting one side of the transducer to the suction and the other to the pressure side of the sail. A diaphragm inside the transducer is deflected according to the pressure difference. This is outputted as a voltage signal; the greater the deflection the greater the voltage. Generally this analogue signal needs to be converted to a digital signal by an analogue-to-digital (A/D) converter.

In a dynamic system the pressures fluctuate constantly, as discussed in the following section 3.2.2. If the dynamic response is of interest then the tube length connecting the pressure tap to the transducer has a significant influence; the longer the tube the longer the response time. This tends to attenuate the peaks of the signal. However when a time-averaged recording is taken the mean will not be affected significantly as the reduction in both the maximum and minimum peaks will negate this influence (11).

Another significant issue is that of the geometry of the tapping. Some research had been carried out by Flay and Millar (11) into how the taps themselves affect the pressure readings. It was seen that pressures were measured lower than a reference flush mounted tap. This may be due to the flow accelerating over the tap and thus reducing the pressure locally. Even in the case of a flush mounted tap, where a PVC tube is trimmed to be flush with the surface, it can often still have a lip after trimming. This lip could create a local separation of the flow over the tapping and reduce the reading. Any proposed surface mounted tap should therefore be tested for its effect on the pressure reading.

3.2.2 Fluctuations in Readings due to Pressure Environment

To illustrate how unsteady the environment is the following observations can be made. Assuming a wind velocity of 3 m/s at model-scale or 10 m/s at full-scale and a $\triangle C_P$ of 4 then the range of pressures to be measured would be ±20 Pa or ±240 Pa respectively. This pressure range is relatively small for the following fluctuations that the environment experiences.

The atmospheric pressure at sea-level can vary between 95,000 – 105,000 Pa due to the main weather systems and shifts over time can be as high as 8 Pa/min with a rapidly approaching low or high pressure. This can significantly affect the pressures measured throughout a day of testing or even between two consecutive runs. Ideally the atmospheric pressure should be recorded during the sampling period as a reference. From equation 3.5 it can be seen that the dynamic pressure is

influenced by the square of the wind velocity. Therefore even a 10% increase in a 10 m/s wind can result in a pressure shift of 12.6 Pa.

The atmospheric pressure also varies in height at around 12.5 Pa/m. This can be significant even at model-scale. The difference in height should be noted between the measurement point and the reference point or alternatively a differential pressure could be recorded, i.e. the difference between both sides of the sail measured on one transducer, as these shifts will then be cancelled out (24).

3.2.3 Difficulties to Zero the System at Full-Scale

Electronic measuring systems have a tendency to drift in the readings. This can cause an error in the readings if it is not accounted for. This applies to the pressure measuring system at both model- and full-scale as well as the force balance in the wind tunnel. In the wind tunnel it is easy to switch the wind off and allow the air to settle so that all the pressure transducers are measuring the same pressure and thus has no deflection of the diaphragm. This allows the measurement equipment to be brought back to a zero reading.

However at full-scale it obviously is not possible to switch off the wind. This poses a serious challenge. In order to apply same pressure on both sides of the transducer some methods were proposed including luffing, furling or dropping the sail.

Luffing is the term used when the sails are eased or the boat heads too directly into the wind so that the sails are left to flap in the wind. No drive is created and it can be assumed that over a period that the pressures will be equal on both sides. This however is dependent on how accurately the helmsman can steer the boat; alternatively he may steer the boat through a zigzag over the direction of the wind so that each side of the sail creates a positive and a negative pressure for equal periods during the zeroing. Another concern is when the sails flap in the wind or *flog* it could potentially damage or dislodge the pressure sensors.

Furling of both the sails is possible on boats fitted with furlers. This is when the sail is rolled up around the forestay for the headsail or inside the boom or mast for the main. Usually the sail is furled tightly but this would not be possible as it would damage or dislodge the sensors. By sailing downwind when furling it is possible to furl the sail loosely but there is no guarantee that it still will not be damaged. Also the trailing edge sensors will likely still be exposed. On the test boat there is no furling mechanism for the mainsail.

The last option, and the most viable, is to drop the sails. The headsail can then be placed into a bag and the mainsail under its cover. Care should be taken to close most gaps in the covers but provided that the pressure inside is reasonably constant inside then a zero can be achieved.

3.3 Theory behind VSPARS

Visualisation of Sail Position And Rig Shape (VSPARS) was used to measure the shape of the sails. It was developed at the YRU by David Le Pelley and Owen Modral and was designed to be a simple system that could handle large perspective effects and sails with large curvatures using off-the-shelf cameras. The system uses one deck-mounted camera for the headsail and one camera for each tack

of the mainsail. It is possible to record in 3D the global position of a specific number of horizontal stripes on the sail, which are marked out in neon orange tape to allow for easy recognition.

The user must input the 3D position of the camera relative to a datum, usually on the centreline at the base of the aft surface of the mast, the length and height along the luff of each stripe and lastly the camera angle. This angle then is used to determine the twist of the stripes in the 3D space. Once everything is setup and running the luff positions of the stripes with the sails under no load need to be manually defined within the image of the sail. This is then used as the base position of the mast and forestay; any deviation from this is then calculated and used to determine the translation of the stripes and the rig deflection.

The system is then ready to capture the sails. The first step of the program is to pass up and down a user defined line that crosses all the stripes and look for pixels of the specified colour. A filter may be necessary to improve this step. Once found the program then sweeps perpendicular to these points and defines the bottom edge of the stripe. This process is aided by user defined settings such as *trim*, which defines how steep the gradient of the curvature can be, or *jump*, which allows the search function to jump an obstruction like a drop of water on the lens or a stay. The pixels of the stripe are then defined in coordinates of the picture.

The luff and the leech are identified and the distance of each from the camera is calculated using the known heights and the calculated twist angle. The chord line is now defined. Using the camera position an Euler rotation is performed so that the camera is numerically placed directly below this line. This allows the stripe and its depth to be seen in 2D. A length is then guessed for the chord and offsets are estimated from the chord to the stripe. The length of the stripe is calculated using a known relationship of millimetre to pixel at varying heights and then compared to the known stripe length. Iterations are performed until they match.

The offsets are then applied to the chord in the global 3D space before the rotation, whereby the coordinates in this space can be calculated. The output is in the form of x, y and z coordinates for each stripe. Other data of the stripes is also calculated and given, such as twist, entry and exit angles (8).

3.4 Full-Scale vs. Model-Scale or Numerical Testing

In a perfect world when designing a new sail the sail would be manufactured and flown by one of two identical boats sailing alongside in a constant breeze. Immediately it would be obvious which design was more suited for the heading chosen. Failing that a VPP is used to predict which will be faster. One of the inputs for these is the principal force components of the sails.

The two most common tools used to find these forces are CFD and wind tunnel testing. Both however have significant drawbacks. CFD is extremely useful for testing of upwind sails where the flow is mostly attached, therefore simple potential flow solvers can be used effectively. Downwind sails on the other hand can be fully separated along a chord; thereby needing more powerful RANSE based solvers which take viscous effects into account. These solvers require much more computing power, take longer to run and need to be validated which makes them extremely expensive. Furthermore modelling a soft sail, where the code is able to predict the flying shape of the sail, makes the process much longer requiring many iterations before the shape is found.

Wind tunnel testing is able to test all kinds of sails in constant, easily recreated conditions and using sail cloth that behave much like the full-scale product. However it is unknown how accurate these results are when scaled to the full dimensions. Scale factors are often not satisfied as getting the sail to fly in the correct shape is of utmost importance. Results comparing two sails are deemed reliable in the qualitative sense but the difference between model- and full-scale is still not understood well enough (16).

3.4.1 Details of the Twisted Flow Wind Tunnel (TFWT)

The TFWT, first built in 1995, was the first wind tunnel purpose built for testing of yacht sails. The feature that made this tunnel famous was the ability to change the flow direction at different heights using vertically twist vanes. This is necessary to accurately recreate the conditions experienced by an actual yacht sailing by the power of the wind. As mentioned in section 3.1.3 all surfaces with a fluid flowing over it has a boundary layer; this is also the case for the earth. This creates a velocity gradient in the vertical direction. When a yacht is moving forward the wind that it experiences is known as the *apparent* wind, as opposed to the *true* wind. This is the resultant velocity between the true wind and the boat's speed. Because of the atmospheric boundary layer the direction of the apparent wind as well as the speed changes vertically. This effect is most notable when sailing downwind (19).

The tunnel itself is an open-circuit wind tunnel 3.5 m high and 7 m wide. Two 46 kW fans with a diameter of three metres each and four blades suck air into the tunnel. Stators then remove some of the rotation applied to the air before it passes through a honeycomb air-straightener. A fine mesh further removes turbulence from the air. The following section of the tunnel can be used to create the vertical velocity gradient by either adding roughness elements to the floor or by placing beams across the width. The twisted vanes are the last stage before the open test platform. The yacht models are placed into frame that sits in a trough filled with water to prevent air flowing below the yacht. The frame is connected below the platform to a six-component force balance capable of measuring the three principal forces and moments. To keep blockage effect to a minimum the models used are limited to roughly 2 m high. More details can be found in (16).

3.5 Curve Fitting Techniques

One of the major parts of this work was to recreate the sails' full shape and pressure distribution from discrete points. In order to 'fill the gaps', especially at the extremities, an interpolation of the data points was necessary. Please note that extrapolations may also be referred to as interpolations when referring to them collectively.

3.5.1 Interpolation

MATLAB has a built-in function for interpolations. It is easy to select either a linear or a spline function for the curve but one has to be careful to use these appropriately. In Figure 3-14 one can see that the spline function recreates the peak very well but the curve veers off significantly towards the trailing edge. This is only one example but it is clear that without control over the degree of the spline curve and good monitoring checks inherent in the process the desired curves could become heavily distorted. Although the linear scheme also has it draw backs, it is much more predictable. It may not be able to recreate the smooth curves that the spline scheme can but neither will it create local peaks or troughs where there should not be any.

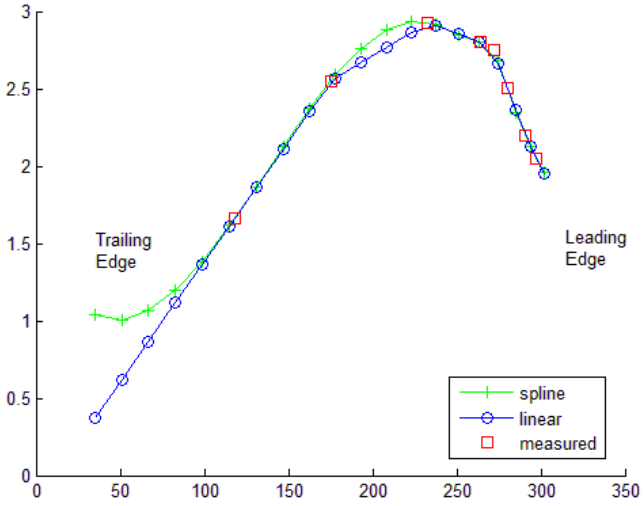

Figure 3-14: Comparison of different interpolation schemes used for a typical chordwise pressure distribution

3.5.2 Least Squares

Least squares curve fitting is also a useful curve fitting technique in cases where it is assumed that there is some deviation in the data points from the actual curve. It is able to find the best fit curve within a scatter of points by minimising the sum of the squares of the vertical distance between the curve and the data points. These are known as the residuals and can be seen in Figure 3-15.

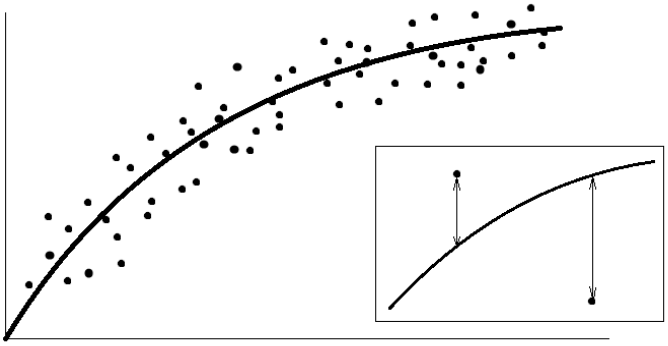

Figure 3-15: The "best" fit curve through a scatter of data points (inset: vertical offsets)

With this method one can then control the degree of the curve relatively easily but constant checks would be necessary to determine which degree works best for each curve. However some curves cannot be represented accurately at all using this method and for some applications it may be desirable for the curve to pass through the actual data points.

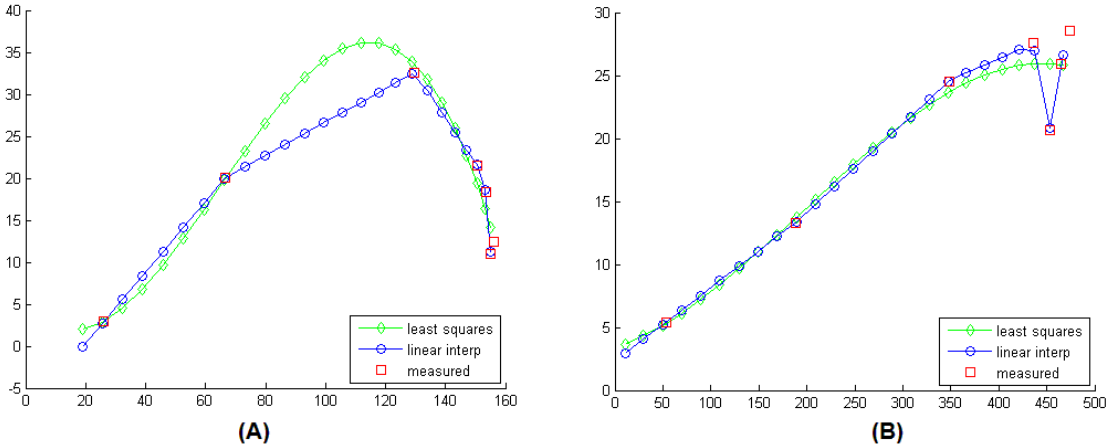

Figure 3-16: Two examples of a 3rd degree least squares curve fitted to a typical pressure distribution compared to a linear interpolation

In Figure 3-16A the least squares method arguably recreates the curve relatively accurately and captures a pressure peak that may have been missed by the sparse measurement points. However when considering Figure 3-16B it is clear that the curve has entirely missed the leading edge separation bubble although the rest of the curve fits the data points very well.

4 Pressure Integration over Sail Shapes

A code was developed using MathWorks® MATLAB to handle the output data from the pressure and shape measuring systems and to predict the forces and moments created by the sails. Firstly the code recreates the sails from the VSPARS coordinates. Then the discrete pressure measurements are extrapolated over the sail area in order to obtain a full distribution. Finally these pressures are multiplied by the normal vectors of a relevant area to find the force and then by moment arms to find the moments.

These steps are described in detail in the following section. Refer to Appendix 1 for the base code, Appendix 2 for some formulas and derivations used in the code and to the attached CD for the full program with data files.

4.1 Inputs for the Integration

Various inputs are required for the recreation of the sails and calculation of the forces. These are detailed in the following sections.

4.1.1 Shape Input

The data of interest from VSPARS is the x, y and z coordinates of each stripe which is used to recreate the sail shape. In order to recreate it as accurately as possible some additional information about the sail is required. A spreadsheet for each sail needs to be filled out so that the code can find this information when necessary. VSPARS also outputs data regarding each stripe such as camber and twist angle, which has not been used to recreate the shape but was useful in validating the code. An example of the data spreadsheet has been given in Table 4-1.

Table 4-1: Data sheet for code

st	NoSS	NoSP	l_h	l_f	z_h	z_f	clew	x_h	leech		
2	3	4	12	702	1880	11	NA	25	1855		
Pressure Data											
	Stripe B	Stripe D	Stripe F	Stripe H				Legend			
Height	300	700	1100	1500				st	Sail Type		
Length	573	439	299	148				NoSS	Number of Shape Stripes		
# of Taps	11	10	8	8				NoSP	Number of Pres. Stripes		
Arc%	0.03	0.04	0.05	0.09				l_h	Length of Head		
	0.05	0.10	0.09	0.17				l_f	Length of Foot		
	0.12	0.12	0.15	0.25				z_h	Height of Head		
	0.16	0.23	0.19	0.32				z_f	Height of Foot		
	0.25	0.29	0.22	0.41				clew	Position of Clew		
	0.32	0.39	0.34	0.52				x_h	Position of Head		
	0.37	0.51	0.54	0.72				leech	Length of Leech		
	0.48	0.64	0.72	0.92							
	0.59	0.78									
	0.79	0.91									
	0.90										

The recreation of different types of sails can vary, for instance the mainsail is constrained by the boom while the headsail is not. The first value, *Sail Type,* prompts the code to use different functions where necessary.

Number of Shape Stripes and *Pressure Stripes* are the number of horizontal coloured stripes or groups of pressure taps along the sail. This aids the extraction of the relevant data from the input files and the subsequent handling of the data within the code; in other words it tells the code how many times a loop needs to be run or how big an array is.

The *Length of Head* is the measured length of the head of the sail. Even in the case of the headsail it should not be assumed that it comes to a point at the head. It can be assumed for a square-top mainsail that the head does not hold any camber, i.e. the head can be assumed to be a straight edge. This length, along with the *Height of Head*, is used to define the head.

For the foot the extrapolated shape down to the Height of Foot may not necessarily be the correct length. The *Clew Position* for the main and the *Length of Leech* for the headsail along with the *Length of Foot* are used to trim and scale the foot. More detail on how this is done can be found in section 4.2.

4.1.2 Pressure Input

In the bottom left-hand block of Table 4-1 some required data about the pressure system is given. The height of the taps can be assumed to be constant along a chord. This height is then used in defining the measurement point on the sails along with the percentage of arc length along the section. The length of each section is used to calculate this, either directly in the spreadsheet or within the code. The number of taps per stripe is also required which the code uses to extract the correct corresponding data from the pressure input file.

The pressure data format for this work varied with each of the tests conducted. Ideally the pressures should be presented as a differential across a singular point on each side of the sail but this was not always possible. For the first test with the Semi-Rigid sails the pressures on either side were recorded simultaneously by separate transducers and presented in the same output file. It was then fairly straight forward for the code to calculate the differentials. For the core flute sails it was only possible to record pressures on one side of the sail at a time and with slightly varying dynamic pressure. Therefore the pressures were first reduced to a coefficient and the differentials were calculated directly in Excel before input into the code. For the full-scale test the pressures were recorded as differentials but were in an entirely different format as it was a totally new system. The output was recorded in bits and had to be converted to pressures within the code using a calibration and a zeros file.

4.1.3 User Input

In order for the code to run correctly there are a few still a few parameters that need to be set by the user. The code can be used to only generate sail shapes and therefore the pressure interpolation and force calculation must be switched on or off. The run numbers of interest need to be selected. This may be for an entire test, just one sweep within it or just one particular run. The resolution of the interpolation, i.e. how many points to use, also needs to be defined. The more points used will increase the accuracy, especially for the sail shape, but that will also decrease the speed of the code.

Finally the tack of the boat needs to be specified to aid the recreation of the head and foot so that they point in the right direction.

4.2 Sail Shape Generation

In order to be able to calculate the forces in the correct directions an accurate recreation of the shape was necessary. Using the output coordinates of the luminescent stripes placed on the sails from VSPARS and some measured data of the sail as well as a few assumptions it is then possible to do so. Furthermore, as VSPARS is a commercial package utilised by top racing teams from the America's Cup, Volvo Ocean Race and more, there may be interest in a code that can output a geometry file for use in CFD. This could be an important tool used to validate the design and manufacturing processes. The steps involved in this recreation are detailed in the following section

The function file 'extract_data3d' is called first. In here a shape file is read and the x, y and z coordinates for each stripe are extracted and isolated. Then for each stripe the coordinates are parametized by their arc length percentage. In other words the arc length from the leading edge to each point is calculated and divided by the total arc length. It is then possible to interpolate using the spline scheme to find the x and y coordinates for the user defined chordwise resolution. This scheme should be able to fit a fair curve for most sail shapes either with a 2^{nd} or 3^{rd} degree function depending if the sail clearly has an inflection point or not. This loop is carried out for each stripe for one sail at a time and independent matrices are outputted for the x, y and z coordinates for each sail. Each column in the matrix is thus one stripe starting with the lowest stripe in the first column. The result can be seen in Figure 4-1.

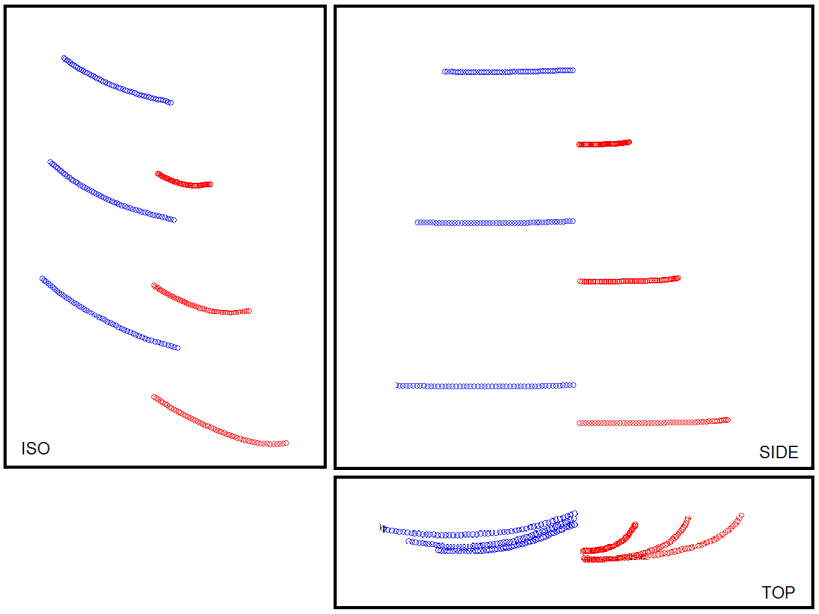

Figure 4-1: Stripes with user defined number of points

The next function file called on is 'get_head_foot'. This file extrapolates the measured stripes to find the head and the foot of the sails. The first step is to extrapolate the luff points to the foot and head. This then gives the shape of the mast. A spline function is used to capture the bend in the tip of the mast. For the head it is assumed that firstly it never comes to a single point and will always have

some length and secondly that it does not carry any camber; in other words the head is always a straight line. This has been seen from experience. The angle of twist is then calculated for each stripe from the luff and leech points and extrapolated. The head is then found using this angle and the measured length of the head. This step requires the user to define whether the yacht is sailing on port or starboard yacht so that the program knows which side to create the head.

The foot is created from the extrapolated luff and leech points plus a point from a predefined camber and draft location. A 2nd degree curve is fitted through these points. On a fair shaped sail, such as those used for the model tests, this step would not be required and all points along the stripes could be extrapolated down to this height, however, as will be seen, the full-scale sails had inflection points along the chord. Ideally the camber and draft should be extrapolated from the known stripes but due to time constraints this has not been implemented.

The above mentioned method to define the foot does not necessarily obtain the correct length of the foot and therefore a scaling of the length is necessary. The main is slightly simpler than the headsail as it can be assumed to be horizontal or constant height at the boom. Thus this is handled within this function file but the headsail is dealt with later. In order to scale the foot it needs to be centred at the origin and rotated by its twist angle so that the trailing edge is on the x axis. The x coordinates can then be scaled by the known clew position:

$$x_i^* = x_i * \left({clew}/{x_n}\right) \tag{4.1}$$

Now the clew is in the correct position but the arc length is still larger or smaller and therefore the Y coordinates are iteratively scaled by the measured length of the foot over the current length of the arc until the length of the arc equals the length of the foot. The foot is then rotated back to the correct twist angle and returned to the correct position of the tack.

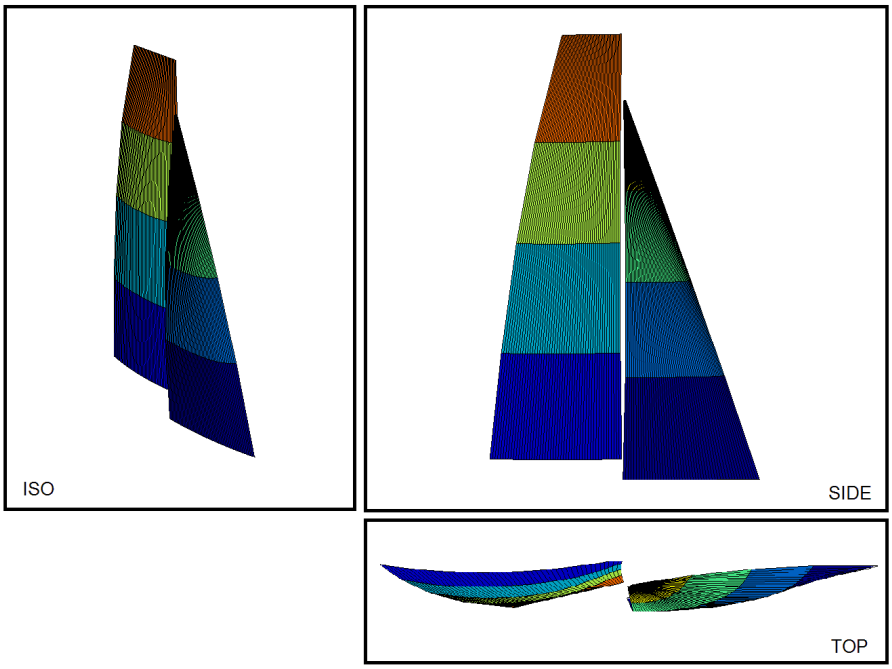

Figure 4-2: The basic sail shape extrapolated to the head and foot

The full sail is now represented by x, y and z matrices with the number of columns equal to the number of stripes on the sail plus one column for the head and one for the foot. At this point the full shape can be recreated but the surfaces are not well defined as the resolution is very poor, as shown in Figure 4-2. The next function file, 'resolution', increases the spanwise resolution by interpolating the x and y coordinates to the user defined resolution of the z coordinates. This again uses a spline function, otherwise the surface would maintain the linear shape of the measured stripes. At this stage the heights of the interpolated pressure points for the mainsail are found simply halfway between the shape points. The sails now have a much more natural shapeas seen in Figure 4-3 and the coordinate matrices now take the following form:

$$\begin{matrix} x_{11} & x_{21} & \cdots & x_{c1} \\ x_{12} & x_{22} & \cdots & x_{c2} \\ \vdots & \vdots & \ddots & \vdots \\ x_{1n} & x_{2n} & \cdots & x_{cn} \end{matrix}$$

where c is the user defined resolution and for $i = 1{:}n$ the subscript $1i$ is now the foot of the sail and ci is the head.

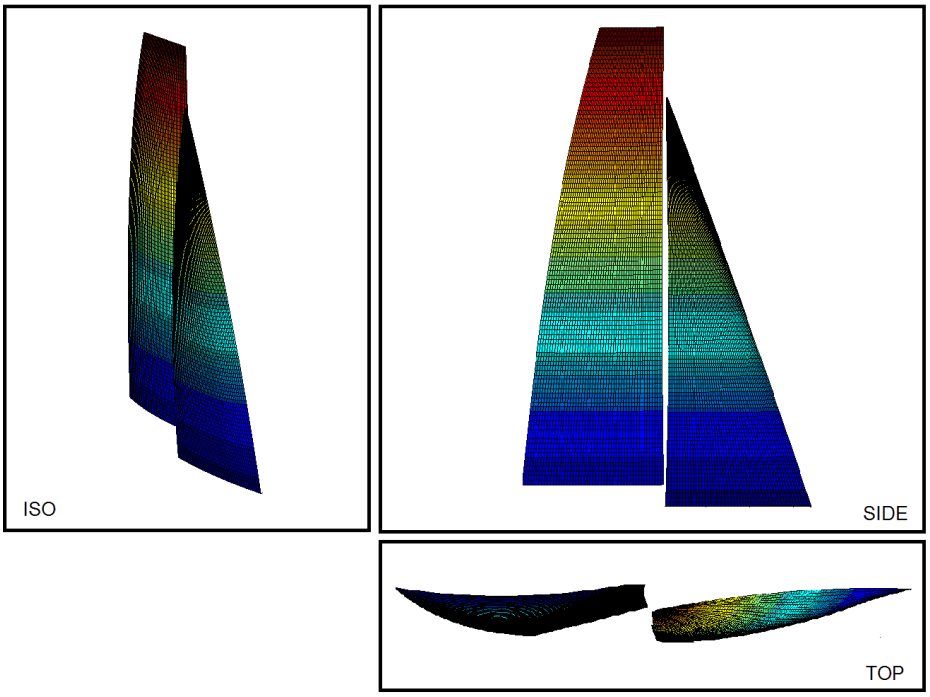

Figure 4-3: Sails generated at a high resolution

Finally the jib foot is dealt with in 'jib_foot'. It is not correct to assume that the jib's foot is horizontal so therefore a method had to be employed to find the correct position of the clew. This is very difficult to measure during testing, especially at full-scale, so a numerical method was developed. The leech length can be measured and so this was used to trim the sail by iteratively calculating the interpolated leech length starting from the head until the length was greater or equal to the measured value. For this operation the higher the spanwise resolution the smaller the error is, as the length will be defined as the next largest pre-existing height of the cells. This data point is then assumed to be the new clew position. The foot coordinates then need to be recalculated along the

line joining the tack and the new clew. First the Z coordinates are found by dividing the clew height by the number of points chordwise. Then for each point along the chord the height is found between it and the head. This height is then divided by the number of points spanwise to give the $\triangle Z$ between each cell. A new Z matrix can then be created using these values. The X and Y coordinates are then interpolated to these Z values. A linear function can be used here as the resolution is now high. As can be seen in Figure 4-4 the cells on the headsail have now been skewed slightly.

Once this is done the foot length can be scaled in the same fashion as for the main. In this case, as the shape matrix is already in the full resolution, the shape needs to be re-interpolated to remove the kink at the foot that has now been created. Five columns are isolated; one for the foot, one for the head and three roughly at the heights of the original stripes, although they have now been skewed. These five stripes are then used to interpolate the full sail shape once again.

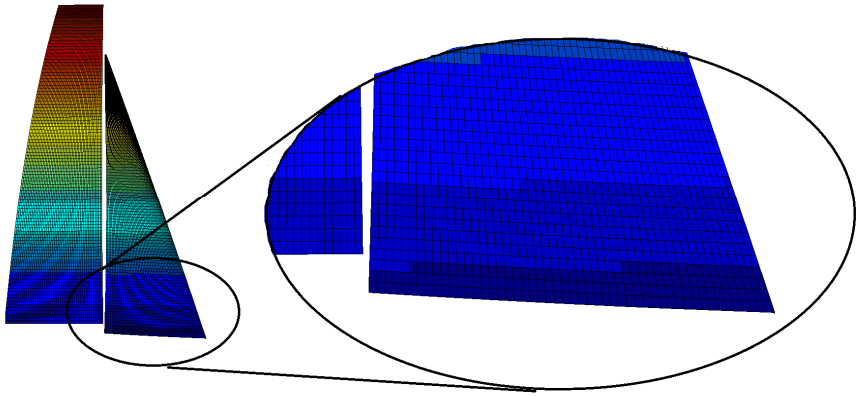

Figure 4-4: Picture showing the cut and skewed cells on the headsail

The desired pressure points are located in the middle of each cell. At this point only the heights are calculated as half the distance between the shape point heights. The sail geometry is now final and the coordinate matrices can be exported.

The final step before moving onto the pressure section is to calculate the normal vector and area for each cell on the sail. The cross product of the diagonals of each cell in fact gives the normal vector in x, y and z components with their respective magnitudes equal to twice the projected area of the cell for each direction. The proof of this theorem can be found in Appendix 2.

4.3 Pressure Integration over the Sail

Once the sail geometry has been defined the next stage is to take the discrete pressure measurements and interpolate them to find the complete pressure distribution over the sail. Once this is found the forces and moments can be found by multiplying the pressure at the centre of a cell by its area in the projected x, y and z directions.

'pressureA' extracts the data form the pressure file. It requires some data regarding the number of the taps which is found in Table 4-1. The pressure data, depending on the system, comes in different formats therefore this file requires some user manipulation before it will function correctly. Some of the variables that require different approaches are the file's format, i.e. text or excel spreadsheet, and if the data is divided into leeward and windward pressures or if it is already a set of differential

pressures. Provided that the pressure variable 'P' is outputted to the base code in the correct format then the code will function correctly. The only difference to this matrix compared to the shape matrix is that if there are different numbers of taps on different stripes then the matrix size will be defined by the stripe with the most taps. An example is given here in Table 4-2 of a data set for 4 stripes with 11 taps on the bottom and lower middle stripe, 10 on the upper middle and 6 on the top stripe. Zeros are used to fill the gaps.

Table 4-2: Example of a pressure matrix with varying number of taps

0.9028	0.8689	1.365	1.4802
1.0612	0.441	1.3851	1.3807
0.6513	0.5682	1.5497	1.4055
0.6611	0.8846	1.3902	1.3171
0.6968	1.1902	0.9668	0.9836
0.7464	1.3438	1.1203	0.7819
0.7929	1.3795	1.4367	0
0.7883	1.3655	1.4662	0
0.7836	1.2724	1.401	0
0.7541	1.1762	0.0818	0
0.3832	0.3336	0	0

Now 'pressresoA' is called to first map where on the sails the measurements are taken and then to interpolate the pressures over the sail at the desired resolution.

In the opposite way that the shape points needed to be parametized into arc length percentages, the pressure points are given in the arc length percentage or distance along the arc and their x and y coordinates need to be found. First coordinates at a known distribution need to be found at the height of the pressure measurements. A simple interpolation is done here between the x and z and then the y and z coordinate matrices to the height of the measurements. These coordinates are at the user defined chordwise resolution which is defined in arc length percentage. They can then be interpolated to the arc length percentages of the actual pressure taps. Now the pressure points are defined in x and y on the sail.

Same as for the distribution of pressure points in the spanwise direction, the chordwise distribution for the pressures are defined as the points halfway between the shape points. The x and y values need to be found for this distribution at the measured heights. This is another simple interpolation of the coordinates from the measured arc lengths to the desired chordwise ones.

It is possible now to interpolate the measured pressure values to these coordinates. The curves of the pressures vary quite significantly and are seldom regular, in other words cannot easily be fitted with a spline curve. These issues are mentioned in section3.5. So the pressures are interpolated linearly from the x and y values of where they were measured to the desired chordwise distribution.

These pressure values, as well as the x and y coordinates, are then interpolated along the spanwise direction. As mentioned in section 3.1.3 in theory there should be a decrease of the pressures towards the head and foot of a sail. However the form of this is not known and therefore cannot be

recreated accurately. It was also mentioned that it can be safely assumed that it occurs fairly rapidly over a short distance and thus the pressures have been left as is.

4.4 Force & Moment Calculation

With the normal vectors of each cell having the magnitude of twice their area, as explained in Appendix 2, and the interpolated pressures at the centre of each cell the forces can now be calculated simply in the x, y and z directions.

$$F_x = \sum p_{ij} * {}^{\boldsymbol{n}_{x\,ij}}/_{2} \tag{4.2}$$

This operation is done for all three directions and for both sails. The contribution from each sail is totalled together to find the resultant force acting on the yacht.

The Side Force reported in the results is in the plane of the force balance therefore it is a function of F_y, F_z and the heel angle (β).

$$F_{side} = F_y \cos\beta - F_z \sin\beta \tag{4.3}$$

To find the moment equation 3.10 is used. The heeling arm is longer than the distance from the data points to the datum and so this needs to be accounted for.

4.5 Verification & Validation

The main purpose of the model testing that is covered in detail in following chapters was to validate the written code. The results for the pressure integration of these tests are covered in their respective sections, but here other results and checks are presented to verify that the code was functioning as desired.

4.5.1 Sail Area Calculation

The theorem that the cross product of the two diagonals of a quadrilateral equals the normal in the x, y and z directions with their magnitudes equal to twice the projected area in that direction was verified by calculating the projected areas of each cell assuming they are parallelograms. The cells are in fact slightly tapered towards the head and therefore a mean base value b between the two sides was used. The difference of this comparison was ±0.9% thus proving the accuracy of the theorem. The area of a parallelogram is given in Figure 4-5 and the equation for its area is as follows:

$$A_{parellogram} = b.h \tag{4.3}$$

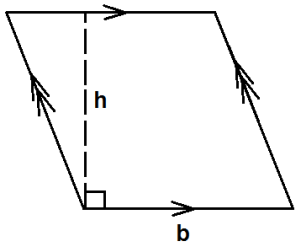

Figure 4-5: Area of a parallelogram

4.5.2 Sail Dimensions

For the mainsail the parameters of the foot length and clew position are scaled to the exact measured values.

The headsail's foot length is also scaled to the measured value but the leech length calculation is dependent on the spanwise resolution. For 50 points the leech length is larger than the measured value by 2% while for 100 points it is only 1% larger.

These scaling operations ensure that the sail has the correct shape and dimensions.

4.5.3 Integration of Uniform Pressure Field

A check was conducted using a uniform pressure distribution, i.e. the pressure distribution across all taps equal to 1 Pa. The result was used to check that the results for the drive and side forces were in fact the pressure multiplied by the area. The results confirmed this with the forces created equal to the projected area in the respective directions.

5 Model Test 1: Semi-Rigid Sails

The main objective of this work was to record pressure distributions and shapes of full-scale sails and to calculate their forces. In order to accomplish this with the required level of confidence the system had to be validated. This was done in the YRU's Twisted Flow Wind Tunnel (TFWT).

The first test was conducted on semi-rigid fibreglass upwind sails. They had been previously used at the YRU and were constructed using glass fibres and epoxy resin on a male mould milled by CNC. The reason for using semi-rigid sails instead of soft, flexible cloth sails was two-fold. Firstly the shape was fixed which allowed it to be easily measured. This helped the development of the sail shape recreation. Secondly the weight of the pressure taps would have distorted the flying shape of the sails as the cloth needs to be extremely light in the wind tunnel. This is highly important for them to function in the same way as full scale sails. Also this would have created an irregular pressure distribution and the shape would have been more complicated to recreate.

5.1 Test Setup: Semi-Rigid Sails

The model rig can be seen in Figure 5-1. This section goes into the details of the testing equipment used and the procedure followed during the test.

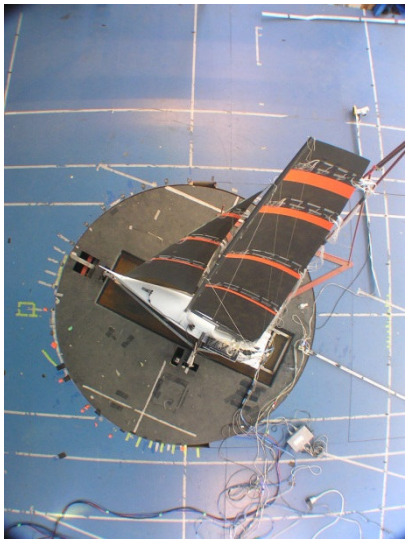

Figure 5-1: Overhead view of the Semi-Rigid test setup in the wind tunnel

5.1.1 Details of Semi-Rigid Sails and Pressure System

It was decided to use three VSPARS stripes on the headsail and four on the main as the headsail was significantly shorter. This is known as a fractional rig, i.e. the headsail terminates at a fraction of the mast height. The stripes were placed at 1/4, 1/2 and 3/4 luff heights on both sails and the fourth one for the main at 7/8. It was felt for the best accuracy in the pressure and shape integration that the pressure taps should be positioned as close to these stripes as possible. It was important to not obstruct the camera's view of the bottom edge of the stripes and therefore the taps were placed above them.

A brief study of the pressure distributions along the intended heights of the taps using a VLM was conducted in order to determine the ideal location of the pressure taps along the chord. By a process of elimination these distributions were recreated using the least number of taps. Figure 5-2

shows a typical recreation of a distribution along a chord using only 7 points. For the full list of pressure tap locations refer to Appendix 4.

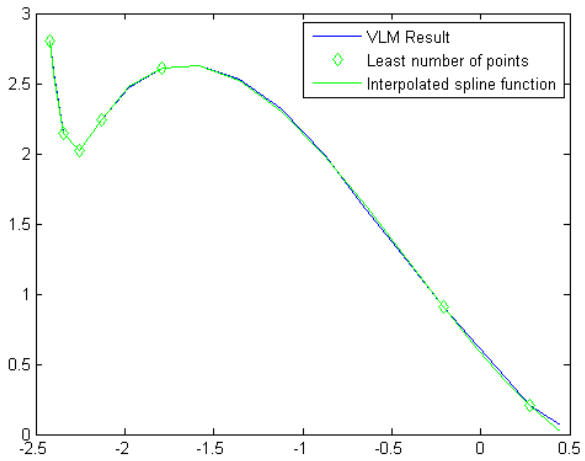

Figure 5-2: Graph showing the recreated pressure distribution along a chord

The same pressure data acquisition system and transducers were used as in (15), (7), (14) and (21). For more details refer to (15). For the pressure taps it was initially desired for them to be able to measure two points directly across the sail thereby a differential pressure could be measured. A concept for a block shaped tap to encase two tappings, one for windward and one for leeward, was proposed. A small hole could be made in the sail with the leeward hole of the tap aligned with it, allowing it to simultaneously measure both sides of the sail. These taps were fabricated and tested against a tap that had previously been used in Flay & Millar (11) at the YRU. These other taps will henceforth be referred to as the *coin* tap. Both taps and their measurements can be seen in Figure 5-3 and Figure 5-4. The results of this test can be found in Appendix 3. Both taps saw a reduced pressure compared to a reference, flush mounted tap. The coin tap's reading was 14% less while the drop was twice as large for the block tap.

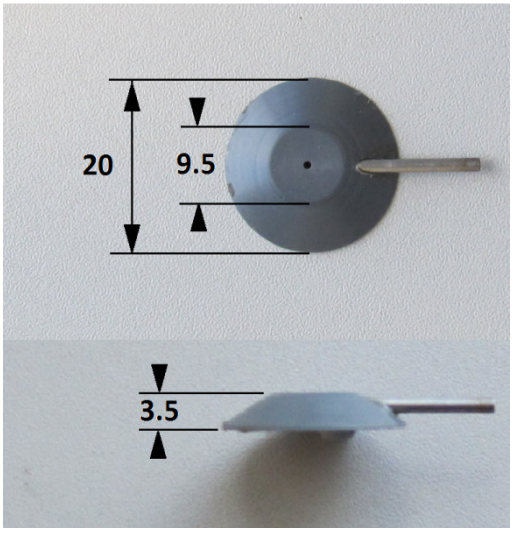

Figure 5-3: Coin tap (dimensions in mm)

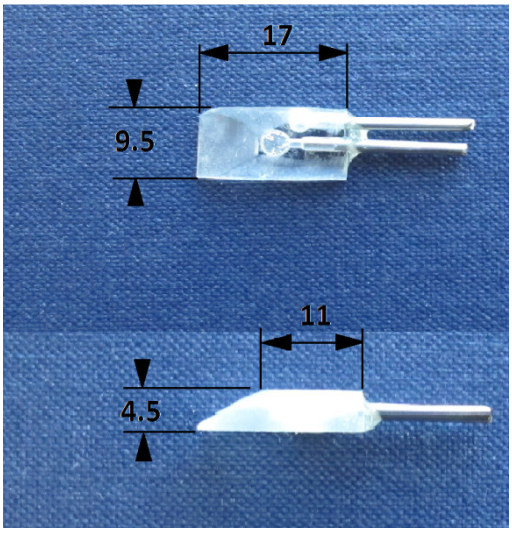

Figure 5-4: Block tap (dimensions in mm)

Following this result it was decided rule out the block tap completely and to use flush mounted PVC taps for the more critical, leeward side and the coin taps for the windward side where the flow is less sensitive to disturbances. Unfortunately the size of the coin tap made it impossible to place the tappings exactly where the VLM study dictated or the leeward and windward tappings on the same chord, especially at the leading edge. Therefore the leeward taps were placed at the intended heights and positions while the windward taps, which see less variation or steep gradients, were placed 10 mm below and when they could not fit in the chordwise direction they were staggered, alternating 10 mm above and below the leeward line. This can be seen in Figure 5-5. For the calculations they were assumed to be at the intended positions. The flush mounted taps were glued in place using a quick curing epoxy while the coin taps were stuck down using double-sided tape.

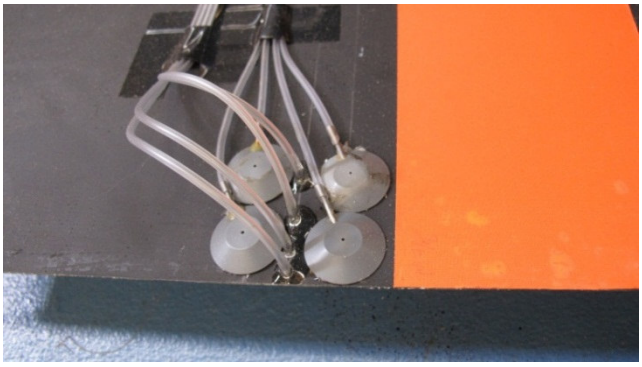

Figure 5-5: Picture of taps on the top stripe at the leading edge of the mainsail

In Figure 5-5 it can also be seen how the PVC tubing is lead aft above the locations of the taps. They continue this way till the trailing edge. For the headsail the tubing was then attached to the shrouds and lead down to the transducer box on the deck, while for the mainsail the tubes were lead onto an independent stand and then back onto the transducers. This can be seen in Figure 5-6. In order to keep the sail's surface as clean or unobstructed as possible this was deemed the best option although the system was then technically not floating free on the force balance. The tubes were given enough slack to minimise this interference.

Figure 5-6: Picture of mainsail, PVC tubing and stand from astern

5.1.2 Test Procedure for the Semi-Rigid Sails

Tests were conducted at 20° heel and an AWA of 25°. Three sweeps of sail trims were tested, meaning the sails were trimmed as tight as possible and then eased out in small increments. The three sweeps were for the mainsail only, the jib only and then both simultaneously, referred to here as the combined sweep. Including the initial trim eight positions were tested for each sweep. The main, jib and combined sweeps are referred to as MS, JS and CS respectively with the suffix 0 indicating the initial trim position and 1, 2, 3… for every trim thereafter.

The YRU have conducted windage tests on their models and have the data readily available. However in this case the influence of the PVC tubing could not be ignored. In order to find the windage of the tubes the test setup had to be recreated without the presence of the sails. Spare tubing was cut, bundled and placed in roughly the same positions and at the same attachment points. The tubes on the mainsail were attached at the same height but directly onto the mast.

Twisting the wind is considered unnecessary for low AWAs as the effects are insignificant. Furthermore the exact simulation of full-scale was unnecessary to validate the system. Therefore no vanes were used for this test.

5.2 Results: Semi-Rigid Sails

The following section presents the most interesting data collected from the test. For a more comprehensive collection of the force and moment results refer to Appendix 5 but for all the test data please refer to the attached CD.

5.2.1 Semi-Rigid: Recorded Pressures

As the pressures were recorded separately for the leeward and windward sides the pressure distributions could be compared to the theory in 3.1.3 and particularly Figure 3-8. For the 1/2 luff height Figure 5-7 clearly shows the leading edge separation and reattachment on the headsail as well as the mast separation and reattachment on the mainsail. The headsail exhibits a small amount of trailing edge separation as the C_P value does not return to zero, whereas the mainsail remains fully attached to the trailing edge.

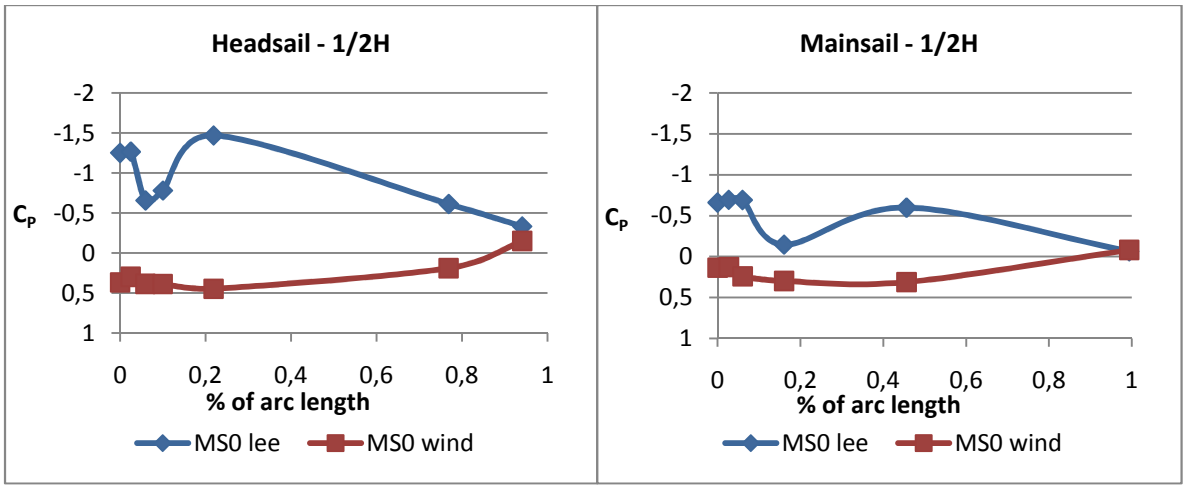

Figure 5-7: Figures of pressure distribution around the Semi-Rigid sails

The sweeping of the sails also exhibited trends that were expected. Figure 5-8 and Figure 5-9 show the 1/4 luff heights on the head and mainsail respectively as the headsail is eased out from the tightest trim possible, trim position 0, to fully out, trim position 7.

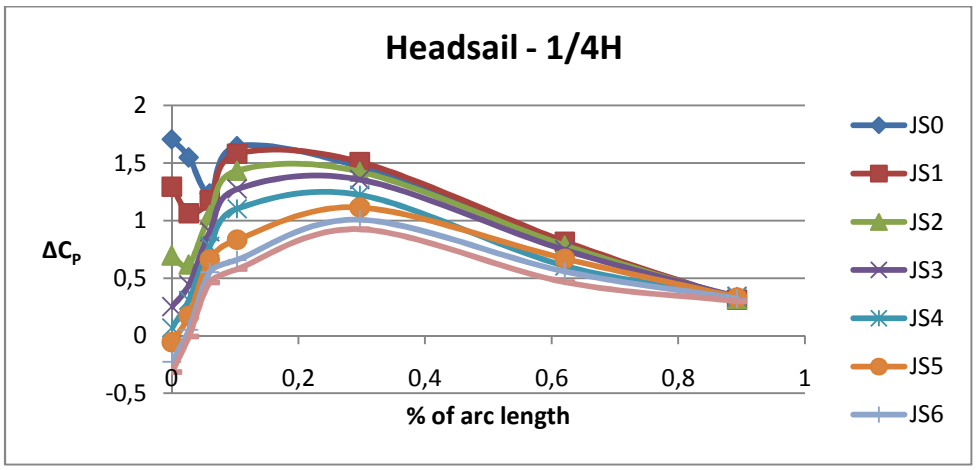

Figure 5-8: Differential pressure reading on Semi-Rigid headsail for the sweep of the headsail

For the headsail:

- For the first change in trim from JS0 to JS1 the separation bubble is decreased but from 20% along the arc the pressure is slightly higher. This could be due to increased upwash as the mainsail loading is increased.
- The following trims see a reduction in the pressure distribution. This is probably due to the decrease in AoA.
- For the leading edge separation bubble it can be seen that as the sail is eased the bubble reduces in size until the sail no longer separates at the leading edge. This occurs between trim position 2 and 3
- After trim position 5 the sail begins to see a positive pressure on the leeward side resulting in a negative $\triangle C_P$. As the sails are Semi-Rigid they did not collapse or deform as a normal cloth sail would and still managed to provide a drive force, but essentially these trim positions are of no interest to normal sailing conditions.

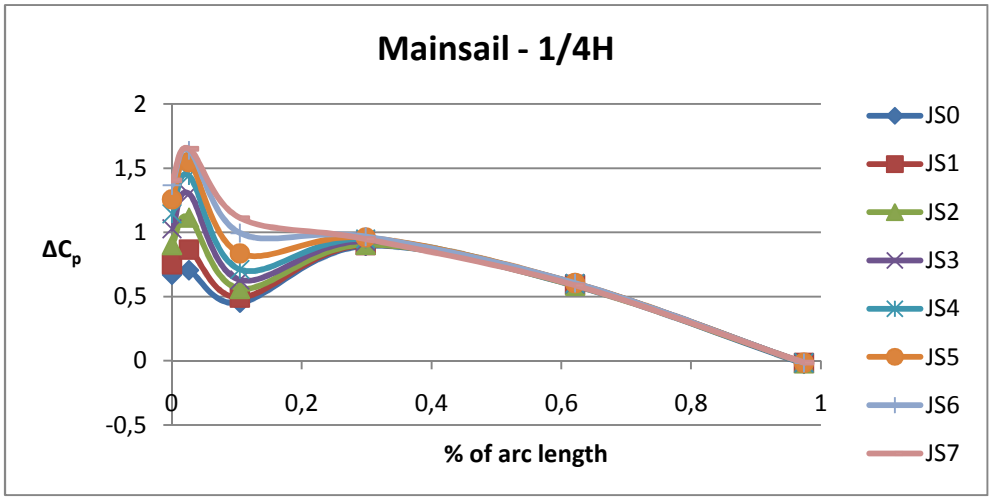

Figure 5-9: Differential pressure reading on Semi-Rigid mainsail for the sweep of the headsail

For the mainsail:

- The high pressure field at the trailing edge of the headsail has a negative effect on the overlap region of the mainsail. As the headsail is eased out the gap is increased and these negative effects are reduced, thus increasing the performance of the mainsail as can be seen in Figure 5-9.

The pressure contour plots for the first run in the jib sweep are shown in Figure 5-10 and Figure 5-11. The contour plots of similar sails using a VLM, developed by Julien Pilate at the YRU, have also been presented in Figure 5-12 and Figure 5-13. Note that the VLM sails are on starboard tack while the Semi-Rigid sails are on port.

Comparing the contours from the VLM to the Semi-Rigid sails there are some marked differences. There appears to be a large trough close to the leading edge of the Semi-Rigid mainsail which is not seen in the VLM, while large pressure peaks at the leading edge toward the head of the VLM sails is not seen on the Semi-Rigid sails. The pressure at the head of the Semi-Rigid headsail starts low and builds to the peak aft of halfway along the chord. This is a very different trend than seen in the VLM.

Generally the pressure distributions and the behaviour through the sweeps looked reasonable across most of the sail except at 3/4H on the headsail. This is where the density of pressure taps was highest and is the most likely location where the flow would have been disturbed.

The results from the VLM are still only theoretical and it has been mentioned that numerical methods such as this cannot capture separation of the flow. Also this method does not include the mast on the mainsail which could account for the lack of a pressure peak on the main. The results from the VLM can show roughly what to expect but cannot be used definitively.

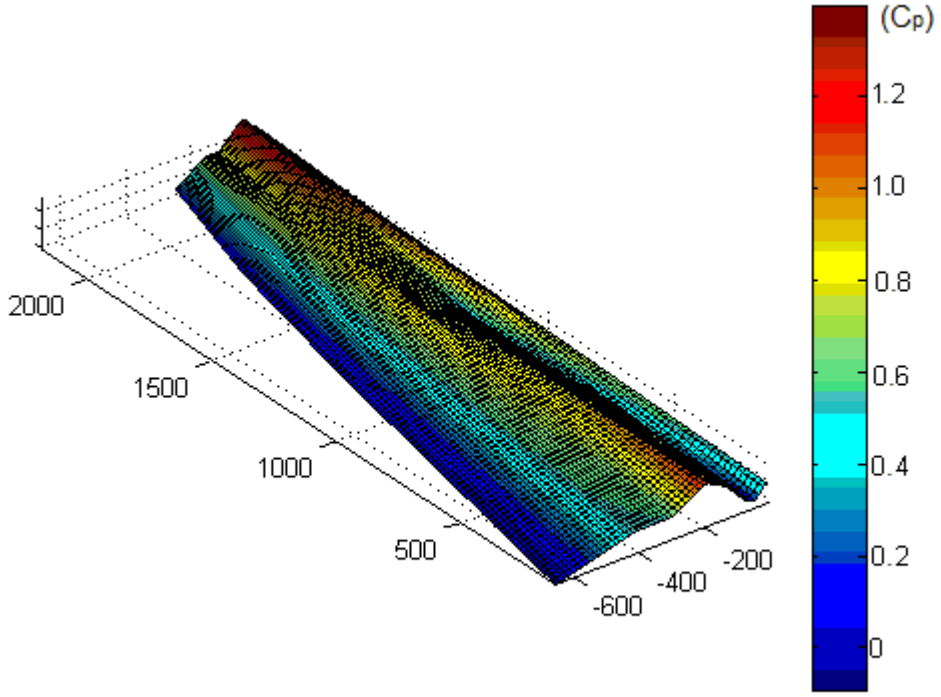

Figure 5-10: Pressure contour plot of Semi-Rigid mainsail for JS0

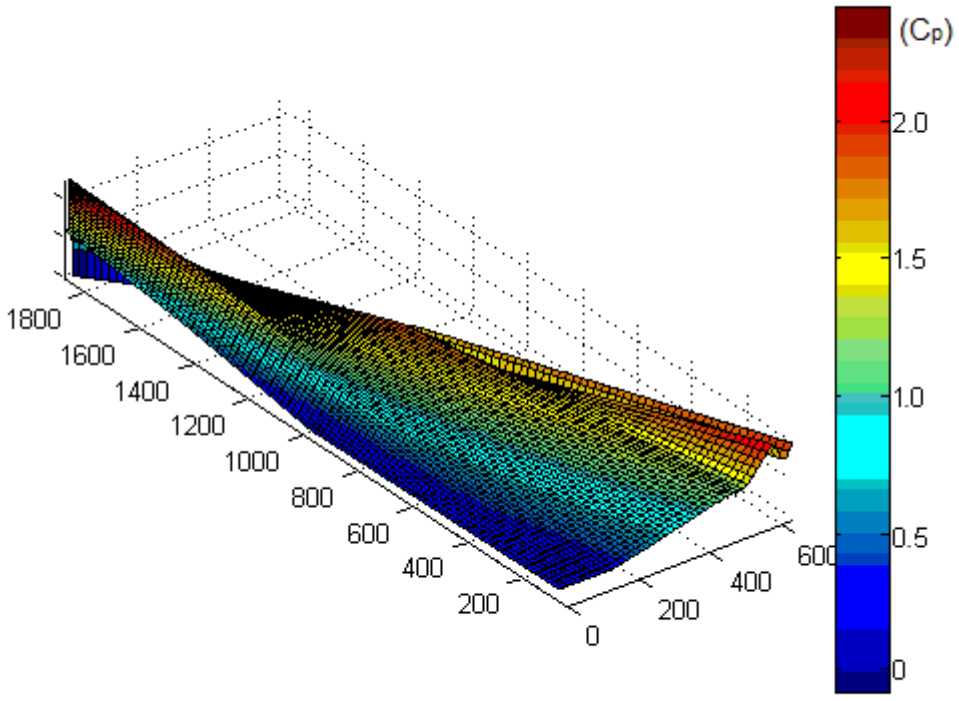

Figure 5-11: Pressure contour plot of the Semi-Rigid headsail for JS0

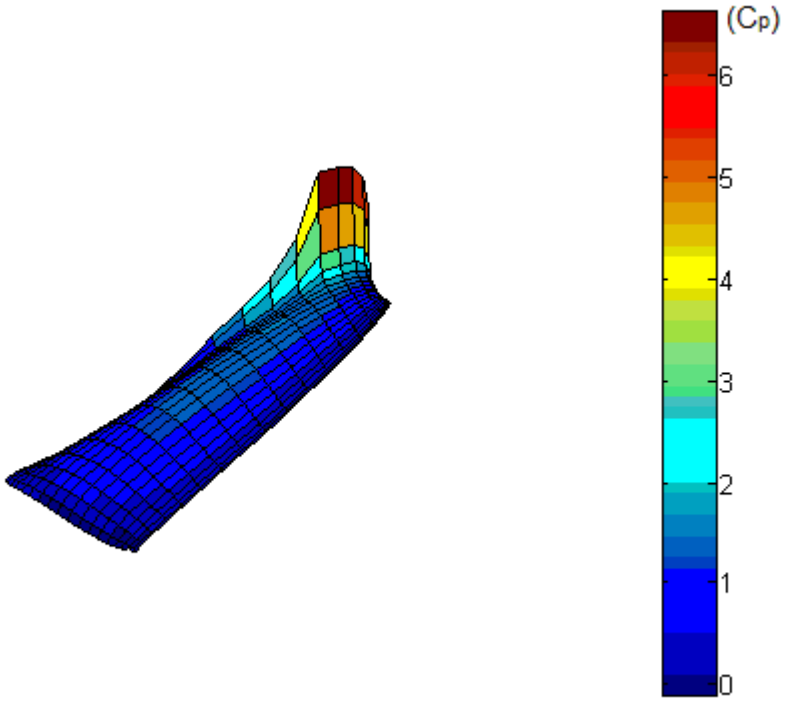

Figure 5-12: Pressure contour plot of the mainsail using a VLM

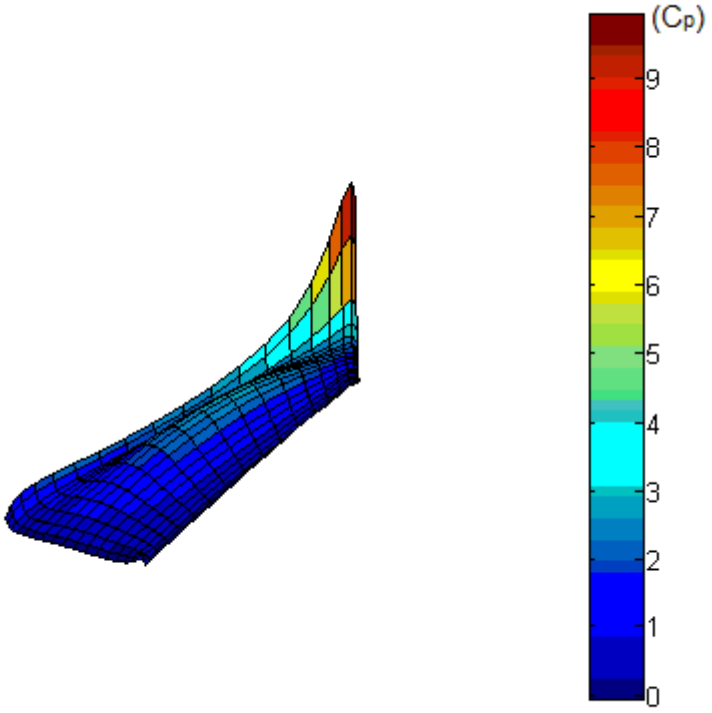

Figure 5-13: Pressure contour plot of the headsail using a VLM

5.2.2 Semi-Rigid: Forces & Moments

Here the results from the code are presented and discussed.

To validate the results the calculated forces were compared to the windage corrected measurements from the wind tunnel force balance using this equation:

$$Average\ difference = \sum \frac{(calculated - measured)}{measured} * 100$$

The sign convention is therefore negative when the calculation is under-predicted and positive for an over-prediction.

The standard deviation, given in percentage, is then a measure of how much the average difference for each run fluctuates around the mean over the entire sweep. This gives an impression of how close the trend is replicated.

Figure 5-14 gives an example of a typical set of results for a sweep. The actual force balance readings and the windage corrected readings are shown against the calculated results. The trends are clearly well reproduced. This is corroborated by Table 5-1 which shows that the standard deviations for all the sweeps were less than 6%. However there is consistently a large under-prediction of the forces and moments.

Table 5-1: Force & moment results for Model Test 1: Semi-Rigid

	Average Difference (%)	Standard Deviation (%)
Jib Sweep		
Drive Force	-31.1	4.8
Side Force	-12.6	3.2
Roll Moment	-19.0	2.5
Main Sweep		
Drive Force	-27.7	3.4
Side Force	-10.0	1.7
Roll Moment	-13.8	1.3
Combined Sweep		
Drive Force	-30.5	4.4
Side Force	-15.2	5.2
Roll Moment	-21.5	5.4

The results from the force and moment calculation are encouraging as the trends are reproduced very well. However they were under-predicted by a margin that was too large to have full confidence in the system.

As mentioned in 3.1.4 the windage correction may be affected by removing the sails when measuring it. If the observations by Richards et al. (23) were applied to these results the correlation would be far better. Without conducting further tests this is merely conjecture.

The code was thoroughly checked for bugs using the methods outlined in section 4.5 and was found to be functioning correctly and could not explain the drastic differences between the calculations and the force balance readings. This lead to the conclusion that the test setup was less than ideal.

5.2.1 Semi-Rigid: VPP Results

The results from the code and the measurements from the force balance were used in a VPP to estimate the boat speed (Vs) and heel angle of the boat. The force balance readings were used as is but for this comparison the calculated results had to be corrected for windage. The VPP can either be run by keeping the heel angle that the boat was tested at fixed and varying the theoretical wind speed to match this heel angle or by fixing the TWS and calculating the theoretical heel angle. For this case both options have their flaws although technically the former is the standard method. By fixing the heel angle it is harder to directly compare between two runs as the TWS will be different, while if the heel angle is allowed to change then the affects that has on the aerodynamics of a sail are not accounted for. These affects are explained in detail in (19), (20) & (5). For the sake of comparison the latter option was used for the following predictions.

The plots of boat speed and heel angle are shown for each run in Figure 5-15 and Figure 5-16. The results for boat speed are, as expected, significantly under-predicted while the trends match fairly well, although there appears to be a slight convergence as the boat speed drops. The heel angle for the calculated force results however does not follow the trend as well. Note from Figure 5-17 that the heeling moment curve is offset as normally the heel would be zero at zero heeling moment. This is because a canting keel is included in the VPP model. This is able to counteract the heeling moment and therefore the heel is zero even when the moment is a substantial.

The VPP results were not encouraging, although the method of fixing the TWS is questionable. This is highlighted by the heeling moment vs heel angle curve in Figure 5-17 where the two curves do not coincide.

Note the two dips in Vs for the jib sweep at run 4 and 7. This is due to the camera having accidentally been slightly moved during the test run. This shows how sensitive the drive force results are, as the same affect is not seen for the heel angle.

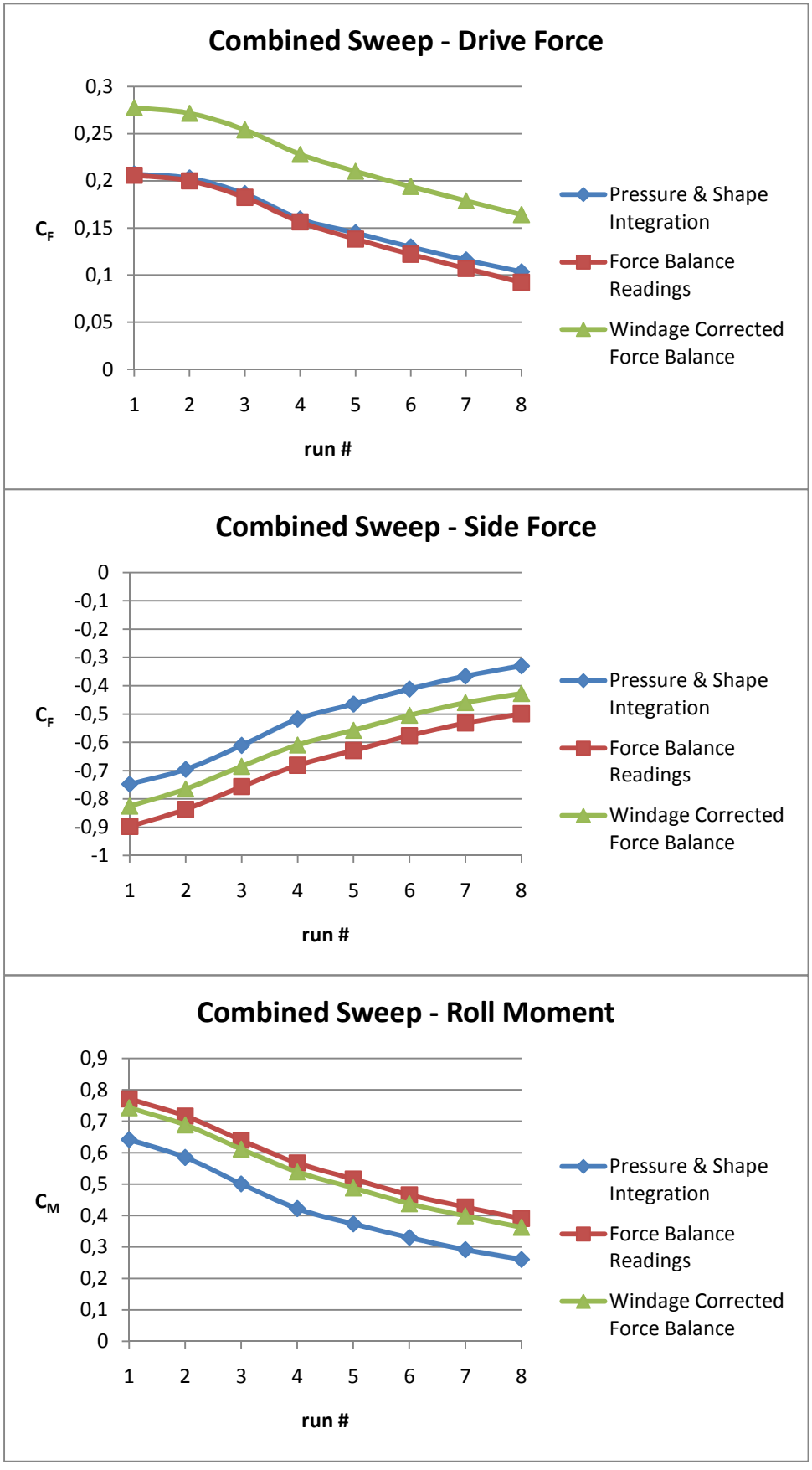

Figure 5-14: Results for each trim position in the combined sweep of the Semi-Rigid Sails

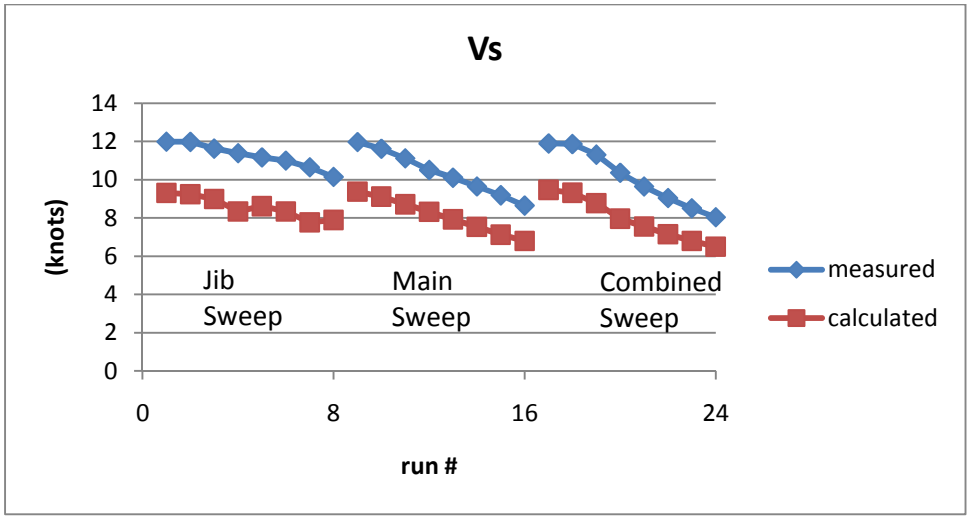

Figure 5-15: VPP predicted boat speed (Vs) for Semi-Rigid

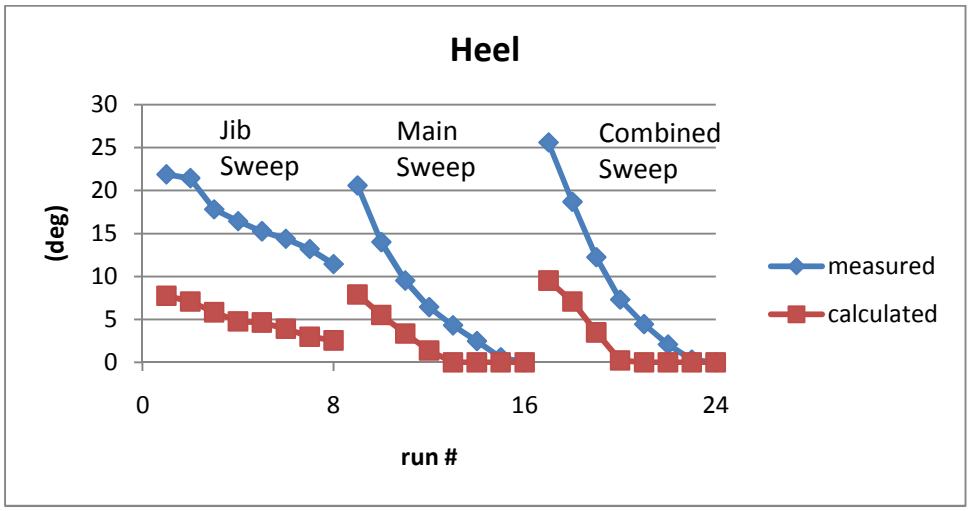

Figure 5-16: VPP predicted heel angle for Semi-Rigid

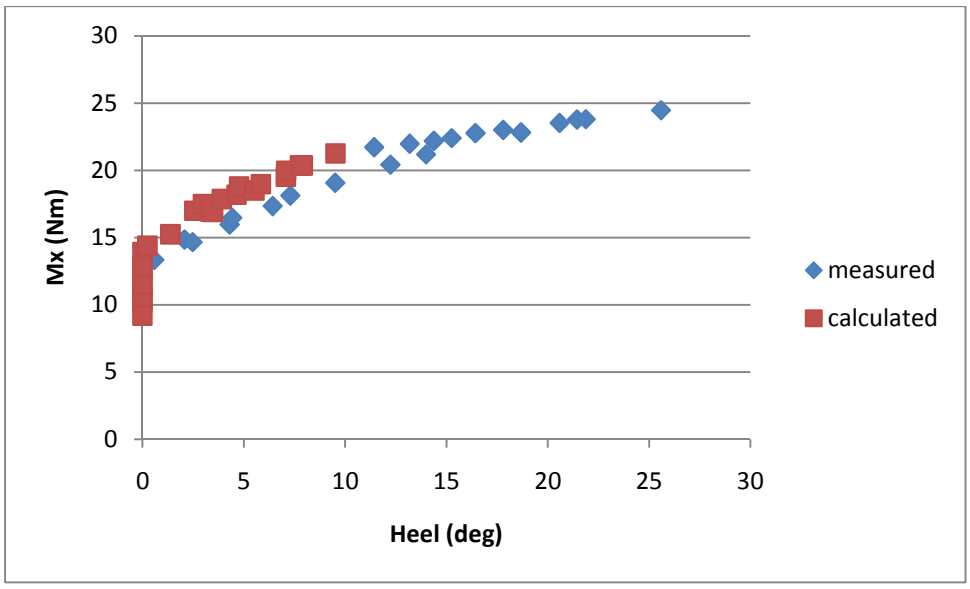

Figure 5-17: Heel moment (Mx) vs VPP predicted heel angle for Semi-Rigid

5.3 Summary of Results for the Semi-Rigid Test

Generally the measured pressures were in good agreement with the previous work. There were however areas where the pressure seemed more distorted than others, in particular the 3/4H of the headsail. This suggests that, at least at model-scale, the effect of the pressure taps, the way in which they are held in place and the presence of the PVC tubing that conveys the pressure to the transducers cannot be ignored. The VPP results show the inaccuracy of the test setup. Therefore an alternative means of testing the system was desired. The possible sources of error are discussed in the following section.

5.3.1 Possible Sources of Error for the Semi-Rigid Test

The reduction in the pressure measurement seen by the coin tap was unavoidable, but when factored in this would reduce the actual pressure differential on average by 3%. The test was for a single tap with no other interference around it, however as seen in Figure 5-5 the pressure taps may have seen even more interference, especially towards the leading edge. Arguably these taps have a larger influence on the drive force as the normal vectors of the relevant surface are oriented more towards that direction.

Upon inspection some of the flush mounted taps on the leeward side appeared not to be trimmed right down to the sail, again especially towards the leading edge. That may have been due to the epoxy used to set the tubes in place not having cured sufficiently and allowing the tubes to move further through. These ridges can be seen in Figure 5-18. This may also have contributed to a reduction in the local pressure at the taps.

The stand used to lead the PVC tubing off the trailing edge of the mainsail may also have influenced the force balance readings. This setup was not ideal but another solution could not be found.

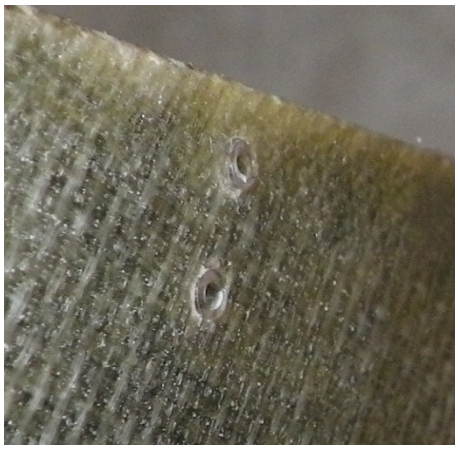

Figure 5-18: Photo of ridges found on the leeward, flush mounted taps

6 Model Test 2: Coreflute Sails

Following the testing conducted on the Semi-Rigid sails it was decided to utilise the sails built and used by Fluck et al. (15). Using a special core they managed to create airtight flutes on the inside of the sail to transfer the pressures down to the transducers on the deck. This eliminated the possible influence from the tubing and the coin taps on the flow around the pressure tappings. The idea was that using these sails would prove if this was what caused the large under-predictions in Model Test 1 of the forces and moments or not.

6.1 Test Setup: Coreflute Sails

The use of the new sails slightly affected the test procedure. These changes are highlighted here along with a description of the sails themselves.

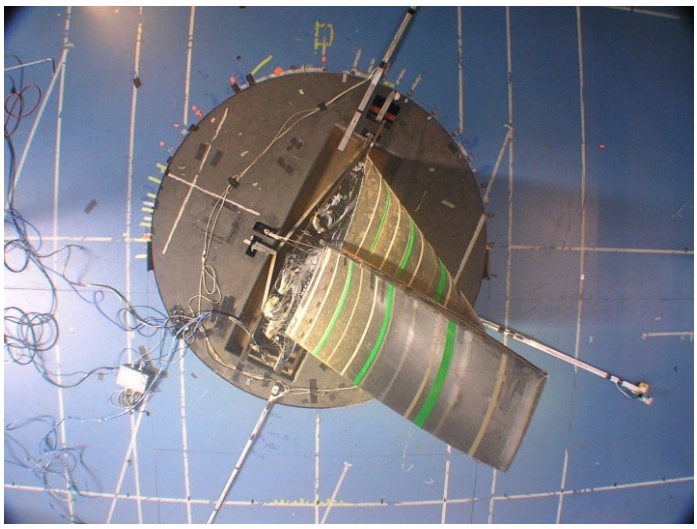

Figure 6-1: Overhead view of the Coreflute test setup in the wind tunnel

6.1.1 Description of the Coreflute Sails

The sails are made of fibreglass reinforced epoxy with a Coreflute® sandwich core. They were laminated on a male mould and put under vacuum pressure to ensure a high quality product. Coreflute® is a corrugated plastic board material most commonly used for advertising or real-estate signs. The product has two sheets of polypropylene joined by transverse walls thus creating airtight flutes. These flutes were oriented in the spanwise direction so that tappings could be perforated straight through the sail and by covering the hole on one side at a time the pressure could be transferred to PVC tubing connected to the foot of the sail. This tubing was then connected to the transducers. In this way no interference on the flow around points of interest would be created. Figure 6-2 shows the sails construction and the heights of the pressure taps (15).

Many tappings were perforated into the sail by the previous users and often more than one tap was connected to a single flute. Furthermore over time through general wear and tear some flutes were leaking and there had been some delamination of the fibreglass/epoxy from the core which rendered some flutes unusable. For the purposes of this work a range of independent tappings over a range of heights was needed, such as for Model Test 1. Much time was spent repairing the sails, locating the usable taps and deciding which rows would give the best distribution over the chord- and spanwise directions.

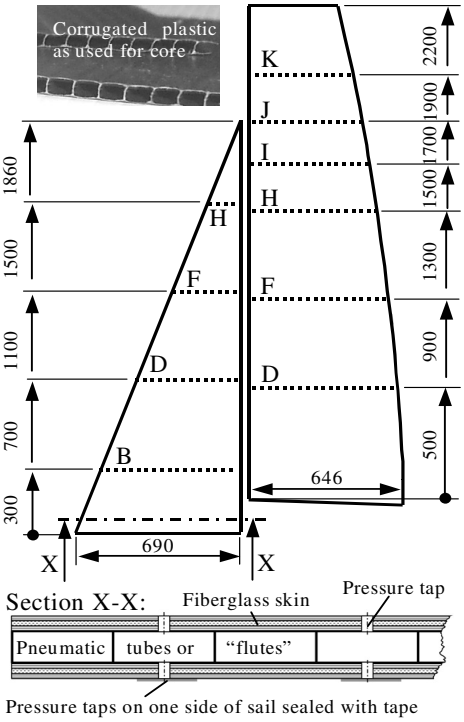

Figure 6-2: Cross-section of the Coreflute sails and location of pressure tap rows (15)

For the Semi-Rigid sails the tap heights were placed at a fraction of the luff height, but as can be seen in Figure 6-2 these taps were placed at 200-400 mm intervals along the vertical height. Table 6-1 shows the rows of taps used in this study and the corresponding percentage of luff height (H). For a full list of locations of the taps refer to Appendix 4.

Table 6-1: Rows used and corresponding percentages

Mainsail			
C	**F**	**I**	**K**
0.14H	0.43H	0.71H	0.90H
Headsail			
B	**D**	**F**	**H**
0.16H	0.37H	0.58H	0.80H

The VSPARS stripes were limited this time to three on both sails. From the previous test it was felt that this was enough to recreate the sails adequately. These were placed at 1/4, 1/2 and 3/4 luff heights on both sails. Thus the pressure taps were not located as close to the VSPARS stripes as before. Neon green stripes were used in this test as a new filter was being tested for the VSPARS system.

For these sails a 3D modelling file in .igs format was available from which the mould was created. This in theory provided the actual sail area with which to validate the code. The sail area and pressures directly influences the results from the integration, so therefore this is a valuable check.

6.1.2 Test Procedure: Coreflute Sails

The same baisc procedure was followed as for the Semi-Rigid sails. The exact trim positions used were not recorded sufficiently to recreate from this test but the same method was used, i.e. the sails were trimmed to the tightest position and gradually eased in small increments. The number of trim positions recorded was reduced to five as during the post-processing of the data from Test 1 it was seen that further easing of the sails resulted in positive pressures on the leeward side. These trims would not be of much interest for normal sailing conditions using flexible cloth sails. They would not be able to hold the same shape that the rigidness of these sails allowed.

As each tapping was connected directly to both sides of the sail two runs were needed for each trim position. The tappings on one side were taped closed so that the measurements could be recorded for the other side. The tape was then switched to the other side and the test repeated for the same trim position before moving to the next one. In order to remove the influence of slight free-stream dynamic pressure variations between the two runs the pressure results were converted to coefficients before finding the differential. The shape data was averaged over both runs, although it was assumed that the shape was constant throughout the testing.

The same pressure measuring system for Model Test 1 was used in this test, but a different model boat and rig were used. It was found that the rig used in the previous test was bent significantly and could not be straightened through tensioning of the rigging. It was also desired to better accommodate the boxes of transducers on the deck.

6.2 Results for the Coreflute Sails

The data presented here aims to highlight the differences from the Semi-Rigid test.

6.2.1 Coreflute: Recorded Pressures

The pressure distributions from Figure 5-7 are included in Figure 6-3 for comparison purposes. It appears in Figure 6-3 that the taps were not close enough to the leading and trailing edges at 0.58H on the Coreflute headsail to capture the separation if it occurred. For the Semi-Rigid headsail the local maximum pressure at the leading edge occurs roughly between 6-10% of the arc length. The taps on the Coreflute headsail are located at around 6 and 10 % and no closer, therefore they may have captured the local maximum but not the steep drop off seen for the Semi-Rigid sails.

What can also be seen here, but will be clearer in Figure 6-4, is that the Coreflute sails manage to produce a higher $\triangle C_P$. The local minimum occurs at around 35% on the Coreflute headsail while there is a large gap on the Semi-Rigid sail from 20-75% arc length. However comparing the values available at 20% arc length on both headsails it can be seen that on the leeward side the Coreflute sails have a C_P of -2 while the Semi-Rigid only have -1.5.

The mainsail is mostly the same in both cases although there is a noticeable plateau of the leeward pressures on the Coreflute sail from 30-60% arc length. This may be visible due to the higher density of taps in this area.

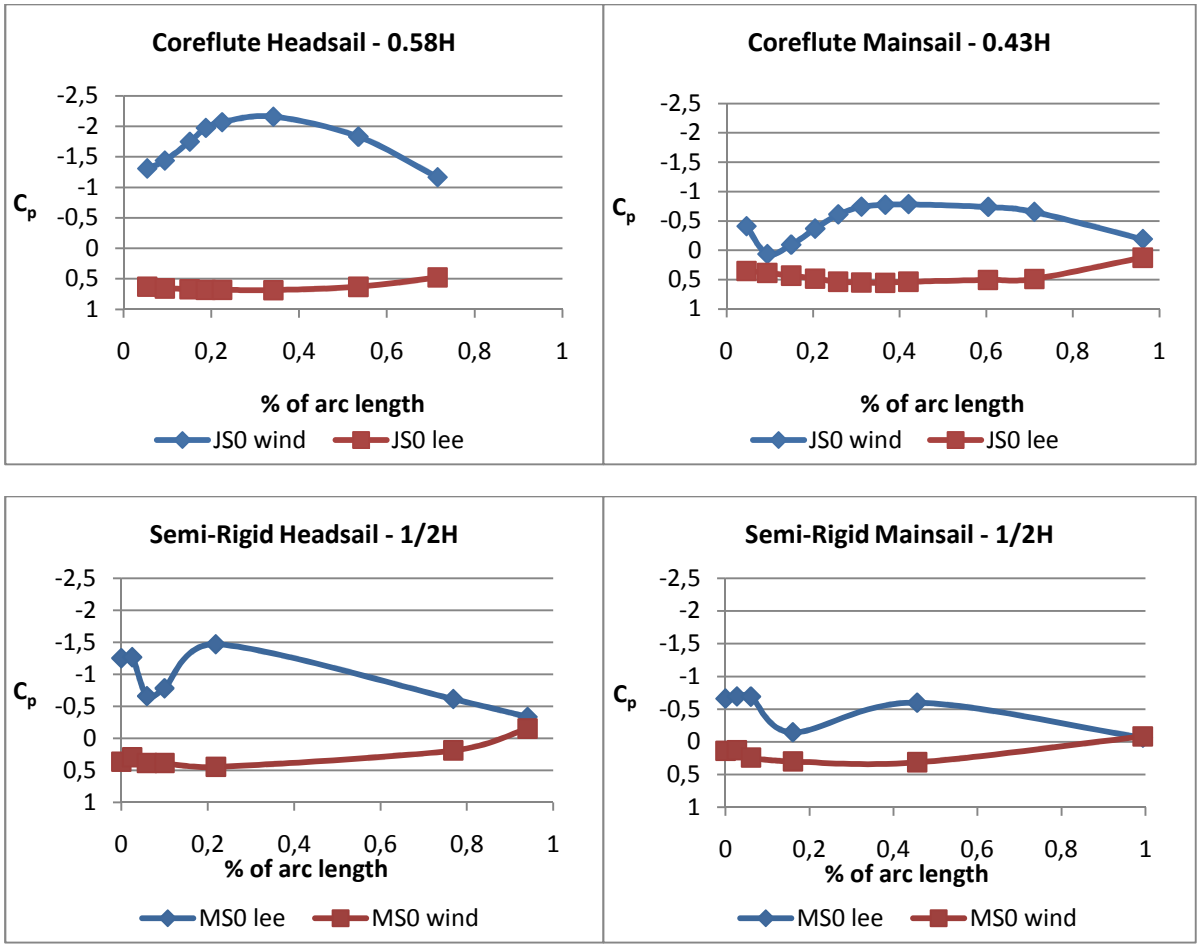

Figure 6-3: Figures of pressure distribution around Semi-Rigid and Coreflute sails

The importance of the pressure tap distribution is highlighted in the above comparisons between the Semi-Rigid and Coreflute results. When extrapolating data points where they have not captured a negative to positive shift in gradient that should have been seen the delta pressure at the leading edge will be greatly under-predicted. Without the taps closer to the leading edge capturing this gradient shift and establishing the correct trend then the pressure distribution will not be captured correctly.

The differential pressure distributions for the Coreflute sails, seen in Figure 6-4 and Figure 6-5 show similar trends for both sails across the sweep compared to the Semi-Rigid sails in Figure 5-8 and Figure 5-9. The obvious differences have been covered above regarding the pressure distribution on both sides of the sails.

The pressure contour plots for the main- and headsail for the initial trim position of the jib sweep are shown in Figure 6-6 and Figure 6-7. For the headsail the same large pressure peak towards the head that was seen in Figure 5-13 of the VLM headsail is present. However this was not the case for all the trims.

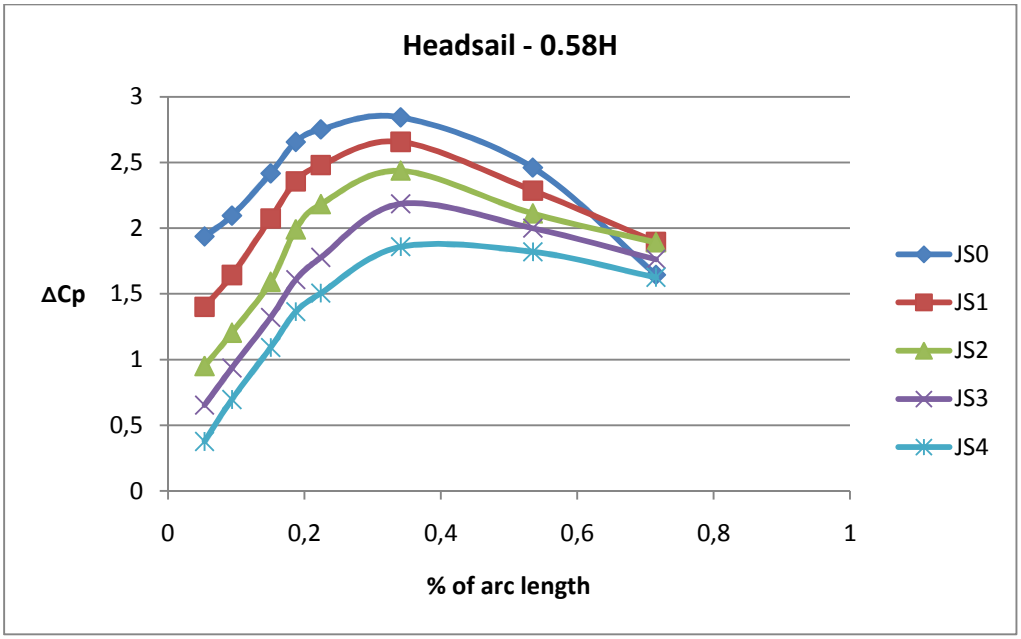

Figure 6-4: Differential pressure reading on Coreflute headsail for the sweep of the headsail

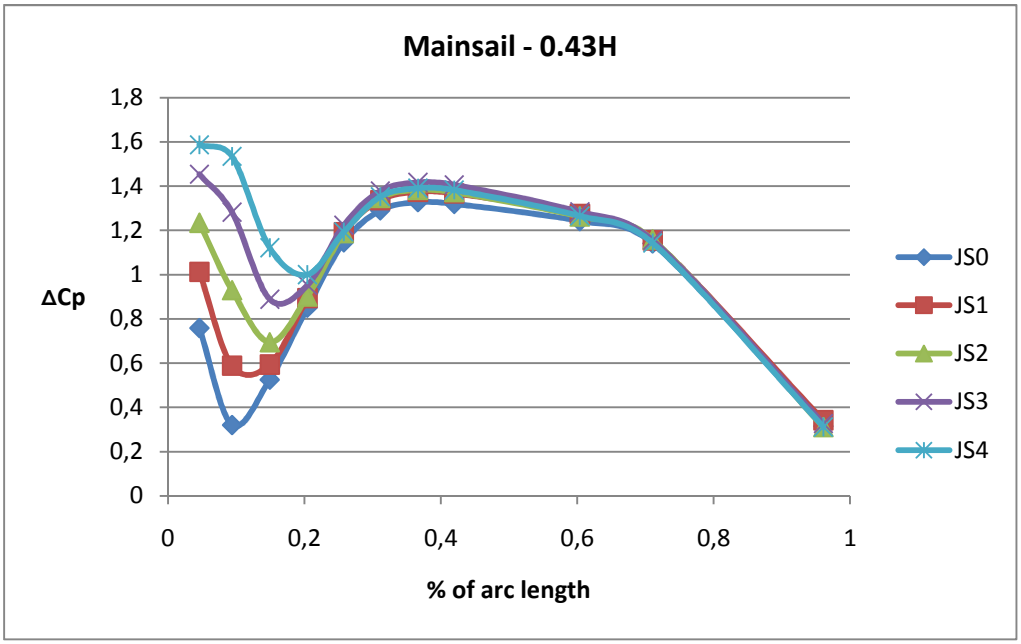

Figure 6-5: Differential pressure reading on Coreflute mainsail for the sweep of the headsail

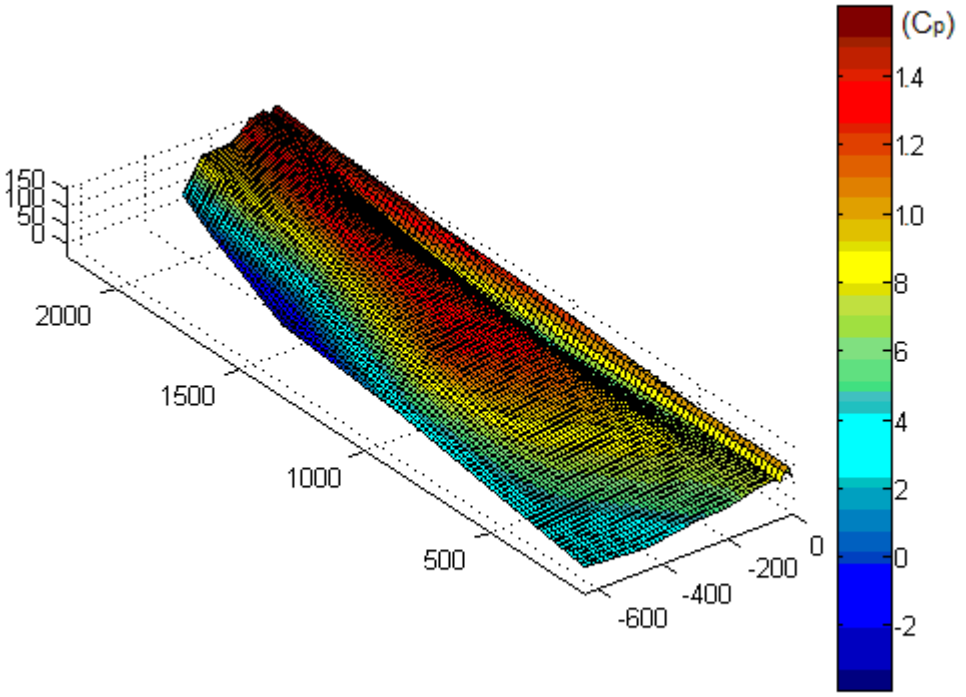

Figure 6-6: Pressure contour plot of Coreflute mainsail

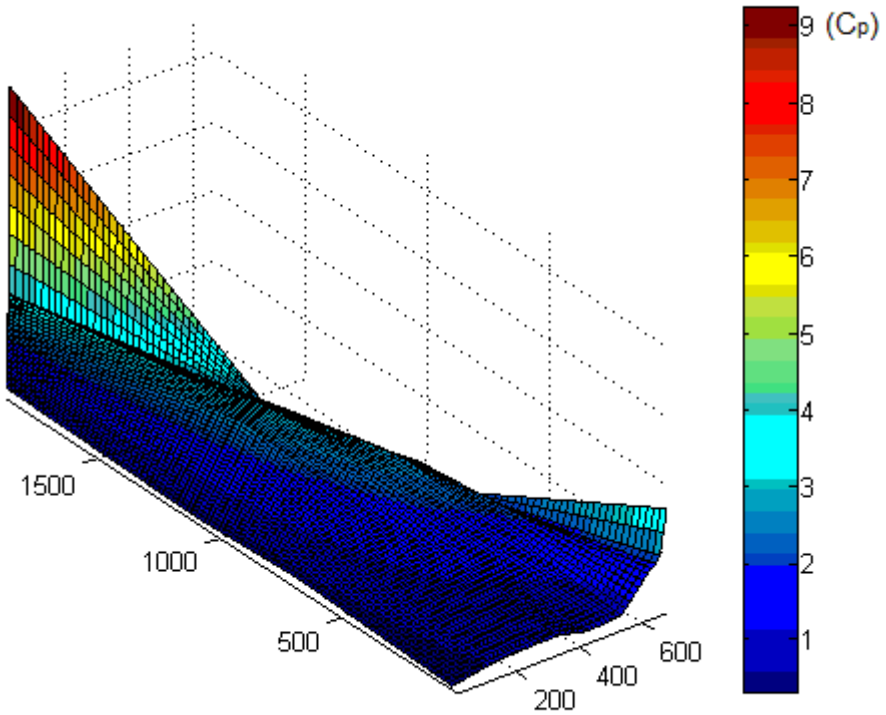

Figure 6-7: Pressure contour plot of Coreflute headsail

Arguably the pressure contours were smoother for this test showing that the flow was less disturbed. This indicates that the tappings were able to capture a better pressure distribution corresponding to the whole sail. This, as opposed to measuring a locally disturbed flow while the rest of the sail operates under an undisturbed flow, would result in a closer match of the force balance and calculated results.

The number of rows of pressure tappings was increased from three to four and the location of the top and bottom stripes were much closer to the head and foot of the sail. This may also have improved the pressure map across the full sail.

6.2.2 Coreflute: Sail Area and Depth

The VSPARS system was validated using the Coreflute sails. Measurements of the depth or camber of the sails were measured at 50 mm increments along the chord line for the first 150 mm and thereafter in 100 mm increments. The estimated error margin in these measurements was ±2 mm. These were then compared to the average sail shape over all the sweeps in the Corefulte test. As the sails were very rigid their shape is assumed to be constant even though they were loaded in the VSPARS measurements and not for the manual ones.

The results are presented as a percentage difference between the VSPARS and measured values over the chord length.

$$percentage\ difference = \frac{(VSPARS - measured)}{chord\ length} * 100$$

The sign convention for draft is thus positive where the VSPARS found the position to be further aft and for camber where it found it deeper.

As can be seen in Table 6-2 the draft is generally found by VSPARS to be further aft and the camber to be deeper than the actual sail. This can be seen visually in Figure 6-8.

Table 6-2: Percentage difference between VSPARS and measured values

Mainsail	(values in %)			
	Top	**Middle**	**Bottom**	**Average**
Draft	4.46	1.44	4.18	3.36
Camber	0.08	0.13	0.48	0.23

Headsail	(values in %)			
	Top	**Middle**	**Bottom**	**Average**
Draft	-1.04	2.98	3.05	1.67
Camber	2.54	1.62	1.18	1.78

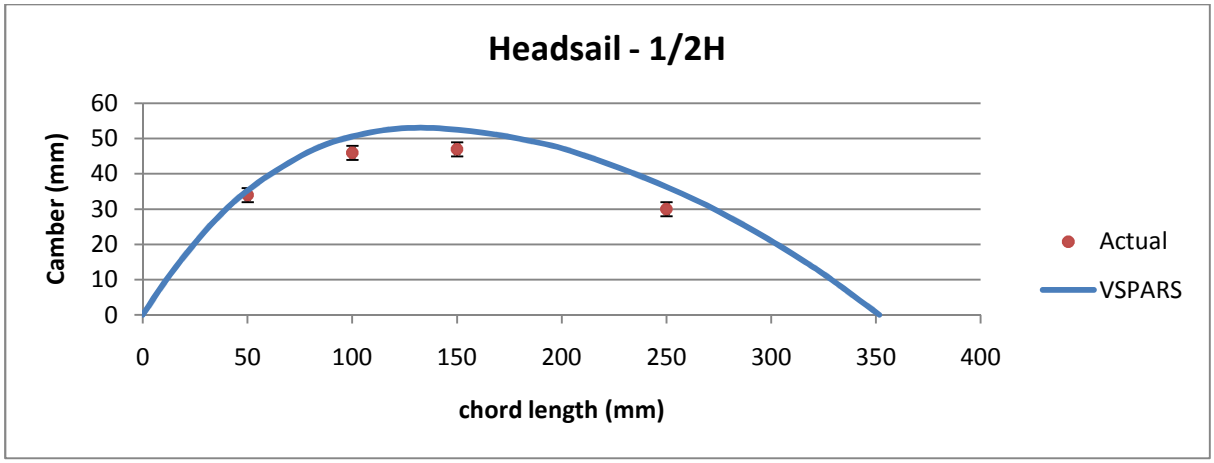

Figure 6-8: Comparison of VPARS to measured values for camber and draft

As mentioned in section 6.1.1 there was a digital 3D model, in .igs format, available for these sails. From this, using 3D software, a precise sail area could be found to validate the area calculation done by the code. The calculated area for the headsail was found to be 8% smaller than what was found using this file, while the mainsail was 4% less. However after comparing the measured values of the edges of the sail, i.e. the foot, luff, etc., it was found that they did not match up exactly. By calculating the nominal area of the sails using equations 3.1 and 3.3 and comparing the difference the error margin was estimated at ±3%.

The results from this section were somewhat contradicting. Although the sail area is under-predicted by the calculation compared to the 3D model, VSPARS has a tendency to over-estimate the depth of the sails which should result in an over-prediction. The accuracy of the 3D model is questionable as it was found that the edge lengths of the sails did not match up.

Without a more accurate measurement of the actual sail area this validation method is misleading.

6.2.3 Coreflute: Forces & Moments

The results here are expressed in the same fashion as for the Semi-Rigid sails, where a negative sign indicates an under-prediction of the results from the code compared to the force balance.

As can be seen in Table 6-3 the average difference and standard deviation for each run was significantly improved, however the drive force was still under-predicted more than the other forces and moments. This could be due to the low density of pressure taps close to the leading edge for some rows. Figure 6-9 shows the same plots as for the Semi-Rigid sails where the trends and differences can be compared visually.

Table 6-3: Force & moment results for Model Test 2: Coreflute

	Average Difference (%)	Standard Deviation (%)
Main Sweep		
Drive Force	-16.5	2.8
Side Force	8.9	5.5
Roll Moment	-5.0	3.7
Jib Sweep		
Drive Force	-12.8	1.9
Side Force	3.2	2.3
Roll Moment	-6.5	1.8
Combined Sweep		
Drive Force	-19.4	6.0
Side Force	5.7	3.0
Roll Moment	-8.9	2.4

6.2.4 Coreflute: VPP Results

The results were run in the same fashion as for the Semi-Rigid sails. The boat speed in Figure 6-10 was still slightly under-predicted, as was expected from the comparison of the forces. Interestingly the jib sweep, which was arguably the most accurate when comparing forces and moments, shows the largest under-prediction in Vs. The comparison of the heel angle in Figure 6-11 shows a good agreement between the two data sets. The righting moment curve in Figure 6-12 are more closely matched than they were for the Semi-Rigid sails.

Again it should be mentioned that the results in this section are not definitive but are an interesting assessment of the quality of the results. The results, as expected from the force and moments compared to the force balance, showed a better agreement for boat speed and heel angle than the Semi-Rigid results.

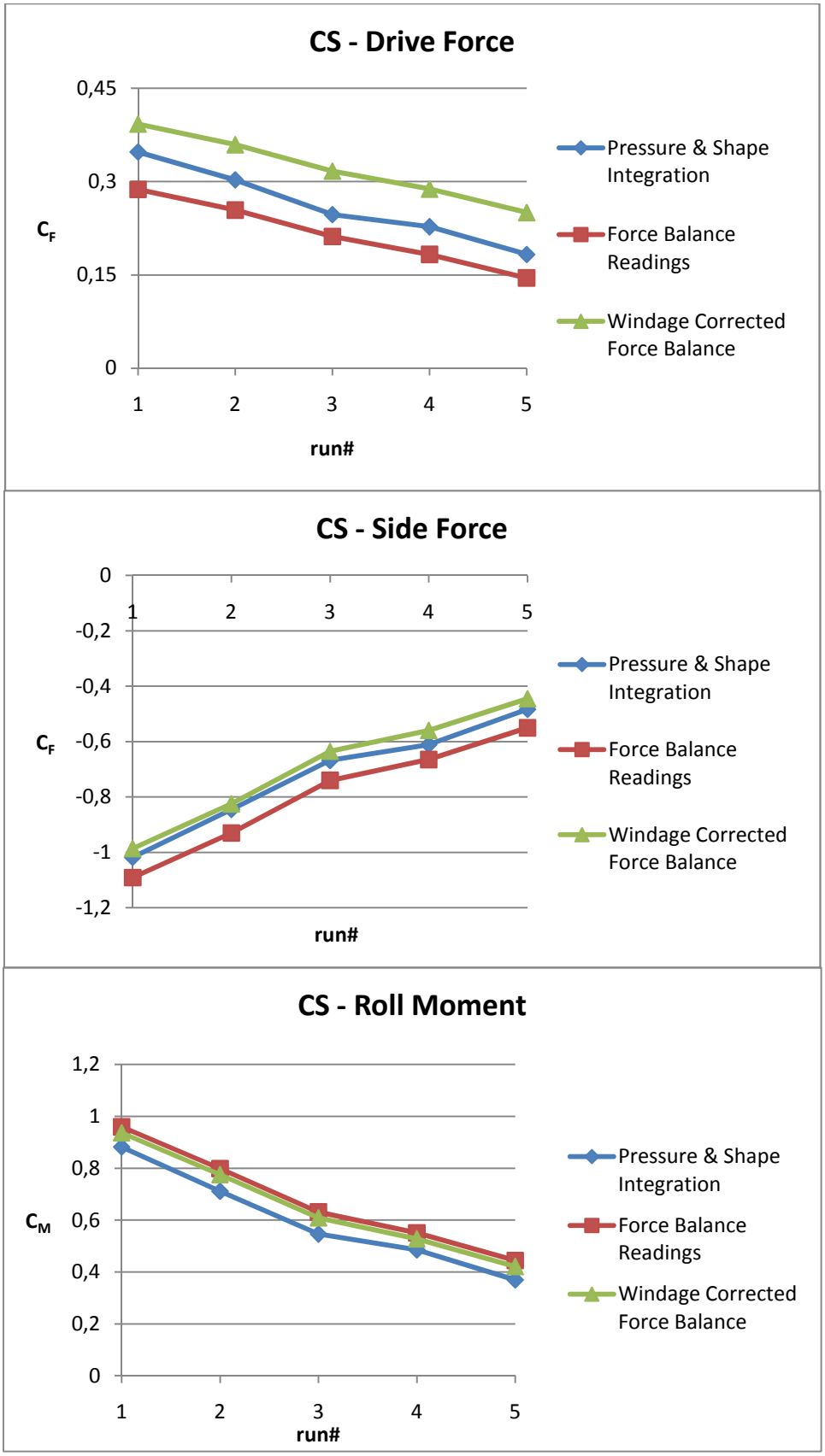

Figure 6-9: Results for each trim position in the combined sweep of the sails

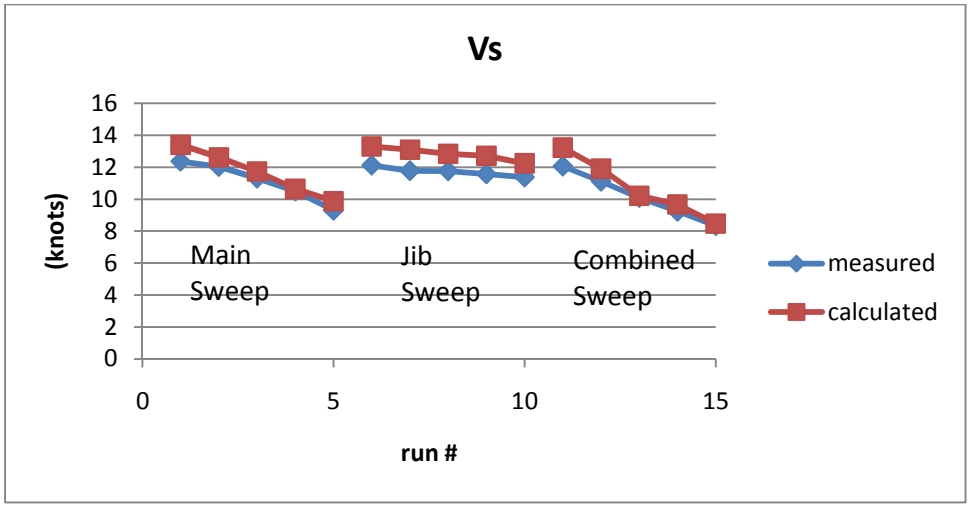

Figure 6-10: VPP predicted boat speed (Vs) for Coreflute

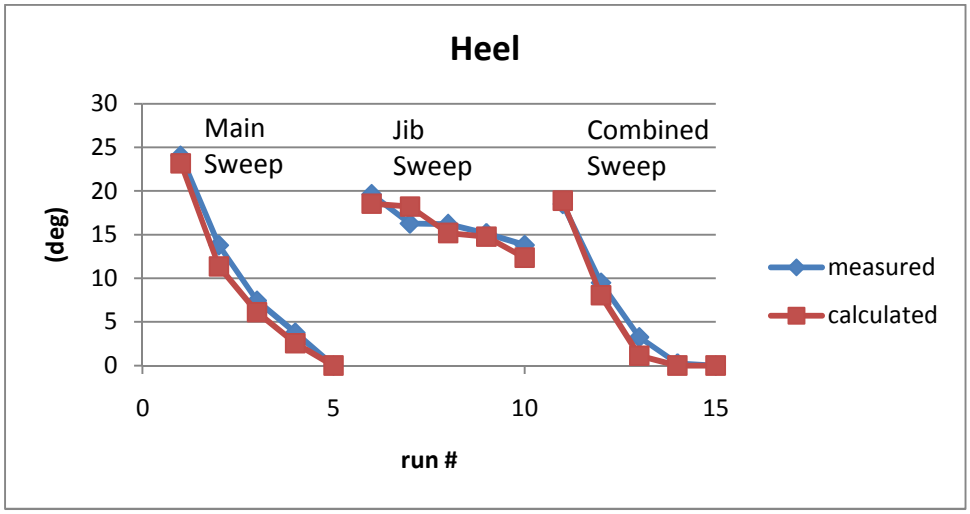

Figure 6-11: VPP predicted heel angle for Coreflute

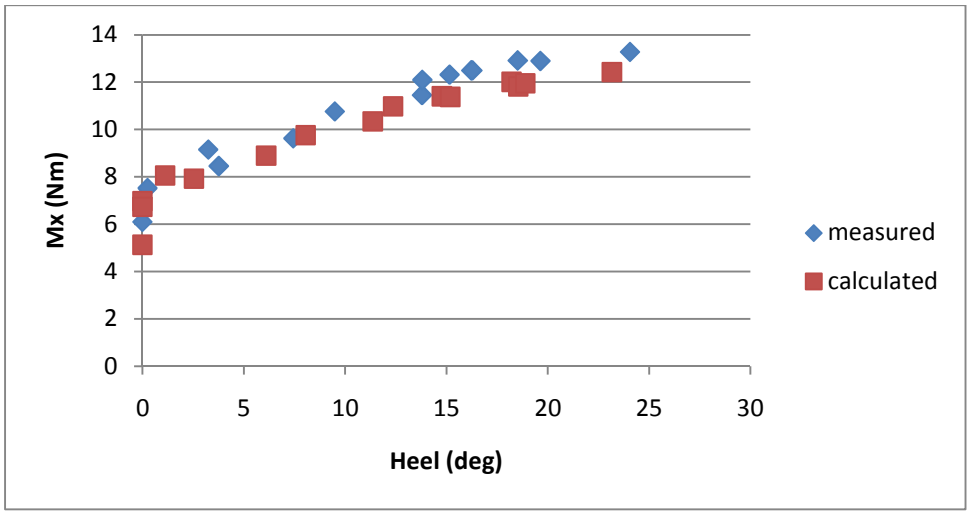

Figure 6-12: Heel moment (Mx) vs VPP predicted heel angle for Coreflute

6.3 Summary of the Results for the Coreflute Test

The results across the board are significantly improved from the Semi-Rigid test. But there are a number of elements that have changed from Test 1 to Test 2. The most obvious change was the removal of the pressure taps, PVC tubing and support stand and the increase in pressure tappings.

The number of taps was increased and this contributed to a better definition of the pressure distribution across the chord. This may have increased the accuracy of the results. Even the large suction peaks seen in the VLM contours were defined, although the constant increase in pressure does not decrease towards the head. The capturing of this was not the case for all the test runs but more research is required as to when this peak should or should not be present. The VLM results can only be used as a rough guide as to what may occur due to the reasons stated in section 5.2.1. Notably it does not include the mast and it is safe to assume that the large peak seen on the main in the VLM does not actually occur in reality.

Overall the agreement between the calculations and the measurements were very good, especially in the VPP results. This proves that this system could potentially be used to assess the performance of sails as it is capable of obtaining the same information as the force balance in the wind tunnel. The advantage of this system is that it can be applied in the same way to sails on a full-scale yacht.

7 Full-Scale Testing

With the confidence attained through the model testing and with a newly developed pressure system ready for use the testing was taken to the water aboard David Le Pelley's Stewart 34. The testing was done over two days with the first predominately used for troubleshooting the issues that came up. The second day saw fine weather with a fresh breeze of around 10-15 knots, ideal conditions for upwind testing.

7.1 Test Equipment

A completely new pressure system was used in this test for the first time. The following section gives the details of this system along with some additional equipment that was used alongside this project.

7.1.1 Details of the Pressure Measuring System

The development of the system detailed below was done by David Le Pelley. Some assembly, calibration and testing was done by the author.

The same type of pressure transducers used at model-scale, Honeywell XSCL04DC, were used at full-scale, however in this case it was desired to place the transducers on the sails. This avoids a number of issues mentioned in 3.2.1, such as the influence of long pressure tubing and not needing to record a reference pressure by measuring the differential pressure across the sail. However the minimum dimensions of the pressure tap were limited by the size of the transducer.

A housing for the transducers was designed with two openings, one on either side, in line with the openings of the transducer when assembled. Figure 7-1 shows the two parts to the housing and the transducer nested in the half which is attached to the sail. They were limited by the transducers to a diameter of 40 mm and a height of ±9.5 mm. Rubber o-rings were used to seal the connection between the transducer and these openings which were clamped in place when the tap was assembled using four screws.

An operation amplifier (op-amp) was connected directly onto each transducer which amplifies their analogue output (in mV) to a signal in the ±2.5 V range. Using ribbon cable and IDC connectors the transducers were easily connected to a ribbon cable running along the chord. A maximum of 8 taps per chord was possible, limited by the number of individual wires in the 11 wire ribbon cable. 3 wires were common for all the taps leaving 8 for the analogue output from each tap to be sent.

Each chordwise cable terminated on an analogue-to-digital (A/D) converter chip which converts the analogue voltage signal into a 12-bit digital signal. Theoretically the system can handle 10 of these chips, and therefore 10 sets of 8 transducers. This work was limited to 3 due to the budget and the infancy of the system. The A/D chips were connected to a continuous ribbon cable along the luff of the sail which terminated at a microcontroller box at the tack. All the A/D chips shared 6 common wires for supply voltage, signal sending, etc. but each required an independent wire that the microcontroller uses to call on each chip one at a time. The microcontroller also provided a time stamp on the recordings. For a diagram of the full system refer to Figure 7-2.

Data acquisition of a single tap could occur at a frequency of 3000 Hz and so for 24 taps, 8 per stripe for 3 stripes, the frequency was reduced to 125 Hz. However there was a high frequency noise from

the power supply that disturbed the signal. It was possible to filter this signal by averaging over 30 readings for each transducer. This resulted in an effective frequency of 7.5 Hz.

The transducers themselves are temperature compensated and provide a range of ±1 kPa. Therefore from the 12-bit A/D resolution the effective resolution was 0.5 Pa per bit. This is a significant improvement on the system used in the full-scale testing done by Viola (7). This can be further improved by changing the resistor adjacent to the op-amp. This can be seen in the calibration file found on the attached CD where the taps towards the leech used different resistors and did not provide a resolution as high as the others (25).

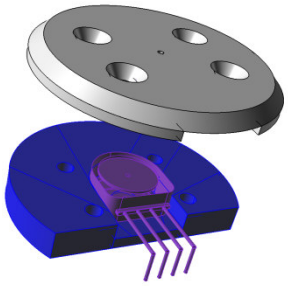

Figure 7-1: Two piece housing for the pressure transducer (25)

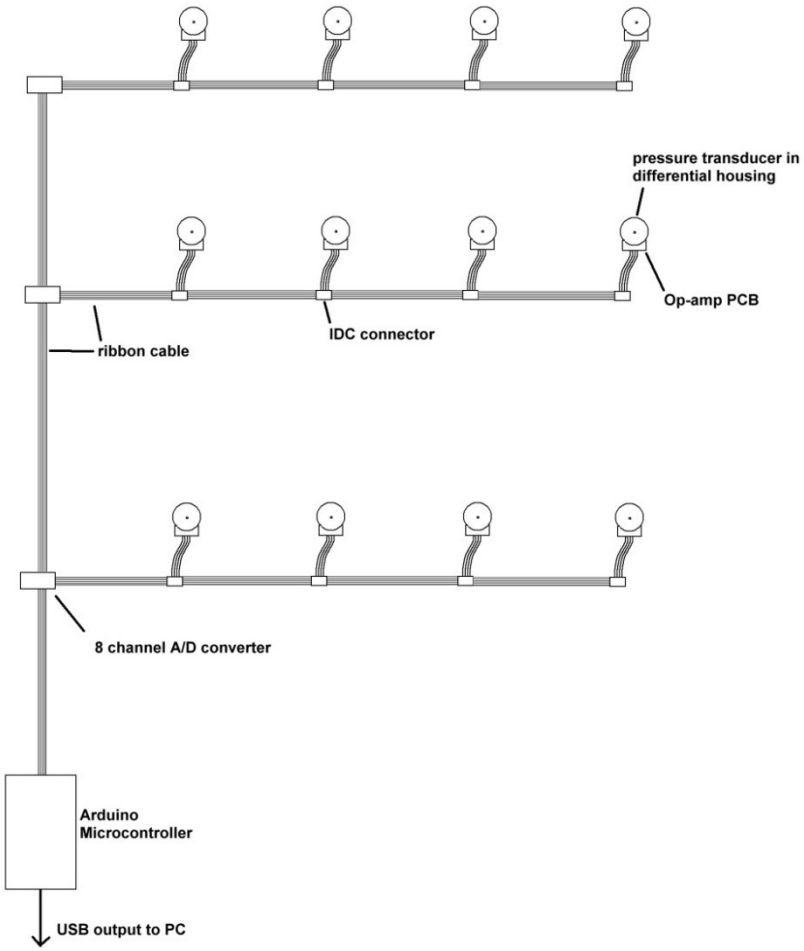

Figure 7-2: Schematic of the wired pressure system (25)

7.1.2 Calibration of the Pressure Transducers

In order to read a pressure from the transducers they had to be calibrated and a zero reading needed to be recorded.

The calibration was dependent on the resistance in the wire connecting the tap to the A/D converter and therefore the taps had to be setup on the sail before this could be done. Before they were finally stuck onto the sails the taps were clamped using a purpose built calibration jig. This jig was designed to secure a rubber tube to one side of the transducer while allowing the ambient pressure onto the other side. Then the tube could be connected to a calibrator so that a known pressure could be applied to the diaphragm inside the transducer. By recording three pressures and the corresponding reading in bits from the data logger a slope could be found. The gradient (m) can then be used along with a zero reading to calculate the pressure for any reading in bits (θ) from equation 7.1.

$$p = \frac{(\theta - \theta_{zero})}{m} \tag{7.1}$$

Once the calibration gradients were found for all the taps they were left for a day. Some taps were then recalibrated to assess the amount of drift. This was found to be negligible and so they did not require recalibration before testing.

For the actual testing the transducers recorded the fluctuating pressures over an acquisition period. The period was determined by how steady the conditions were. The time was increased if the conditions were more erratic. The results were then averaged over this period.

7.1.3 Setup of the VSPARS Stripes

The 3 VSPARS stripes used in the Coreflute test proved adequate to recreate the sails. Again they were placed at 1/4, 1/2 and 3/4 of the luff height. The sail shapes, much the same as for the pressures, were averaged over the data acquisition period to account the fluctuations of the unsteady environment.

7.1.4 Setup of the Pressure Taps

Again it was desired to locate the taps close to the VSPARS stripes as it was thought that this would improve the accuracy. The tap location study conducted using the VLM for the Semi-Rigid test proved to be ineffective. The nature of the peaks and troughs of a pressure field move depending on the trim of the sail. The limit on the number of taps meant that the placement of them needed to be refined for this test. The pressure results of both model tests were thoroughly analysed to assess the most appropriate positions.

For the mainsail the first tap was placed as close to the leading edge as possible, 35 mm from the luff, to capture the leading edge suction peak. It was seen that any measurements taken within the first 10% of the arc length were likely to be located in the large separation bubble created by the mast and thus record similar pressures as to the first tap. Then the highest gradients in the pressure field occur between 10% and 25%. To capture this four taps were placed, starting at 10%, at 5% intervals. The pressure peaks between 25% and 45% after which it plateaus until around 70%. Three taps were therefore placed at these percentages. The last tap was placed at 95% to be able to assess the trailing edge separation.

The pressure distribution at the leading edge of the headsail is more critical and the high gradients occur earlier on along the arc length. The first tap was again placed as close as possible to the leading edge followed by three taps placed at 4% intervals going up to 12% along the arc. The rest of the distribution follows what can be described as a sine curve. To capture this adequately the remaining taps are placed at regular intervals of 24% starting from 24%, i.e. 24%, 48%, 72% and 96%.

Perforations were burnt through the cloth at the desired locations to connect the taps to both sides of the sails. For areas of more than a single layer of cloth, such as near the luff rope and on other patchings, the layers were melted together thereby sealing them. The tap could then be stuck to the sails using double-sided tape placed around the opening as seen in Figure 7-3A. This also provided a sufficient seal enclosing the opening of the transducer and the perforation in the sail. From the study conducted on the full-scale tap geometry, refer to appendix 3, a patch of sail cloth with a hole perforated in the middle was used to cover the tap in order to improve its aerodynamics, this can be seen in Figure 7-3B. This was also stuck to the tap using double-sided tape. The edges of the patch were stuck down onto the sail in the same fashion. The density of the taps at the leading edge of the top stripes made it difficult to use separate patches for each tap and were placed under the same patch. This can be seen in Figure 7-3C. It can also be seen how the ribbon cables, IDC connectors and A/D chips were secured to the sail using sticky-backed sail cloth.

The taps were placed on the starboard side of the sails. This means that on port tack they were on the leeward side and windward on starboard.

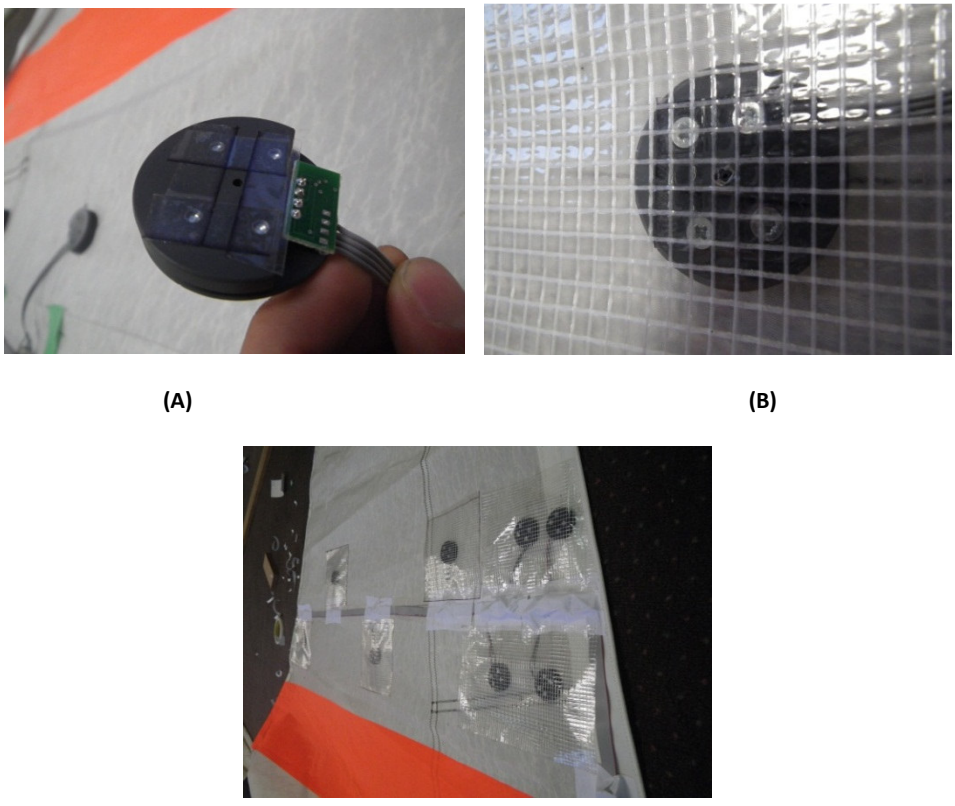

(A) **(B)**

(C)

Figure 7-3: Pictures of the pressure taps being mounted to the sail

7.1.5 The Sails Used

An old main and headsail were used for the test. They were the only sails available that the owner, David Le Pelley, was willing to have holes burnt into. They were fairly stretched and thus much deeper than the sails that would normally be flown on this type of boat. It was seen through the VSPARS program that the average depth of the mainsail was 15% of the chord length while a *good* sail should be no more than 10%.

The headsail was an overlapping jib hoisted on a roller-furler. The roller-furler forestay was relatively large with a cross-section of roughly 30x15 mm.

7.1.6 Additional Equipment

Full advantage of all the resources of the YRU was taken. The boat was rigged with as much data capturing equipment as possible. A GPS and all the data from the boat instruments were logged to provide additional information regarding the speed of the boat, heading, AWA and AWS.

Two sonic anemometers were installed at the top of the mast and off the stern to measure the wind velocity and angle and boat motions, while an Inertial Measurement Unit (IMU) was used to measure the boat motions at the masthead. These measurements were part of a project conducted by Boris Horel who was researching the turbulence of the wind. However some of the data from this equipment was useful for the work presented here, such as the heel angle from the IMU and the AWS and AWA from the anemometers.

7.2 Test Procedure and Observations

The test was heavily weather dependant as the taps would be rendered useless if the holes became water logged and the sails and sheets used were old and stretched making sailing difficult in heavy winds. The testing was scheduled for the 18^{th} – 20^{th} of July, right in the middle of the New Zealand winter. Fortunately these days were graced with ideal weather for testing. The first day, when all the equipment was setup, the wind was a light breeze which made the process easier. Once everything was operating correctly it was possible to sail out and mark the sheets on either tack to the same positions. The wind was not strong enough to collect any useful data that day. The sheets were removed from the headsail at the end of the day as the sail required some extra work. It was attempted to mark the position of the knot although it proved difficult to reattach them the next day at the same place.

On the morning of the second day the wind had increased to a very stable, moderate breeze around 10-15 knots with a sea state of 3-4 on the Beaufort scale. A zero reading of the pressure system was taken on the way out of the marina with the sails in their covers. The sails were then hoisted but it was noticed that the zero readings on some taps on the headsail were not taken correctly. These taps were located towards the luff and so a furling method to zero the taps was tried. This seemed to work adequately and it was proved that the taps and A/D chips could handle being loosely furled without damage.

Referring to Figure 7-4, the number 1 course was the jib sweep on starboard (stbd) tack. Number 2 was again the jib sweep but on port. This was followed by the main sweep on port at 3 and then on stbd at 4. Number 5 was the stbd combined sweep. All sweeps were begun with the sails sheeted

tightly in and eased in increments of 100 mm on the sheet. The final trim returned the sails to the initial position of the sweep.

During the tack to port after this sweep the sails accidently were allowed to flog and a pressure tap was dislodged from the headsail but remained attached to the ribbon cable. Repairs were required and so the anchor was dropped in Te Whau Bay on Waiheke Island. A zero reading was taken at this point. Repairs were done and another zero reading was taken. Finally course number 6, the port combined sweep, was done. However the wind had died down and had begun to shift considerably and thus the conditions for this sweep were erratic. It was felt that enough data had been recorded by then to be satisfied with no need for testing the following day.

The sails were less than ideal due to their age. The mainsail clearly was backwinding on most runs and the headsail did not either fly in the typical shape that would be expected.

All the tests were conducted from around 11:30am till 1:00pm on Tuesday 19 July 2011. High tide of 3.1 m occurred at 10:06am on this day (26).

Figure 7-4: Rough representation of the course sailed

7.3 Results for the Full-Scale Test

The results for the full-scale test are presented below.

7.3.1 Full-Scale: Recorded Pressures

The pressure distributions for course 6, the combined sweep on port tack, showed that a couple of taps had been damaged or disconnected. This sweep was therefore unusable and is not presented here. The taps were secured robustly enough to last half a day of regular tacking, hoisting, dropping and furling. It was only when the sails were allowed to flog that any damage occurred. Ideally they should be able to handle this too.

It was extremely fortunate to have had such steady wind for the morning of the testing. The results from the afternoon, once the wind became more erratic, were less useful for direct comparisons

between runs although they still produced consistent results. The malfunctioning of the taps during this run also would have contributed to this.

For the zero readings on some taps very little drift was seen between the readings at the start of the day and those at the end. However in some instances random taps recorded strange values that were extremely high or low. In order to get usable values for post-processing, averages were taken of the different zero readings with the anomalies omitted. These zero values were less than ideal as there was a clear offset between the two tacks for a few taps. For an example refer to

Figure 7-5 where all the pressure curves have a kink in the same direction at the second tap from the leading edge. This indicates that the zero value was too low which resulted in pressures that were too high. For reference the taps generally recorded a positive differential on starboard tack a, i.e. when there was a negative pressure on leeward and positive on windward, and a negative of port.

The attempt to get corresponding results for both tacks was unsuccessful. The fact that the sheets for the headsail were removed the previous day negated the exercise of marking them in corresponding locations. Had this worked well it would have been very useful in determining the correct zero values as a symmetry in the readings would be expected and any deviation from this could be corrected.

The pressure distributions were not similar to what was seen for the Coreflute model testing. This was expected due to the large areas of backwinding on the main and poor behaviour of the headsail. In other words the flying shape was not the same therefore the pressure distribution was not either. Although the distribution shown in

Figure 7-5 is fairly regular, it is of the top stripe on the mainsail it was less affected by backwinding. Figure 7-6 clearly shows the affect where the recorded leading edge pressures were in fact the differential pressure crosses the x axis indicating that there was a positive pressure on leeward. In the end the mainsail displayed the pressure distribution that was expected considering its shape. The high pressure created from the headsail's trailing edge flow impinging on the main created a high pressure on the leeward side thereby resulting in a negative $\triangle C_P$, taking into consideration the sign convention between the two tacks.

Furthermore the pressure tap distribution was not justified due the non-corresponding flying shapes between model- and full-scale. Had they not been backwinding the pressure distribution may have been much more similar. Sail shapes as these have had no previous work conducted on them in regards to pressure measurement. That made it difficult to judge exactly how well the pressures were measured. The full pressure map is shown in the pressure contour plot in Figure 7-7.

Figure 7-8 shows the pressure distribution over the headsail. The expected large pressure peak at the leading edge was not present. The size of the forestay may have influenced the readings.

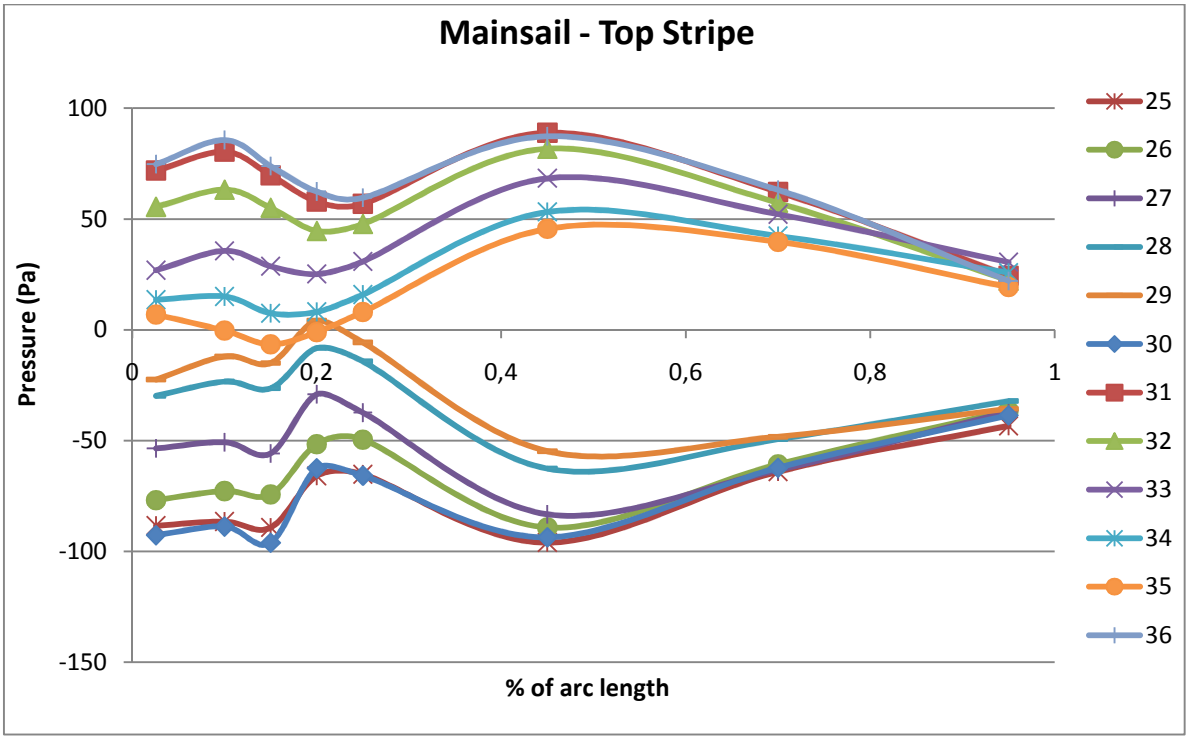

Figure 7-5: Pressure distribution on the main top stripe for main sweep for both tacks

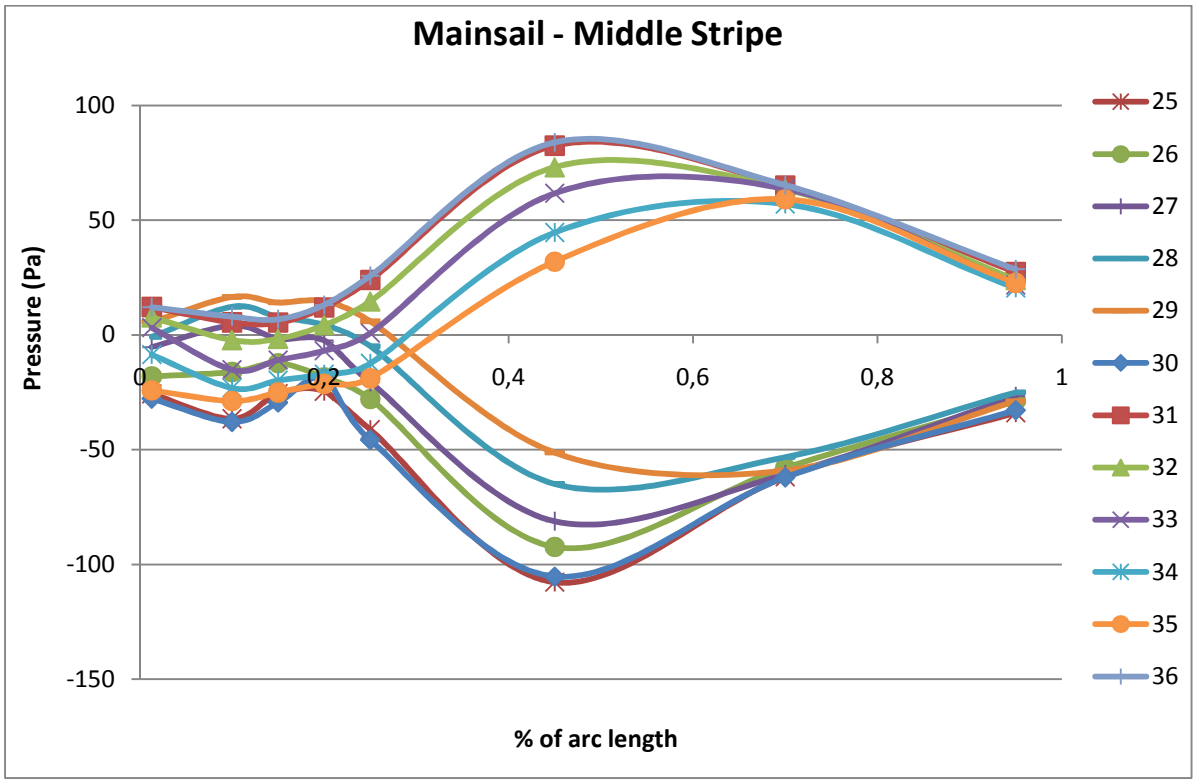

Figure 7-6: Pressure distribution on the main mid stripe for main sweep for both tacks

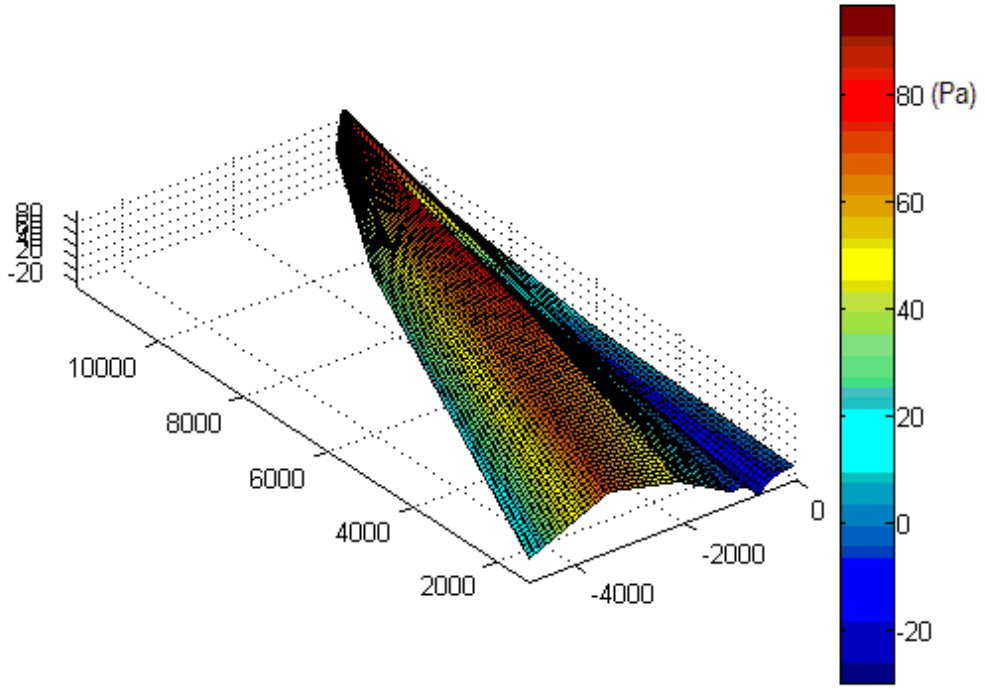

Figure 7-7: Pressure contour plot of full-scale mainsail

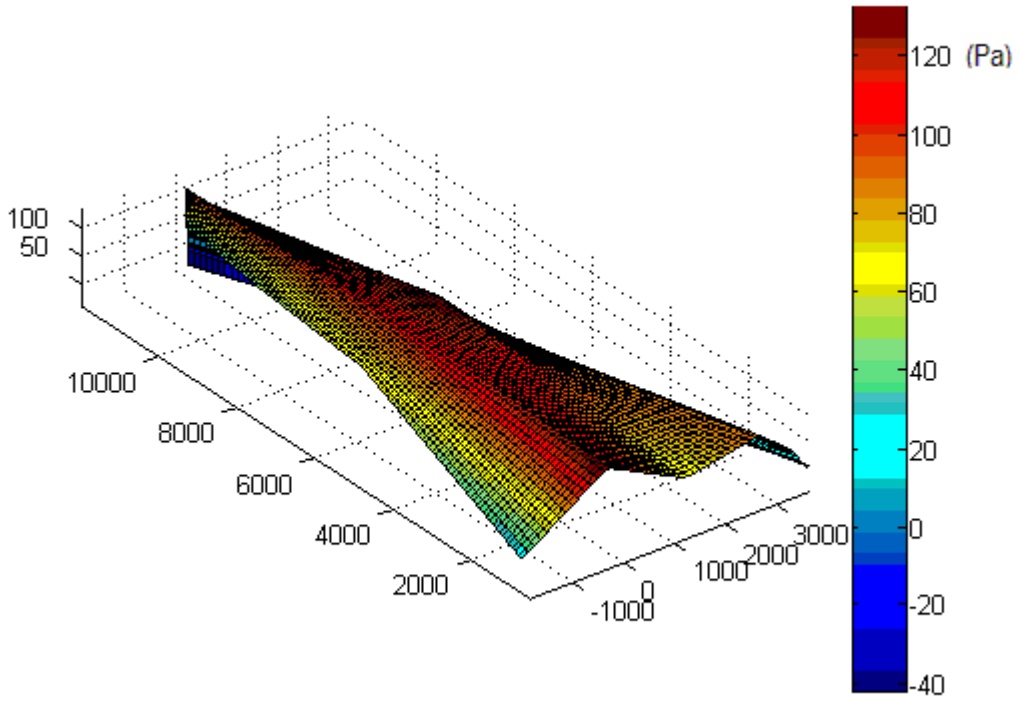

Figure 7-8: Pressure contour plot of full-scale headsail

7.3.2 Full-Scale: Comparison of Various Measurements

Initially the Speed Over Ground (SOG) from the GPS was used to compare with the drive force (F_x) derived from the pressure and shape measurements as the GPS was more trusted than the paddlewheel sensor measuring the boat speed (Vs). Although they displayed similar trends there was a significantly large gap between the two tacks. The comparison then between Vs brought the data points closer together. This may indicate that there was a tidal stream contributing to the SOG. The time of the tests coincided with the strongest tidal streams at mid-tide. The area where course number 1 and 2 were sailed, between the two islands, is believed to have been the most likely areas for this to affect the results. Without actual tidal stream charts available the exact influence cannot be determined, but this did prompt further comparisons to be made using Vs instead.

The data can be seen in Figure 7-9. There was however still a gap between the data points which is unaccounted for. The difference in results between each tack could be due to a variety of reasons. Some boats have a characteristic asymmetry in performance between one side and another due to hull shape or its centre of gravity.

Figure 7-10 shows the drive force compared to boat speed for all the sweeps on the starboard tack. The jib sweep shows an increase in boat speed with an increase in drive force. The main sweep however has roughly the same drive force across the sweep but a range of different boat speeds. The combined sweep, as would be expected, shows characteristics of both.

Figure 7-10 is interesting in that it highlights the contribution from each sail. It is apparent that the headsail provides the majority of the total drive force as there is only a noticeable change in it when the headsail is eased. Normally this difference in contribution may not be as drastic but the backwinding of the main may have seriously reduced the drive force produced by it. However the main still produces a large heeling moment and so when eased the significant reduction in heel increases the boat speed. This is confirmed in Table 7-1 where the heel moment of the main is reduced from 40% to 20% of the total, while for the drive force the main initially only contributes 20% and this is reduced to 10% at the end of the sweep.

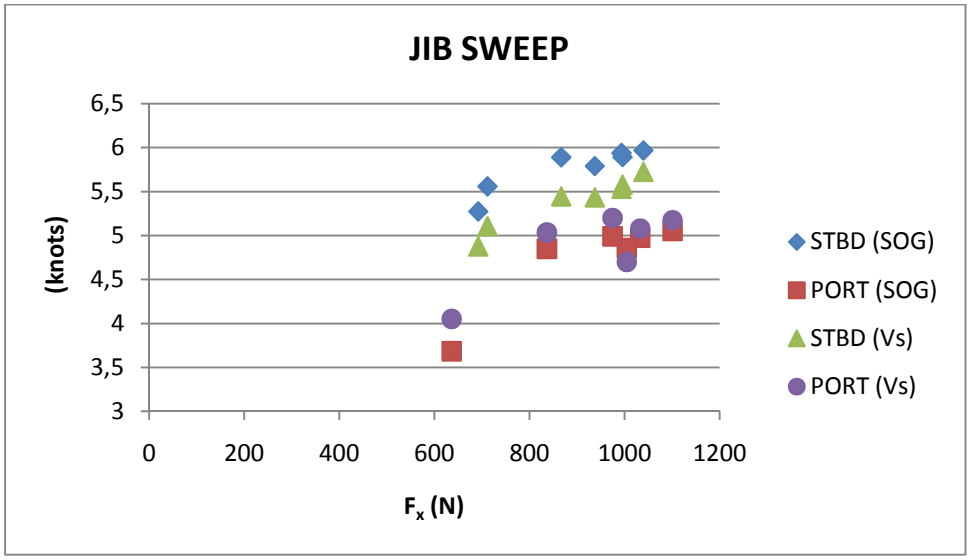

Figure 7-9: Comparison of SOG and Vs to Fx for both jib sweeps

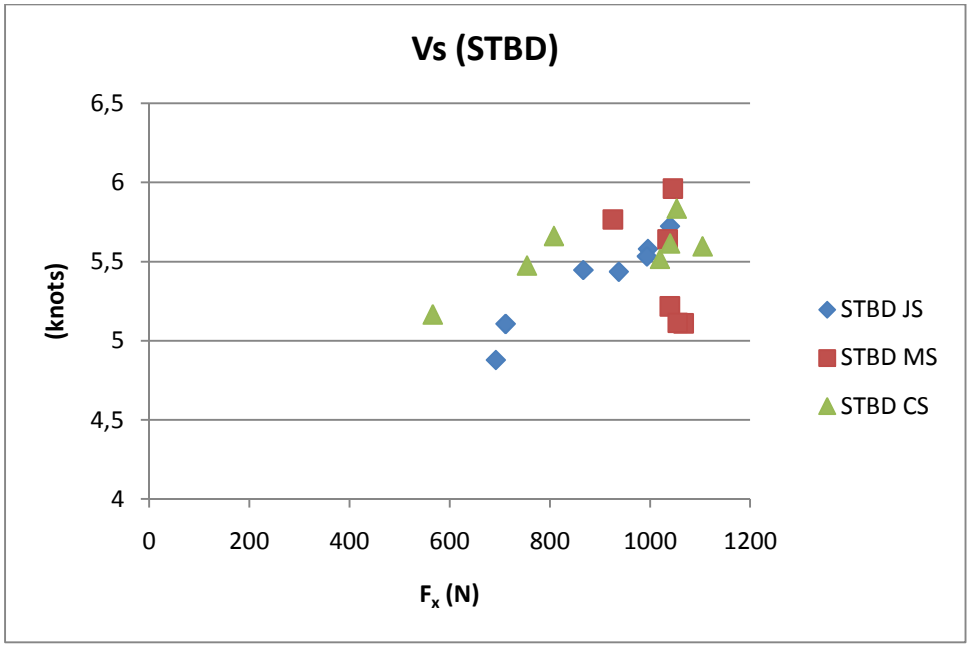

Figure 7-10: Comparison of Vs to F_x for all stbd sweeps

Table 7-1: Relative contribution of main and headsail on F_x and M_x

	Drive Force (N)		Heel Moment (Nm)	
Run #	**Main**	**Head**	**Main**	**Head**
31	253	838	-10516	-14921
32	223	843	-9346	-14850
33	177	888	-7797	-15519
34	118	841	-5817	-14680
35	104	979	-4779	-16007
36	251	828	-10671	-15236

The heel angle was recorded by the IMU at the masthead. This has been compared to the calculated heeling moment in Figure 7-11. The result is a classic righting moment curve.

In Figure 7-12 the heel angle was also compared against the boat speed measured by the paddlewheel sensor. It shows that there is a deterioration in boat speed over a certain heel angle. In this case the maximum boat speed is achieved at a heel angle of 25°. The agreement between the these parameters was very good. As was seen for the model testing the heeling moment is generally better predicted than the drive force.

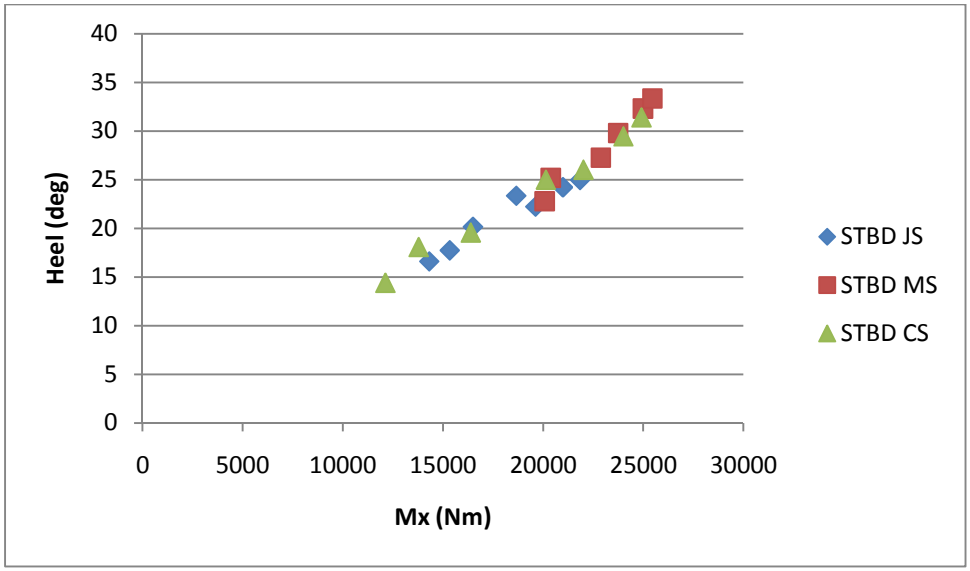

Figure 7-11: Comparison of heel angle to heeling moment for all stbd sweeps

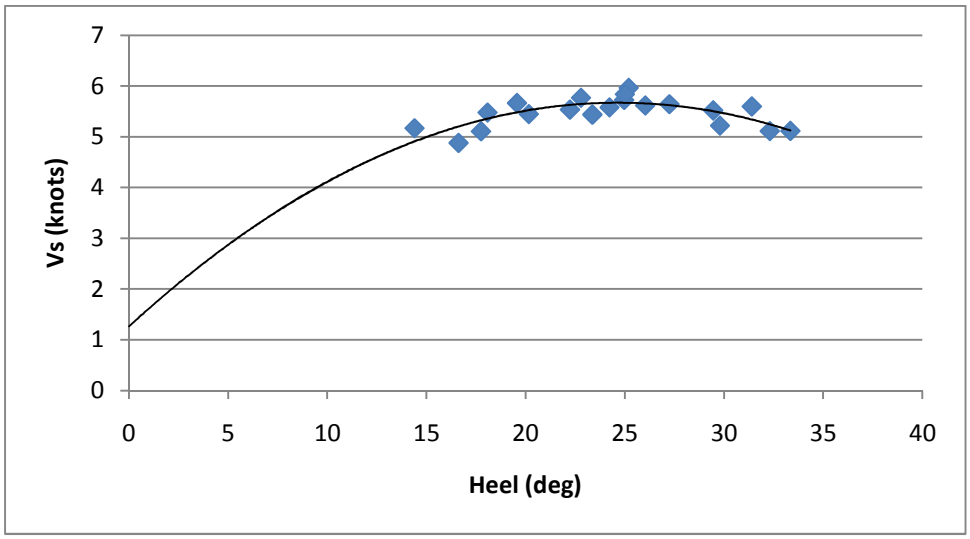

Figure 7-12: Comparison of heeling angle to boat speed for all stbd sweeps

The results for the boat speed compared to the drive force were not quite as expected, although the comparison between the boat speed and heel angle shows that the connection between the former is not as straight forward. In order to clearly see what occurred during the trim all the relevant parameters are shown together for each sweep in Figure 7-13.

For the jib sweep and combined sweep it has already been seen that the boat speed is generally related to the drive force as the sail is eased. The main sweep however clearly shows the inverse relationship of the boat speed to heel angle while the drive force remains relatively constant. These figures again show the strong correspondence between heel angle and heeling moment, while other fluctuations in the trends are likely due to variations in AWS and AWA.

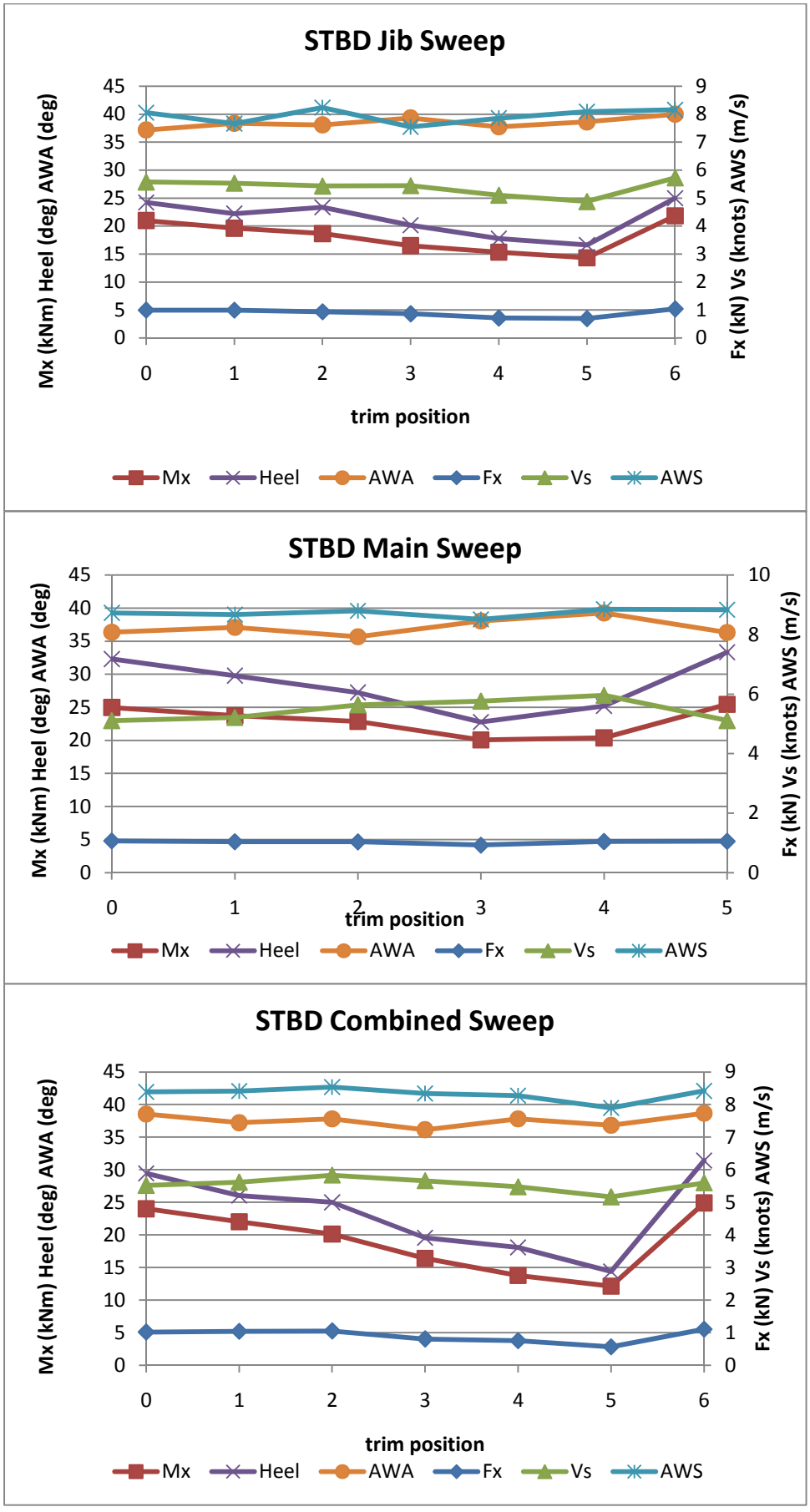

Figure 7-13: Comparison of heeling moment, heel angle, AWA, drive force, boat speed and AWS for all stbd sweeps

7.4 Summary of the Results for the Full-Scale Test

Some of the recorded zeros were not completely trusted but generally the results for the pressure measurements were satisfactory. Pressures were recorded that were of the correct magnitude and showed plausible distributions for the behaviour of the sails. In retrospect some of the test procedure could have been improved for instance the zero readings should have been taken more regularly during the testing and using purpose built covers that ensure no flow resulting in pressure variations.

However, even considering the above, the results were good and showed plausible trends. The contribution to the forces and moments of the each sail shows some interesting relationships between them on what was occurring. This is not possible to see using a force balance in the wind tunnel. Once the system is mature, with most of the limitations dealt with, it could be an interesting tool for further research topics.

The unsteady nature of full-scale testing makes comparison of the results between different runs difficult. Because of this model and numerical testing will never be replaced by full-scale testing, but there certainly is a potential for this system to be used to close the loop between the design and the finished product.

8 General Discussion

The difference between the pressure tappings in the two model tests made for some interesting comparisons.

The placement of the pressures taps proved to be of utmost importance in order to capture the correct pressure distribution. There was no way to determine if a local trough or peak was missed for any particular run and the results had to be used in blind faith that they represented the true values. More work could have been done to predict where the peaks and troughs were likely to occur. For a random sail it would likely have its own optimum tap distribution and therefore a generic sail study is not suitable.

Although the placement is of most importance and accuracy can be improved greatly with a smart distribution the number of taps used plays a large role too. The more taps used the more likely that the critical points would be captured, although the numbers suggested by Graves et al. (12) of 89 differential readings over both sails may be excessive.

There is a price to an increase in tap numbers. The pressure field around a sail appears to be highly sensitive and any interference introduced will affect the flow. The more taps used the more interference there will be. In order to counteract this, the taps could be staggered further apart in the spanwise direction.

A staggered setup goes against the desire for the pressure readings to be as close to the shape inputs as possible. The thought behind this was to ensure accuracy but the results between the model tests proved that this is not necessarily the case. The fact that assumptions can be made to the shape of the foot and head of a sail negates the need to measure the shape in these areas, however the same is not possible for the pressure. In fact it could be said that the increased span between the pressure measurements ensured a greater accuracy. In other words it is far more important for the interpolated values to be as accurate as possible than for the discrete values of the shape and pressure to be measured at the same point.

Where a high density is necessary is the area close to the leading edge of the sail. Arguably this area contributes the most to the drive force due to its orientation and large differential pressures. Thus it is critical that the sail shape and pressure field here are captured correctly. This is where the gradients are highest in the pressure distribution and the curvature is greatest for the sail shape which makes this the most difficult area to measure.

The VSPARS system was not 100% accurate although it was close. However for the cells away from the leading edge where their orientation is more sideways the drive force component is affected more than the side force by a small error in the cells orientation. In other words if the cell's orientation is rotated slightly then the force component in the x direction will be affected by a larger percentage than that for the side force. This has to do with the relative magnitudes of the two components. This again highlights the sensitivity of measuring the drive force compared to the heeling moment.

The easy comparison between the model tests was possible due to the steady conditions and repeatable test procedures. The data captured there was enough to validate the system and prove the value of it. The confidence in the system should then be applicable at full-scale provided the sail

shape and the scale of the taps are held constant. The Full-Scale test in this case resembled the Semi-Rigid test more than the Coreflute. Although not as quantitatively accurate as the Coreflute test, the results from the Semi-Rigid test do provide a qualitative comparison between trim positions. This was proven again in the Full-Scale test although more information was required regarding the conditions to fully understand what was occurring between the different trims.

9 Conclusions

The main aim of the project was achieved. Overall the system proved itself to be a valid method for measuring forces at full-scale, although full-scale testing is unsteady and as such direct comparisons of trim adjustments are difficult. All parameters need to be taken into account when analysing the results.

Using simple interpolations of discrete data points it is possible to recreate a sail's shape and the pressure distribution around it. From this the resultant forces and moments can be derived with reasonable accuracy by discretising the shape into many cells and summing the product of the unit normal vector and area of each cell by the corresponding pressure at their centres.

The pressure distribution over a sail is dynamic; the peaks and troughs migrate and the maximum and minimum pressures fluctuate depending on the sail's trim. The effectiveness of the system developed in this work is dependent on the limited number of pressure taps capturing the local maxima and minima and the transition between them.

The flow over the sail is highly sensitive and the introduction of pressure measuring devices onto the sail's surface will influence the flow and thus the recordings. This can be minimised through the devices shape or size and density around a point on the sail.

10 Recommendations for Future Work

For increased accuracy of the pressure map and therefore the accuracy of the system the following recommendations can be made:

- Test the relative accuracy of the system using varying number of taps and locations, but the following suggestions can be made:
    - Spread the taps widely over the sail from the foot to the head while maintaining a high density at the leading edge.
    - Place the first tap as close as possible to the leading edge. The flow in this area is likely to be separated and so tap aerodynamics is less important. A specialised leading edge tap design could be used.
- Improve the aerodynamics of the taps at full-scale. This can be achieved through an intelligent housing design or by merely reducing the size.

The written code can be improved in the following areas:

- Certain user inputs can be extracted or interpolated from the shape inputs, namely the tack of the run and the camber and draft of the foot of the sail.
- A function should be found for the decrease of the pressure field towards the head and foot and applied to the interpolated field.
- The code should be made to run in real-time thereby information on the quality of the trim can be seen immediately.

More validation of the results would be valuable, namely:

- Precise measurements of the sails' areas should be done to validate the calculated areas.
- Results from a VPP using the calculated forces at full-scale. More hydrodynamic data of the boat used is necessary for this.

The system can be used for further studies in:

- The effect at full-scale of secondary sail controls, such as the main sheet traveller or the jib sheet car.
- The effect at full-scale of various AWA's on the performance of a set of sails.
- The contribution on drive force and heeling moment of each sail when acting together.
- The contribution on drive force and heeling moment of various areas on a sail, e.g. the first 10% of the chord length compared to the rest of the sail or the top half of the sail compared to the bottom.

11 Bibliography

1. **Herman, J. S.** *A Sail Force Dynamometer: Design, Implementation and Data Handling.* Cambridge : Massachusetts Institute of Technology, 1988.

2. *Full Scale Measurement of Sail Force and the Validation of Numerical Calculation Method.* **Masuyama, Y. and Fukasawa, T.** Annapolis : SNAME, 1997. The 13th Chesapeake Sailing Yacht Symposium.

3. **Hochkirch, K.** *Entwicklung einer Meßyacht zur Analyse der Segelleistung im Orginalmaßstab (Design and Construction of a Full-Scale Measurement System for the Analysis of Sailing Performance).* Berlin : Technische Universität Berlin, 2000.

4. *Experimental full scale study on yacht sails and rig under unsteady sailing conditions and comparison to fluid structure interaction unsteady models.* **Augier, B., Bot, P. and Hauville, F.** Chesapeake Bay : s.n., 2011. The Twentieth Chesapeake Sailing Yacht Symposium. pp. 19-32.

5. **Marchaj, C. A.** *Sailing theory and practise.* London : Adlard Coles Limited, 1964.

6. *Full scale investigation of one-design class catamaran sails.* **Puddu, P, et al., et al.** Auckland : s.n., 2006. Proceeding of the Second High Performance Yacht Design Conference. pp. 14-16.

7. *Full-scale pressure measurements on a Sparkman and Stephens 24-foot.* **Viola, I. M. and Flay, R. G. J.** 2010, Journal of Wind Engineering and Industrial Aerodynamics, pp. 800-807.

8. *V-SPARS: A Combined Sail and Rig Shape Recognition System Using Imaging Techniques.* **Le Pelley, D. and Modral, O.** Auckland : University of Auckland, 2008. The Third High Performance Yacht Design Conference. pp. 57-66.

9. *The Aerodynamics of Sail Interaction.* **Gentry, A.** Redondo Beach, California : s.n., 1971. the Third AIAA Symposium on the Aero/Hydronautics of Sailing.

10. *Static pressure distribution over 2D mast/sail geometries.* **Wilkinson, S.** 1989, Journal of Marine Technology 26 (4), pp. 333–337.

11. *Experimental considerations concerning pressure measurements on sails: Wind Tunnel and Full-Scale.* **Flay, R. J. and Millar, S.** Auckland : s.n., 2006. The Second High Performance Yacht Design Conference. pp. 123-130.

12. *Measurements and simulation of pressure distribution on full size scales.* **Graves, W., et al., et al.** Auckland : s.n., 2008. ProceedingsoftheThirdHighPerformance YachtDesignConference. pp. 2-4.

13. *Wind tunnel and CFD modelling of pressures on downwind sails.* **Richards, P J and Lasher, W C.** Milan : s.n., 2008. Proceedings of the Sixth International Colloquium on Bluff Bodies Aerodynamics & Applications. pp. 20-24.

14. *Force and pressure investigation of modern asymmetric spinnakers.* **Viola, I. M. and Flay, R. G. J.** 2009, International Journa lof Small Craft Technology, pp. 31–40.

15. *Comparison of Potential Flow-Based and Measured Pressure Distributions over Upwind Sails.* **Fluck, M., et al., et al.** 2010, Journal of Aircraft, pp. 2174-2177.

16. **Hansen, H.** *Enhanced Wind Tunnel Techniques and Aerodynamic Force Models for Yacht Sails.* s.l. : PhD Thesis, University of Auckland, 2006.

17. *12 meter design: state of the art in 1986.* **van Hemmen, R. F.** s.l. : Marine Technology, 1986, Marine Technology, pp. 320-338.

18. *Modelling IACC Sail Forces by Combining Measurements with CFD.* **Milgram, J. H., Peters, D. B. and Eckhouse, D. N.** Chesapeake Bay : s.n., 1995. The Eleventh Chesapeake Sailing Yacht Symposium. pp. 65-73.

19. **Fossati, F.** *Aero-Hydrodynamics and the Performance of Sailing Yachts. The Science behind Sailing Yachts and their Design.* Milan : International Marine/McGraw-Hill, 2009.

20. **Larsson, L. and Eliasson, R. E.** *Principles of Yacht Design.* Camden, Maine : International Marine/McGraw-Hill, 2007.

21. *Pressure Measurements on Full-Scale and Model-Scale Upwind Sails.* **Viola, I.M., Gauvain, E. and Flay, R.G.J.** Auckland : s.n., 2010. 17th Australasian Fluid Mechanics Conference.

22. **White, F. M.** *Fluid Mechanics.* New York : McGraw-Hill, 2008.

23. *The Use of Independent Supports and Semi-Rigid Sails in Wind Tunnel Studies.* **Richards, P., et al., et al.** Auckland : University of Auckland, 2006. The Second High Performance Yacht Design Conference. pp. 114-122.

24. **Viola, I. M.** *PMonS overview report.* Auckland : Internal report for YRU (UoA).

25. **Le Pelley, D.** *Wired Pressure System (Internal report for the YRU).* 2011.

26. *http://www.linz.govt.nz/hydro/tidal-info/tide-tables/index.aspx.* Land Information New Zealand : s.n., 07/08/2011.

27. **Jr., James Stackpole Herman.** *A Sail Force Dynamometer: Design, Implementation and Data Handling.* Cambridge : Massachusettes Institute of Technology, 1988.

APPENDIX 1 – Base Code

```
%%%%%%%%%%%%%%%%%%%%%%%%%%%%%%% BASE CODE %%%%%%%%%%%%%%%%%%%%%%%%%%%%%%%%%
clear all
close all
clc
clf

%% %%%%%%%%%%%%%%%%%%%%%%%%%%%%%% INPUTS %%%%%%%%%%%%%%%%%%%%%%%%%%%%%%%%%%%
global l lp N res pressures heel tack pressures_display sr fr Pplot Pchord;

%Sail generation only (0)
%or pressure integration included (1)??
pressures = 1;

%Displays
sails_low_display = 0;     %surface plot of sail shape - initial resolution
sails_high_display = 0;       %surface plot of sail shape - high resolution
pressures_display = 1;           %contour plot of pressures over the sails
Pplot = 0;                      %pressure plot along chords for full scale
Pchord = 0;      %plot of measured and interpolated pressures along a chord
Pcheck = 0;           %writes measured pressures to excel (full scale only)
tap_distr = 0;                  %pressure point distribution over the sails

%%%Specify test runs for computation:
sr = 18;                                                  %start of sweep: run#
fr = 23;                                                 %finish of sweep: run#

size = 1 + fr-sr;                                                %number of runs

%%%Specify which tack the run was recorded on
%PORT(1) or STBD(2)
tack = 1;

%Heel angle of test runs
heel = 20;

%%%Specify chordwise resolution for interpolated data points
l = 0 : 1/50 :  1;             %chord-wise arc% resolution for shape points
N = length(l);                                  %number of points chord-wise

%%%Calculate arc% for pressure points (halfway between shape points)
lp(N-1) = 0;
for i = 1:N-1
    lp(i) = l(i) + 0.5 * (l(i+1) - l(i));
end

%%%Specify spanwise resolution for interpolated data points
res = 100;              %span-wise resolution of pressure (shape = res + 1)

%%%Specify Data file
file_D = 'Data\File D\full scale';

%%%Specify Pressure file
file_P = 'full scale';

Result(size, 8) = 0;                                %initialise result matrix
c = 0;                                             %loop counter for each run
```

```
%Loop for each test run specified for computation
for run = sr:fr;

%%%Specify VSPARS file for Mainsail
M_VSPARS = sprintf...
    ('Full Scale\\VSPARS\\Jib Sweep PORT 18-23\\Main\\%d.txt', run);

%%%Load sail data sheet
M_sheet = 'Main';                  %name of relevant sheet in excel data doc
[num] = xlsread(file_D, M_sheet);                           %read excel file

Mst = num(1,1);                                        %sail type mainsail = 1
M_NoSS = num(1,2);                    %number of shape stripes on each sail
M_NoSP = num(1,3);                      %number of pressure stripes
Ml_h = num(1,4);                                          %length of head
Ml_f = num(1,5);                                          %length of foot
Mz_h = num(1,6);                                          %height of head
Mz_f = num(1,7);                                          %height of foot
Mclew = num(1,8);                                %position of clew along boom

%%%Specify VSPARS file for Headsail
H_VSPARS = sprintf...
    ('Full Scale\\VSPARS\\Jib Sweep PORT 18-23\\Head\\%d.txt', run);

%%%Load sail data sheet
H_sheet = 'Jib';                   %name of relevant sheet in excel data doc
[num] = xlsread(file_D, H_sheet);                           %read excel file

Hst = num(1,1);                                     %sail type jib/genoa = 2
H_NoSS = num(1,2);                    %number of shape stripes on each sail
H_NoSP = num(1,3);                      %number of pressure stripes
Hl_h = num(1,4);                                          %length of head
Hl_f = num(1,5);                                          %length of foot
Hz_h = num(1,6);                                          %height of head
Hz_f = num(1,7);                                          %height of foot
%Hx_h = num(1,9);                             %distance of head fore of mast
H_leech = num(1,10);                                      %length of leech

%% %%%%%%%%%%%%%%%%%%%%% SAIL SHAPE GENERATION %%%%%%%%%%%%%%%%%%%%%%%%%%%%
%%%Import data from VSPARS and manipulate into usable structure
[Mx, My, Mz] = extract_data3D (M_VSPARS, M_NoSS, Mst);
[Hx, Hy, Hz] = extract_data3D (H_VSPARS, H_NoSS, Hst);

%%%Extrapolate to get points for the head and foot of the sail
[MX MY MZ] = get_head_foot (Mx, My, Mz, Ml_h, Mz_f, Mz_h, Mclew, Ml_f,...
    Mst, M_NoSS);
[HX HY HZ] = get_head_foot (Hx, Hy, Hz, Hl_h, Hz_f, Hz_h, 0, Hl_f,...
    Hst, H_NoSS);

%%%Increase number of data points to desired resolution
[MXr, MYr, MZr, MPZr] = resolution(MX, MY, MZ, M_NoSS, Mst);
[HXr, HYr, HZr, HPZr] = resolution(HX, HY, HZ, H_NoSS, Hst);

%%%Trim and scale jib foot to correct dimensions
[HX_new, HY_new, HZ_new, HPZr] = jib_foot(HXr, HYr, HZr, Hl_f, H_leech);

%%%Calculate normals on sail surface
[Mnx, Mny, Mnz] = normals(MXr, MYr, MZr);
```

```
[Hnx, Hny, Hnz] = normals(HX_new, HY_new, HZ_new);

%%%Calculate sail areas
M_SA = sqrt(sum(sum(Mnx))^2 + sum(sum(Mny))^2 + sum(sum(Mnz))^2)/2;
H_SA = sqrt(sum(sum(Hnx))^2 + sum(sum(Hny))^2 + sum(sum(Hnz))^2)/2;

%% %%%%%%%%%%%%%%%%% PRESSURE INTEGRATION OVER THE SAIL %%%%%%%%%%%%%%%%%%%
if pressures == 1
%%%Extract & isolate pressure data from file
[MP, M_tapno] = pressureA(file_P, file_D, run, M_NoSP, Mst, M_sheet);
[HP, H_tapno] = pressureA(file_P, file_D, run, H_NoSP, Hst, H_sheet);

%%%Interpolate measured pressures to desired resolution
[MPrh, MPYrh, MPXrh, MPs] = pressresoA(file_D, M_sheet, M_NoSP,...
    MXr, MYr, MZr, MP, MPZr, M_tapno, Mst, run);
[HPrh, HPYrh, HPXrh, HPs] = pressresoA(file_D, H_sheet, H_NoSP,...
    HX_new, HY_new, HZ_new, HP, HPZr, H_tapno, Hst, run);

%%%Calculate forces in x,y,z directions
[MFx, MFy, MFz] = forces(MPrh, Mnx, Mny, Mnz);
[HFx, HFy, HFz] = forces(HPrh, Hnx, Hny, Hnz);

%%%Sum the forces from the main and foresail
FX = sum(sum(MFx)) + sum(sum(HFx));
FY = sum(sum(MFy)) + sum(sum(HFy));
FZ = sum(sum(MFz)) + sum(sum(HFz));

%%%Calculate the heeling moment
[MRM, MYM] = moments(MFx, MFy, MFz, MPZr, MPYrh, MPXrh);
[HRM, HYM] = moments(HFx, HFy, HFz, HPZr, HPYrh, HPXrh);

%%%Sum the moments from the main and foresail
ARM = HRM + MRM;
AYM = HYM + MYM;

%%%Step the loop counter before recording
c=c+1;

%%%Record the measured pressures (full scale only)
if Pcheck == 1
    presscheck(1:24,1) = [MPs(1:8, 3);MPs(1:8, 2);MPs(1:8, 1)];
    presscheck(1:24,run+1) = [MP(1:8, 3);MP(1:8, 2);MP(1:8, 1)];

    presscheck(26:49,1) = [HPs(1:8, 3);HPs(1:8, 2);HPs(1:8, 1)];
    presscheck(26:49,run+1) = [HP(1:8, 3);HP(1:8, 2);HP(1:8, 1)];
end

%%%Record the forces and heeling moment for each run
Result(c,:) = [run, FX, ARM, FY, FZ, H_SA, M_SA, AYM];

end
end

%%%Write the final result to excel
xlswrite('Result', Result);
if Pcheck == 1
xlswrite('Presscheck', presscheck);
end
```

APPENDIX 2 – Formulas used in Code

Cross-Product Theorem

This theorem proves that the magnitude of the normal calculated using the cross product of two diagonals of a quadrilateral is equal to twice the projected area in each direction

This proof is shown for a rectangle but it can easily be extended for any quadrilateral.

Given the rectangle:

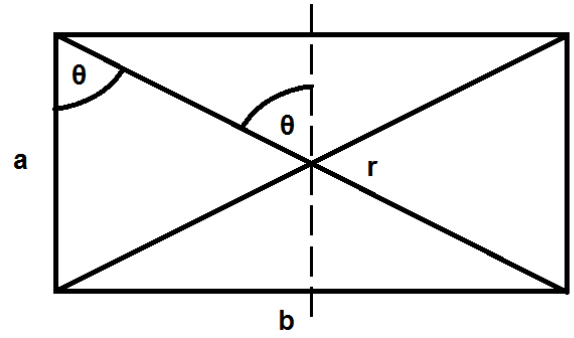

Where a and b are the lengths of the sides and r is the length of the diagonals and θ is the angle between the diagonal and the short side. The area of this rectangle is therefore ab.

We know that the cross product of 2 vectors equals their magnitudes multiplied by each other times by the sine of the angle between them. It can also be seen that the angle between then equals 2θ. Therefore:

$$rxr = r^2 \sin 2\theta$$

$$= r^2 \, 2\sin\theta \cos\theta$$

$$= 2r^2 \frac{b}{r}\frac{a}{r}$$

$$= 2ab$$

Arc Length

For the task of calculating the arc lengths of curves such as the chordwise sections of the sail an iterative calculation is used which approaches the actual value by increasing the number of data points. For a simple explanation refer to Figure 11-1

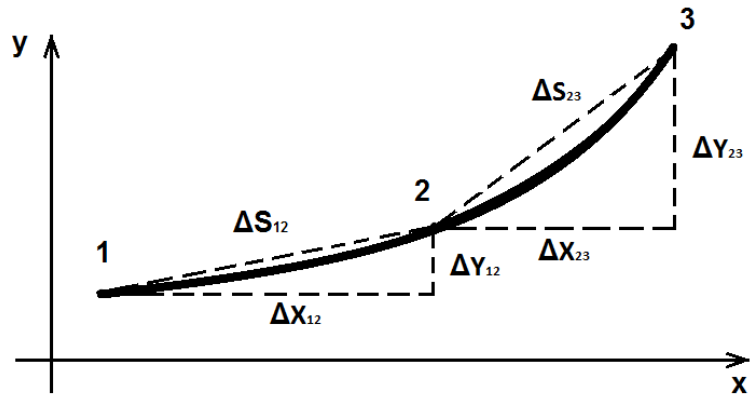

Figure 11-1: Calculation of arc length

Using Pythagoras it is possible to find the straight line distance between two points from their X and Y coordinates.

$$\Delta s_{12} = \sqrt[2]{(x_2 - x_1)^2 + (y_2 - y_1)^2} \tag{A2.1}$$

Then for n number of points the curve length s equals:

$$s = \sum_{i=1}^{n} \sqrt{\Delta x_i^2 + \Delta y_i^2} \tag{A2.2}$$

Least Squares Curve Fitting

For a k^{th} degree polynomial:

$$y = a_0 + a_1 x + \cdots + a_k x^k, \tag{A2.3}$$

the residuals can be described as:

$$R^2 = \sum_{i=1}^{n} \left[y_i - \left(a_0 + a_1 x_i + \cdots + a_k x_i^k \right) \right]^2. \tag{A2.4}$$

By taking the partial derivatives:

$$a_0 n + a_1 \sum_{i=1}^{n} x_1 + \cdots + a_k \sum_{i=1}^{n} x_i^k = \sum_{i=1}^{n} y_i \tag{A2.5}$$

This polynomial can be written:

$$\begin{bmatrix} y_1 \\ y_2 \\ \vdots \\ y_n \end{bmatrix} = \begin{bmatrix} 1 & x_1 & \cdots & x_1^k \\ 1 & x_2 & \cdots & x_2^k \\ \vdots & \vdots & \ddots & \vdots \\ 1 & x_n & \cdots & x_n^k \end{bmatrix} \begin{bmatrix} a_0 \\ a_1 \\ \vdots \\ a_k \end{bmatrix}$$

or expressed as:

$$\mathbf{y} = \mathbf{X}\mathbf{a} \tag{A2.6}$$

To solve for $\mathbf{a}$ premultiply by $\mathbf{X^T}$:

$$\mathbf{X^T y} = \mathbf{X^T X a} \tag{A2.7}$$

and then:

$$\mathbf{a} = \left(\mathbf{X^T X} \right)^{-1} \mathbf{X^T y} \tag{A2.8}$$

APPENDIX 3 – Pressure Tap Testing

Taps for the Semi-Rigid Sails

The results of the test of the taps referred to in section 5.1.1 are shown here. They were placed on the headsail of the Semi-Rigid model along a line of constant percentage of chord length. The sail was then trimmed in a sweep starting from tightly trimmed in. The vertical order of the taps was then varied to make sure that the results were consistent.

The results are referenced to the flush mounted tap. It can clearly be seen that the block tap was not suitable for testing and had to be discarded. The coin tap was not ideal either but there were no other taps available. The results are presented in Figure 11-2 and

Table 11-1:

Table 11-1: Table of average difference of different model-scale tap geometries

	Coin	Block
Avg Diff (Pa)	0.82	1.82
Avg Diff (%)	14	31

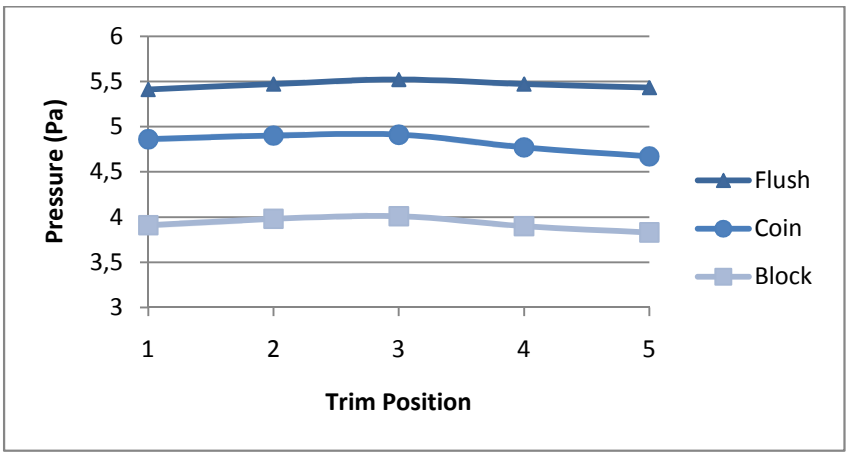

Figure 11-2: Graph of pressure readings for model-scale taps for one sweep of the headsail

Various Full-Scale Tap Geometries

The pressure system developed for full-scale required taps that encased the transducer. This limited the minimum thickness of the tap to 9mm. This is a significant thickness and therefore the geometry of the tap had to be designed to minimise the influence on the flow.

Mock-ups of a range of pressure taps were fabricated out of MDF with varying side gradients and curvatures. They were tested for a range of AoA but they were all deemed unsuitable as they did not follow the trend of the reference pressure. The standard deviation ranged from 0.7 – 1.5.

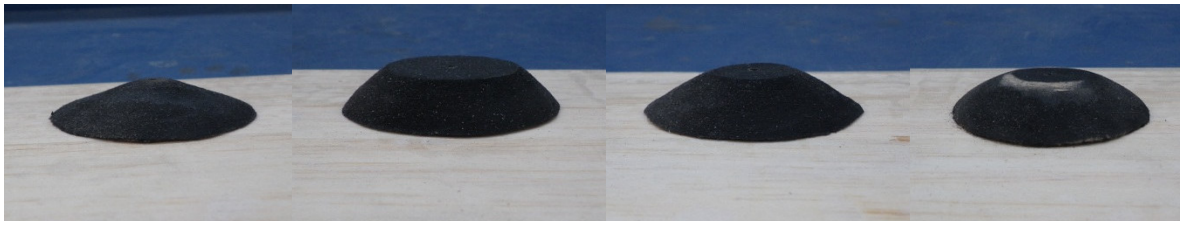

Figure 11-3: Various tap geometries (from L-R: Volcano, Steep, Gradual, Rounded)

Table 11-2: Table of average difference and standard deviations for various full-scale tap geometries

	Volcano	Steep	Gradual	Rounded
Avg Diff (Pa)	1.24	1.73	1.01	0.94
Std Dev (Pa)	1.01	1.52	0.70	0.68

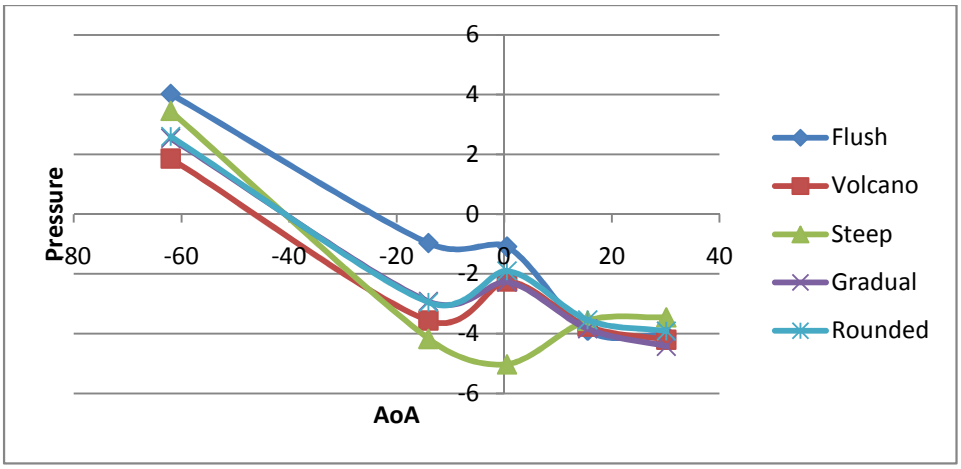

Figure 11-4: Graph of pressure readings for various full-scale tap geometries

Full-Scale Taps with Sail Patches

The next step was to test the same sized tap, with suitable dimensions to house the transducer, but covered with a patch of sail cloth. The patches used were circular and a range of patch diameters were tested. They were mounted on a flat plate and tested at a range of AoA's. These were again referenced to a flush mounted PVC tube.

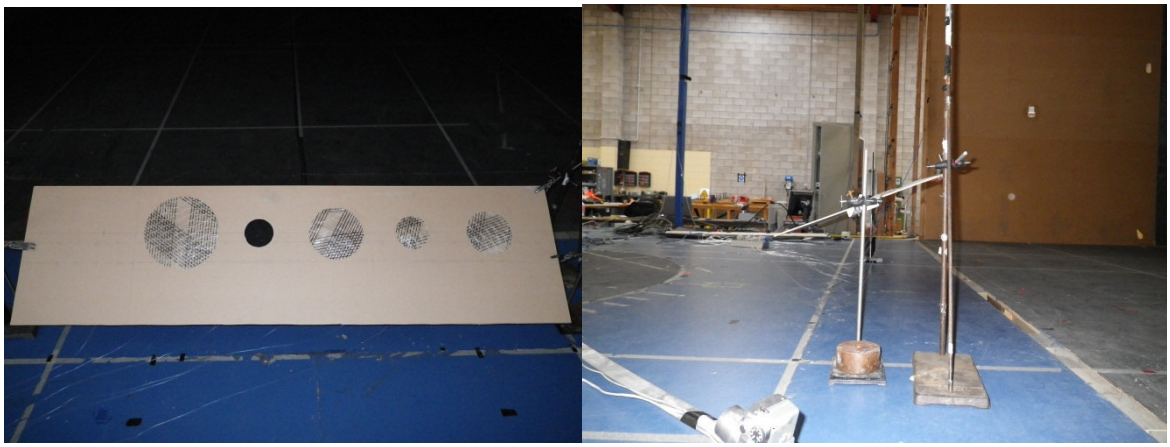

Figure 11-5: Top and side views of the testing of full-scale pressure taps

Table 11-3: Table of average difference and standard deviations for full-scale taps with sail patches

	Blocks with patches of sail - Diameter (mm)			
	270	200	165	120
Avg Diff (Pa)	0.86	1.16	0.82	0.65
Std Dev (Pa)	0.48	0.53	0.44	0.64

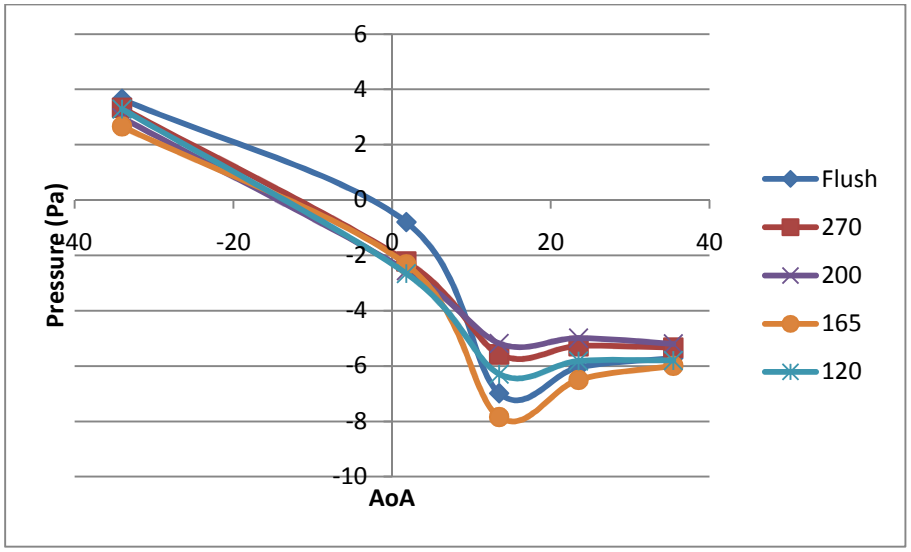

Figure 11-6: Graph of pressure readings for full-scale taps with sail patches

Although the D120 tap recorded values closer to the reference pressure than that of the D165, its standard deviation was higher. This is evident of the curve's intersection with the reference curve. Therefore the D165 patch was chosen for the full-scale measurements.

Note that the patches actually used in testing are square. The circular shape was exceedingly difficult to affix without distorting the shape. The sides of the square patch were then made to be 165mm.

APPENDIX 5 – Pressure Tap Locations

(Locations given in percent of arc length across a chord)

Semi-Rigid Sails

Mainsail	Tap	1	2	3	4	5	6	7
Stripe	0.25H	0.02	2.6	5.9	10	37	70	97
	0.50H	0.01	2.7	5.9	10	37	62	97
	0.75H	0.01	2.7	6.0	16	46	99	
	0.875H	0.01	2.7	11	30	62	97	

Headsail	Tap	1	2	3	4	5	6	7
Stripe	0.25H	0.03	2.4	5.5	10	29	70	94
	0.50H	0.02	2.6	5.8	10	22	77	94
	0.75H	0.01	2.7	5.9	10	30	62	89

Coreflute Sails

Mainsail	Tap	1	2	3	4	5	6	7	8	9	10	11
Stripe	0.90H	3.6	12	29	36	60	78	97				
	0.71H	2.2	2.9	5	9	14	22	36	40	48	86	
	0.43H	4.6	9.4	15	20	26	31	37	42	60	71	96
	0.14H	1.8	3.7	6.4	9.3	15	19	28	32	35	45	92

Headsail	Tap	1	2	3	4	5	6	7	8	9	10	11	12	13
Stripe	0.80H	9.5	17	25	32	41	52	72	92					
	0.58H	5.4	9.4	15	19	22	34	54	72					
	0.37H	4.1	10	12	23	29	39	51	64	78	91			
	0.16H	3.3	5.4	12	14	16	23	25	32	37	48	59	79	90

Full-Scale Sails

Mainsail	Tap	1	2	3	4	5	6	7	8
Stripe	0.25H	2.6	10	15	20	25	45	70	95
	0.50H	1.3	10	15	20	25	45	70	95
	0.75H	0.9	10	15	20	25	45	70	95

Headsail	Tap	1	2	3	4	5	6	7	8
Stripe	0.25H	3.0	4.0	8.0	12	24	48	72	96
	0.50H	1.3	4.0	8.0	12	24	48	72	96
	0.75H	0.8	4.0	8.0	12	24	48	72	96

APPENDIX 5 – Results

Results for the Semi-Rigid Test

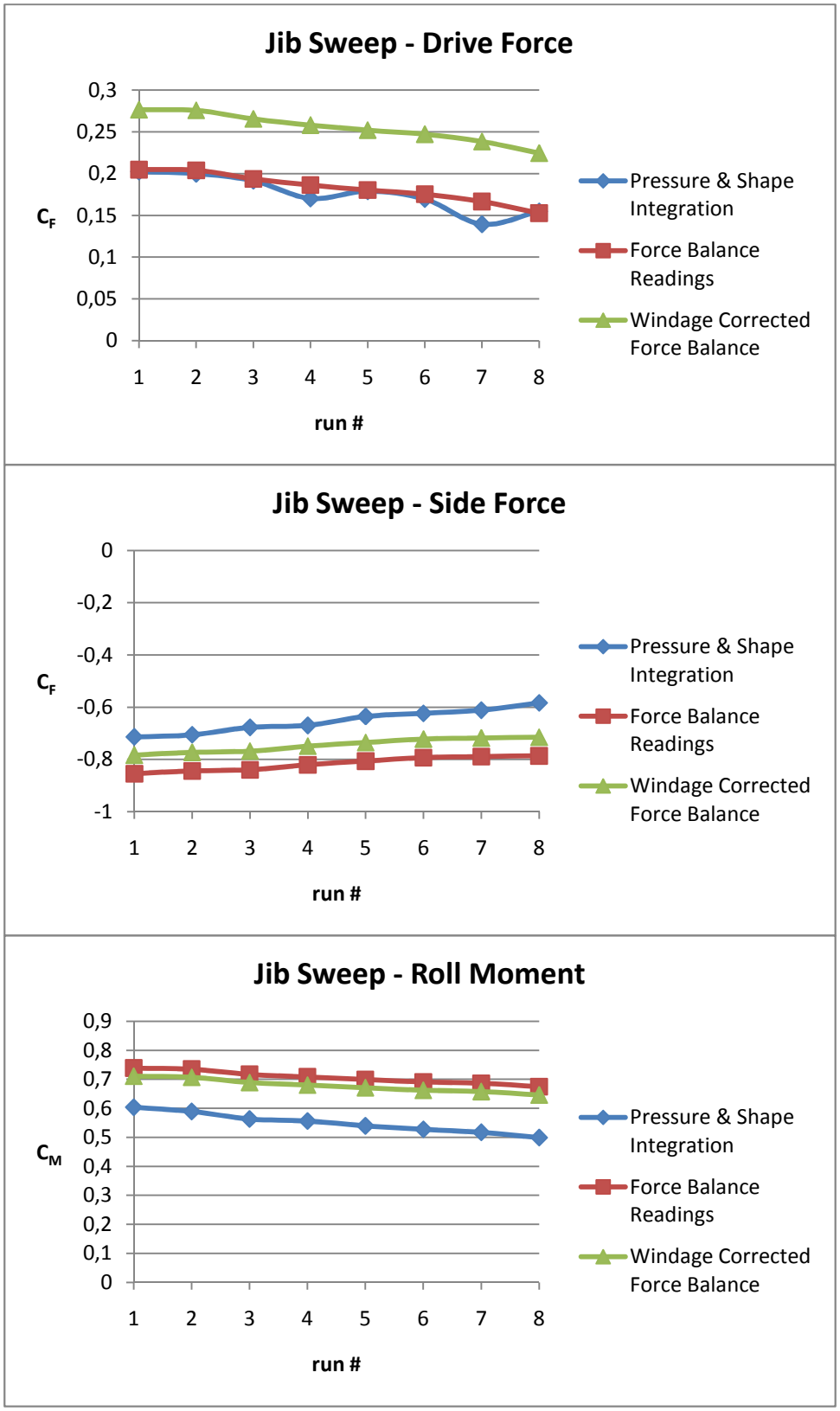

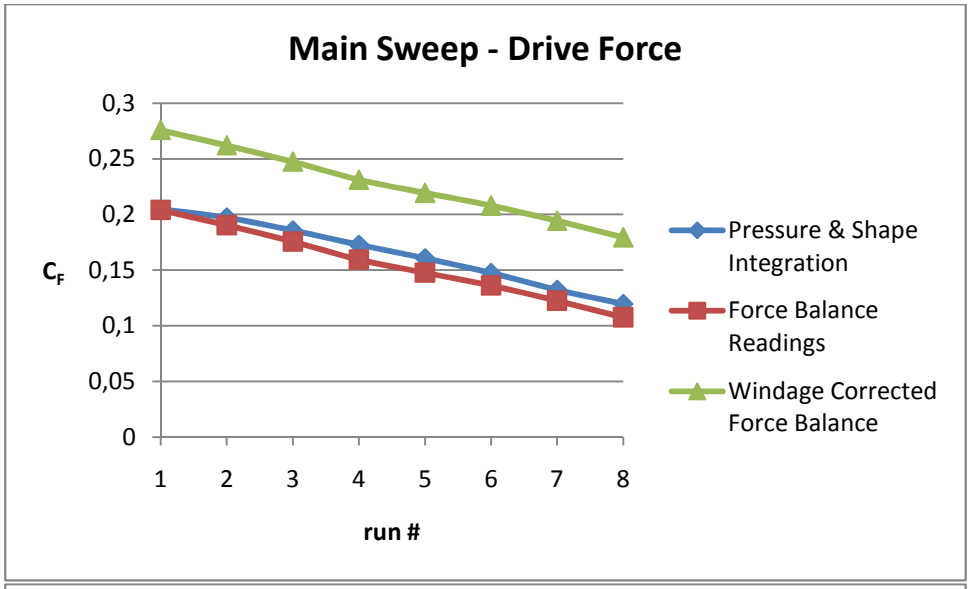
Main Sweep - Drive Force
0,3
0,25
0,2
0,15
0,1
0,05
0
C_F
1 2 3 4 5 6 7 8
run #
Pressure & Shape Integration
Force Balance Readings
Windage Corrected Force Balance


Main Sweep - Side Force
0
-0,1
-0,2
-0,3
-0,4
-0,5
-0,6
-0,7
-0,8
-0,9
-1
C_F
1 2 3 4 5 6 7 8
run #
Pressure & Shape Integration
Force Balance Readings
Windage Corrected Force Balance

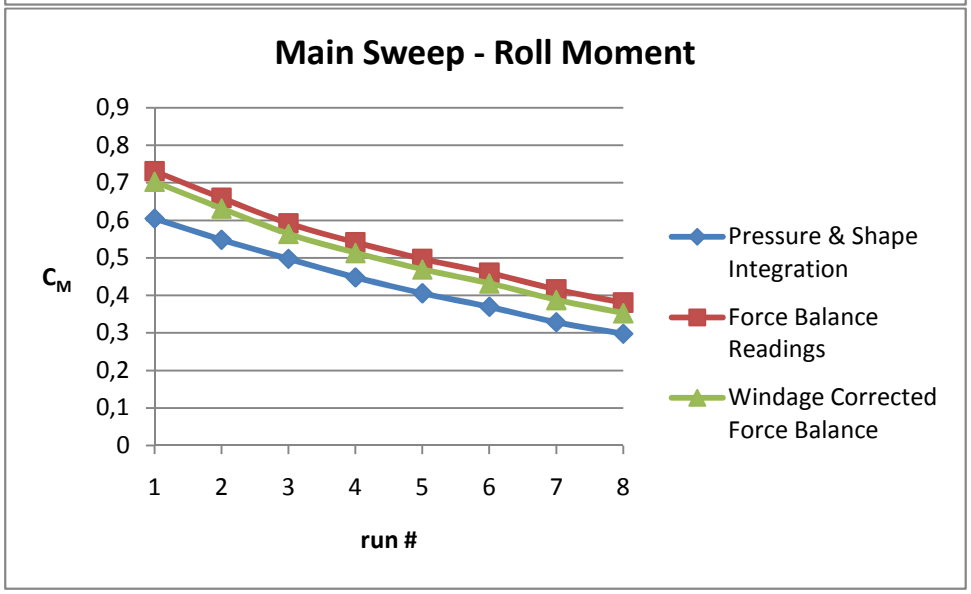
Main Sweep - Roll Moment
0,9
0,8
0,7
0,6
0,5
0,4
0,3
0,2
0,1
0
C_M
1 2 3 4 5 6 7 8
run #
Pressure & Shape Integration
Force Balance Readings
Windage Corrected Force Balance

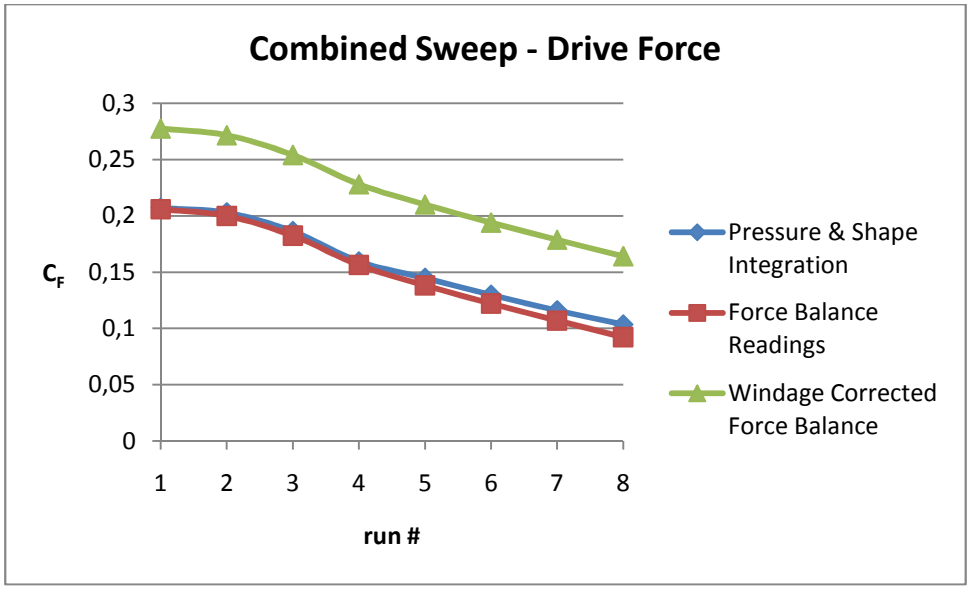
Combined Sweep - Drive Force
0,3
0,25
0,2
0,15
0,1
0,05
0
C_F
1
2
3
4
5
6
7
8
run #
Pressure & Shape Integration
Force Balance Readings
Windage Corrected Force Balance

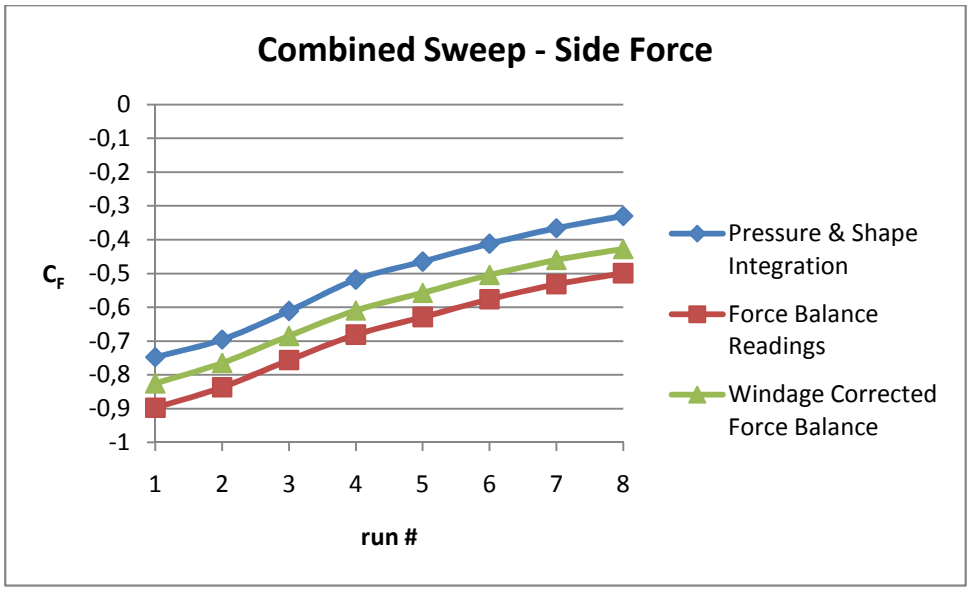
Combined Sweep - Side Force
0
-0,1
-0,2
-0,3
-0,4
-0,5
-0,6
-0,7
-0,8
-0,9
-1
C_F
1
2
3
4
5
6
7
8
run #
Pressure & Shape Integration
Force Balance Readings
Windage Corrected Force Balance

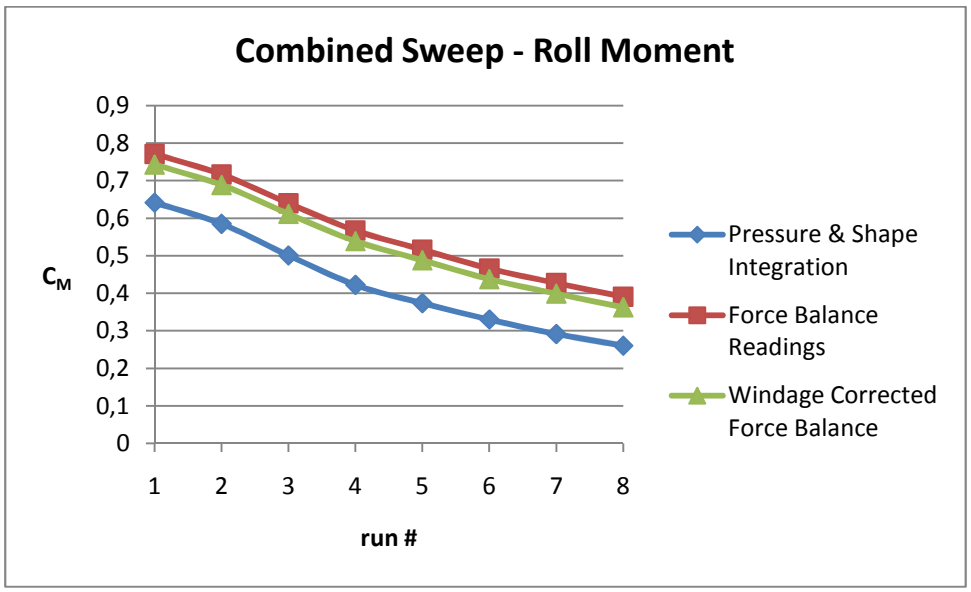
Combined Sweep - Roll Moment
0,9
0,8
0,7
0,6
0,5
0,4
0,3
0,2
0,1
0
C_M
1
2
3
4
5
6
7
8
run #
Pressure & Shape Integration
Force Balance Readings
Windage Corrected Force Balance

Results for the Coreflute Test

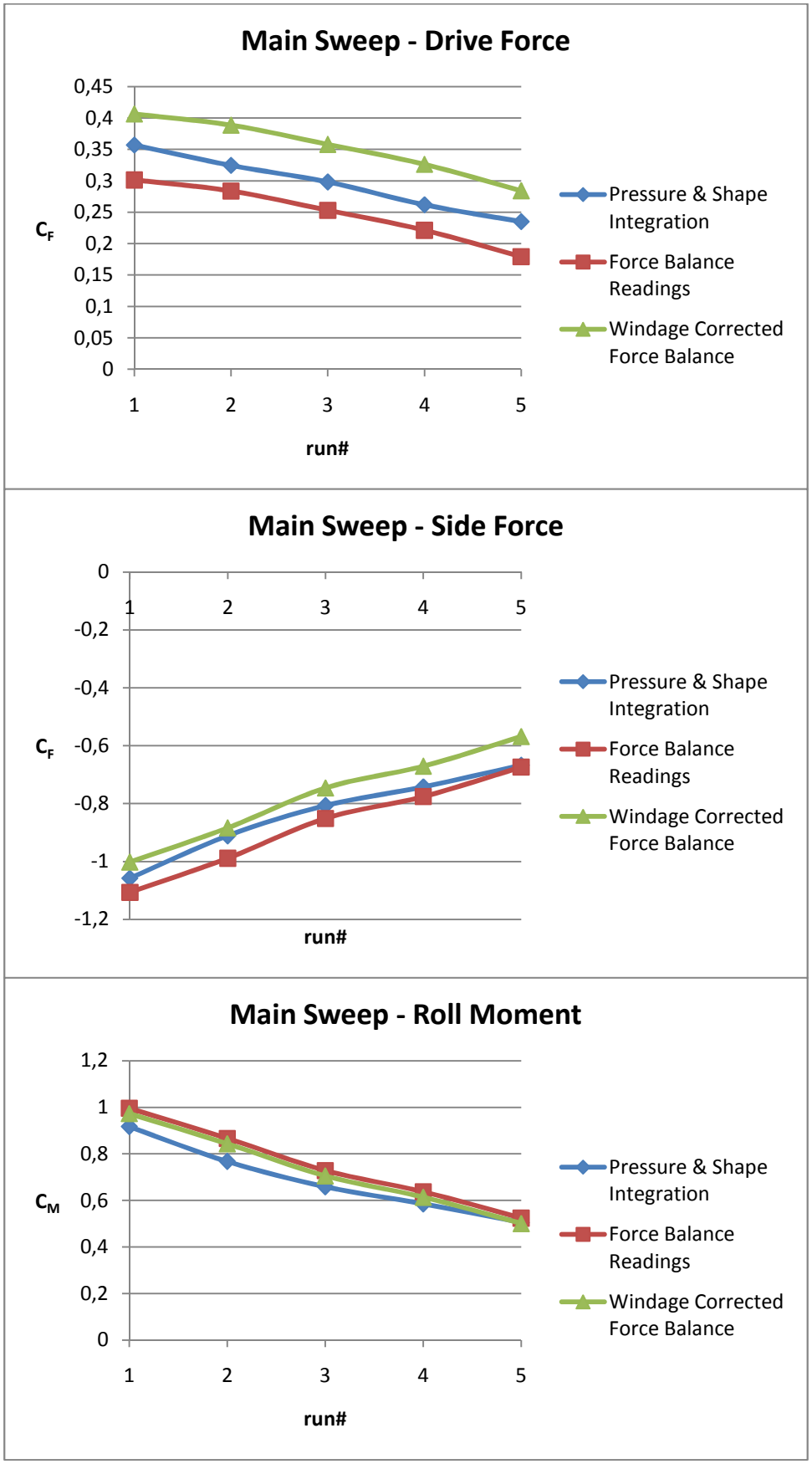

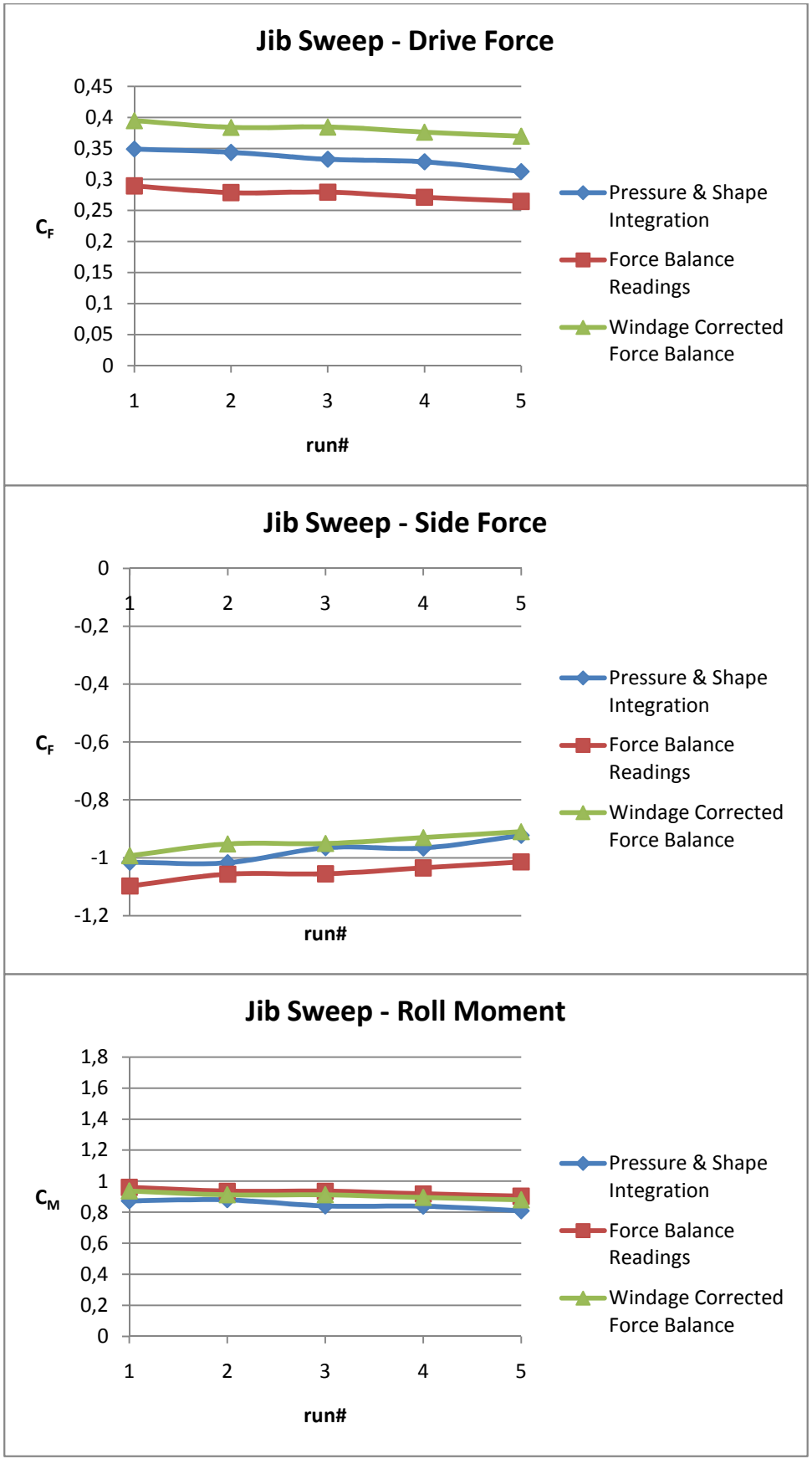
Jib Sweep - Drive Force
0,45
0,4
0,35
0,3
0,25
0,2
0,15
0,1
0,05
0
C_F
1
2
3
4
5
run#
Pressure & Shape Integration
Force Balance Readings
Windage Corrected Force Balance
Jib Sweep - Side Force
0
-0,2
-0,4
-0,6
-0,8
-1
-1,2
C_F
1
2
3
4
5
run#
Pressure & Shape Integration
Force Balance Readings
Windage Corrected Force Balance
Jib Sweep - Roll Moment
1,8
1,6
1,4
1,2
1
0,8
0,6
0,4
0,2
0
C_M
1
2
3
4
5
run#
Pressure & Shape Integration
Force Balance Readings
Windage Corrected Force Balance

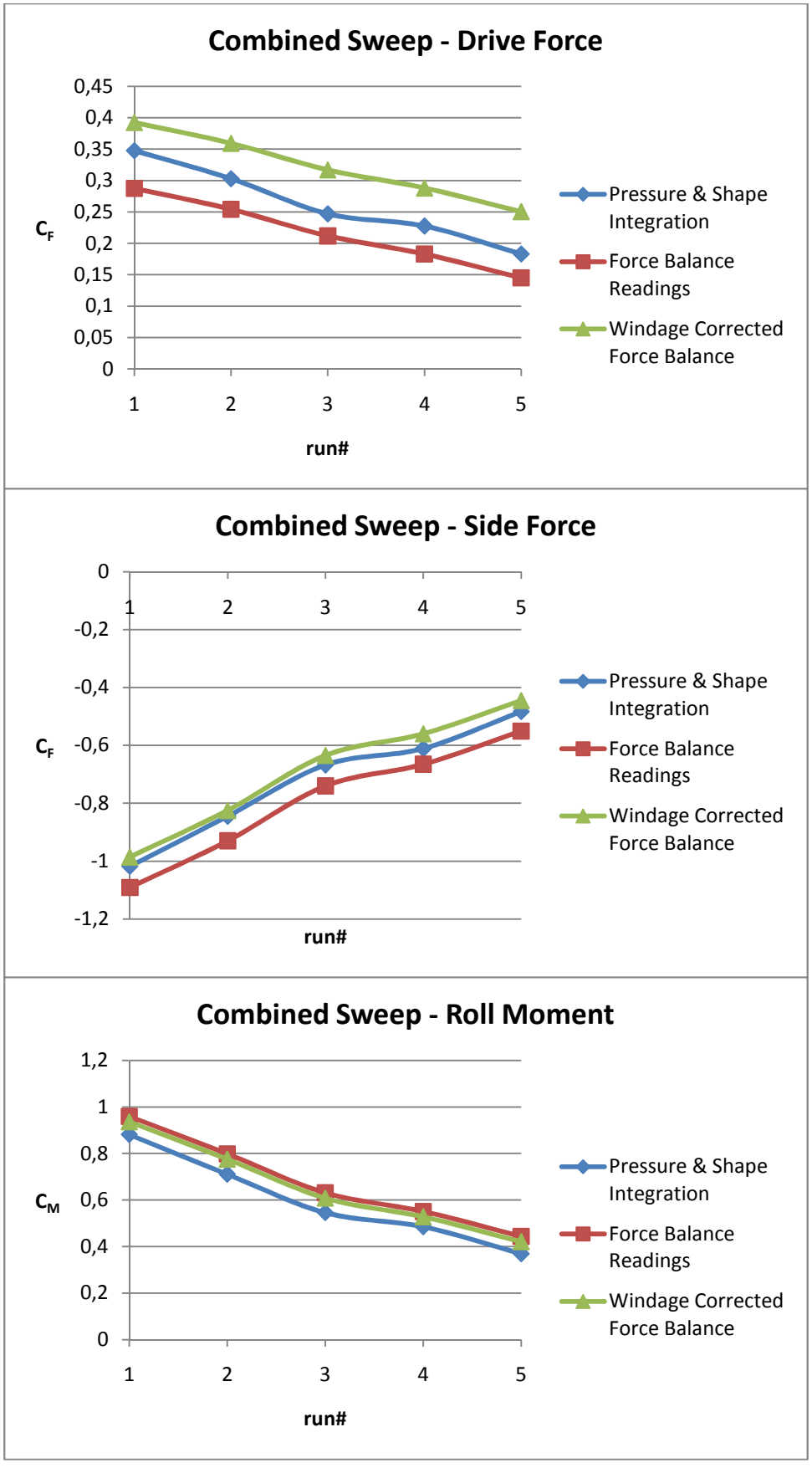
Combined Sweep - Drive Force
0,45
0,4
0,35
0,3
0,25
0,2
0,15
0,1
0,05
0
C_F
1
2
3
4
5
run#
Pressure & Shape Integration
Force Balance Readings
Windage Corrected Force Balance
Combined Sweep - Side Force
0
-0,2
-0,4
-0,6
-0,8
-1
-1,2
C_F
1
2
3
4
5
run#
Pressure & Shape Integration
Force Balance Readings
Windage Corrected Force Balance
Combined Sweep - Roll Moment
1,2
1
0,8
0,6
0,4
0,2
0
C_M
1
2
3
4
5
run#
Pressure & Shape Integration
Force Balance Readings
Windage Corrected Force Balance